Master thesis : Dynamics and control of a future off-shore wind power hub

Auteur : Bastin, Bertrand
Promoteur(s) : Van Cutsem, Thierry
Faculté : Faculté des Sciences appliquées
Diplôme : Master : ingénieur civil électricien, à finalité spécialisée en "electric power and energy systems"
Année académique : 2018-2019
URI/URL : http://hdl.handle.net/2268.2/6802

UNIVERSITY OF LIEGE
FACULTY OF APPLIED SCIENCES

DYNAMICS AND CONTROL OF A FUTURE OFFSHORE WIND POWER HUB

Master thesis conducted by

BASTIN BERTRAND

with the aim of obtaining the degree of Master in Electrical Engineering

SUPERVISOR
Thierry Van Cutsem

JURY MEMBERS
Bertrand Cornélusse (ULiège)
Patricia Rousseau (ULiège)
Lampros Papangelis (External)

ACADEMIC YEAR 2018-2019

Abstract

In the past decades, the increased carbon dioxide released by burning fossil fuels has been urging the demand for decarbonisation of our society. However, even if local renewable solutions are necessary, mass-scale production and management will soon be of crucial interest if fossil energies have to be replaced in due course and efficiently. In that context, it is very likely that offshore wind turbines will become an important electricity provider. Nevertheless, nowadays, technical obstacles remain and prevent the global implementation of such technologies. Indeed, the substitution of the classical synchronous machine by converter-based technologies induces a lack of inertia in the network, rendering the system more vulnerable to disturbances and source-outage. The present work aims at highlighting a possible transition technology : the Synchronous Condenser.

This project is drawn within the context of a large scale and international study: the North Sea Wind Power Hub. The principal idea is to connect onshore network from several countries with an artificial island collecting wind power. Mainly, the efficiency of a Synchronous Condenser to handle the power balance and the voltage control on the island is investigated. Two study cases are performed: a single DC link model and a five link system. Our leading aim is to propose a preliminary tuning of the parameters involved in the VSC controllers and specifically the control of active and reactive power on the island. The control of the active power is based on the rotor speed of the Synchronous Condenser and a Hub Coordinator used to synchronise all DC links together.

A first approach of the design is conducted through a linear study on the single link system. The poles location allows to determine the required value of the gains to fit specific dynamic constraints. Afterwards, a nonlinear analysis enables to impose additional complementary constraints on the gains. Thanks to those two analyses, the control of the VSC is entirely designed. The main conclusion of this chapter concerns the stability of the system. Indeed, a wide range of values for each gain is determined. Those ranges provide space for the tuning of the gains to fit desired dynamics constraints.

The final chapter, dedicated to the five link system, focuses on advanced analyses such as $n-1$ criterion or the operating point. The parameters study of the Synchronous Condenser highlights the large possibility in term of size and nominal power to ensure stability.

The general conclusion of this work is the feasibility of the Synchronous Condenser implementation and the strong stability of the system. It is viable to tune the gains to provide expected behaviours. Therefore, a Synchronous Condenser may be considered as a solution to sustain the current power transition and especially while awaiting the improvement of grid-forming technologies.

Acknowledgements

It has been a first experience for me to undertake such an important project in a research field. Choose my own subject, defining the pathway and the study fields and how to obtain useful results has been a real stimulating challenge and I definitely would not have been able to complete this work without help.

I would like to express my gratitude to my supervisor Professor Thierry Van Cutsem. First and foremost to giving me the possibility to work on such an exciting subject.But I am especially grateful to having been helpful and responsive all along the fulfilment of this work. Besides from providing me indispensable advice, he has always been enthusiastic towards my work and supportive, even during setbacks. Thank you for all the exciting discussions about the project or not, for your motivation and your inspiration.

I also want to thank the PhD students of Mr. Van Cutsem. Lampros Papangelis for all the works, codes and papers that have been helpful for my own project. The advice and time that you grant me have been helpful. Gilles Chaspierre for all the advice regarding the uses of software.

Moreover, I am deeply grateful to my family that has provided unwavering moral support all along the ups and downs of this project and my studies. My thesis being also the conclusion of my five years of study, I feel particularly lucky that they have been so encouraging and stimulating during all this time, whichever way I went. Your trust and your attendance have always made of this family a linchpin for me and a refuge in case of doubt and fears.

Finally, I want to specially thanks my girlfriend, for your support, your patience and your motivation. Your presence helps me to become a better person. Your reflection, your curiosity and your interest are a real inspiration for me.

Contents

Chapter 1

North Sea Wind Power Hub

Due to increasing demand for decarbonization, new solutions, able to bring huge amounts of renewable energies, are becoming urgently required. The North Sea Wind Power Hub (NSWPH) project is one of the several projects suggested to move towards a free-carbon electricity production world. This project consists in creating a big artificial island in the North Sea to collect wind power and connecting it to several European countries. The main goal of this chapter is to present the NSWPH project, together with what are the contribution of this work regarding the NSWPH. All the main abbreviations used in this report are given in Appendix A.1.

1.1 Purpose of the project

The NSWPH has two main purposes: harvesting the benefits of a mass scale offshore wind power and interconnecting countries across North Sea through high voltage direct current (HVDC) links [1]. According to the Paris Agreement, a significant increase of renewable energy sources is needed [2]. The North Sea offers a consequent opportunity to create off-shore wind power with a combination of shallow water, strong and relatively stable wind speeds and closeness to consumption centers [3]. This large-scale project, which aims at providing 180 GW thanks to far offshore wind, could be one solution for this new "green" electricity and be a springboard for new off-shore projects.

1.1.1 Hub and spoke

The purposes of this project can be condensed into its two main actions: "Hub and spoke". The Hub is responsible for harvesting wind power, which is distributed to European market through interconnectors, the spokes. This configuration should allow to share power through DC links even in the case of no wind power production. This configuration is also called *Internationally Coordinated Roll-Out (ICRO)* [5] and comparisons are drawn with a *National Incremental Roll-Out (NIRO)* configuration for an equivalent power. NIRO configuration is, currently, the most common architecture for offshore project. These distinct architectures are represented in Figures 1.1 and 1.2, respectively.

Generally, the increasing cost and losses with distance from onshore is restraining the feasibility of far offshore projects [4]. In our case, the combination of Hub and spoke could allow to reduce the cost up to 30%. These cost reductions arise from several factors[5]:

- Reduced onshore grid reinforcement cost: in the ICRO approach, the Hub is connected to parts of onshore grid where excess transport capacity is available. In the NIRO approach, it is generally the nearest connection point.

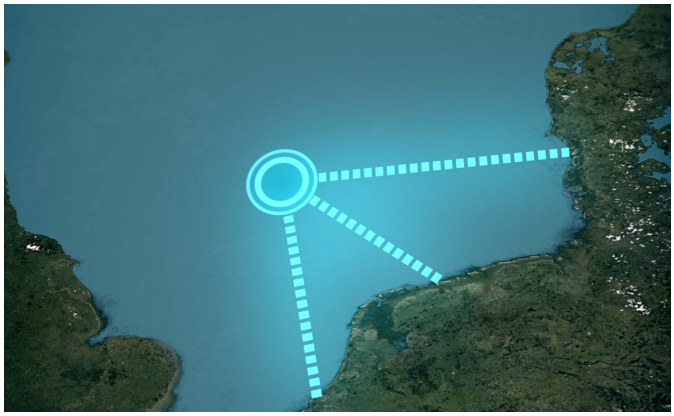

Figure 1.1: ICRO configuration [5]

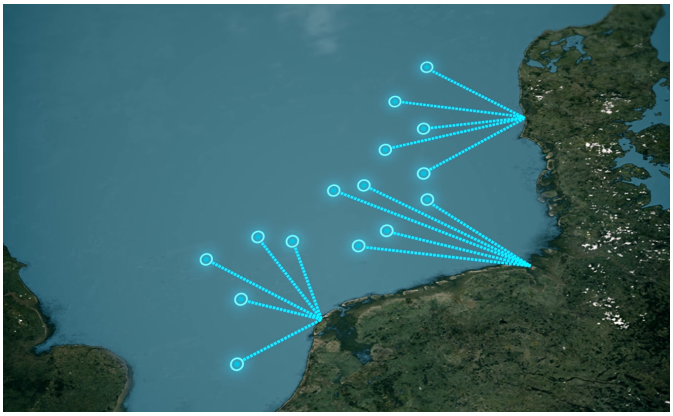

Figure 1.2: NIRO configuration [5]

- Reduced interconnector costs: the combination of Hub and spoke reduced the total cable length and the cost for substation in comparison with two distinct network for both applications.
- Export cable cost: the larger scale power of the project allows to work at higher voltages and consequently reduce the relative cable cost €/ (GW.km).

These advantages come on top of a better continuity of the wind in far offshore. Moreover, in this case, other cost savings could appear thanks to power to gas. The cost advantages are not the only assets of this project. The interconnection between countries could make other projects feasible, such as the use of Norway's pumping station storage for Europe [6]. This could also, in turn, lead to a decreasing cost of electricity and increase the global welfare of the electricity market.

1.1.2 Grid connection options for offshore wind

Even if the offshore wind has been exploited for many years, there exists several techniques to connect it to onshore grid [8]. Some of the possible connections are covered in this section.

HVAC platform

In this type of architecture, the wind farms are connected to an AC platform, which is connected to the onshore network thanks to AC links. This is illustrated in Figure 1.3a. However, when distance to shore and wind farm size increase, the losses increase as well in addition to consequent capacitive effect induce in the cables. This is the main limitation of HVAC uses [11, 14]. Above a certain distance, the losses of HVAC cables become greater than the ones for DC cables [30]. This distance depends mainly on the nominal power of the cables. Due to the consequent remoteness at the basis of the project, this solution is not considered any further.

HVAC collector platform

In this case, the connection between onshore and offshore is ensured by an HVDC cable. However, an AC platform is used to collect the power from the wind farms and step up the voltages for transmission to the HVDC converter

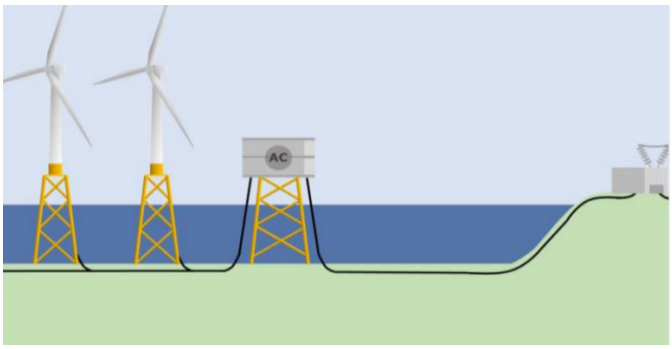

(a) HVAC platform

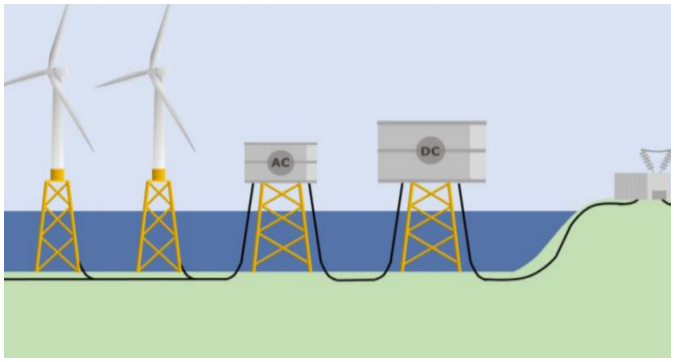

(b) HVDC platform with HVAC collector platform

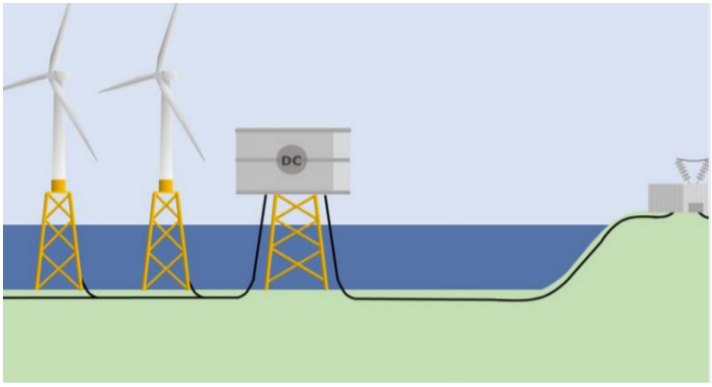

(c) HVDC platform

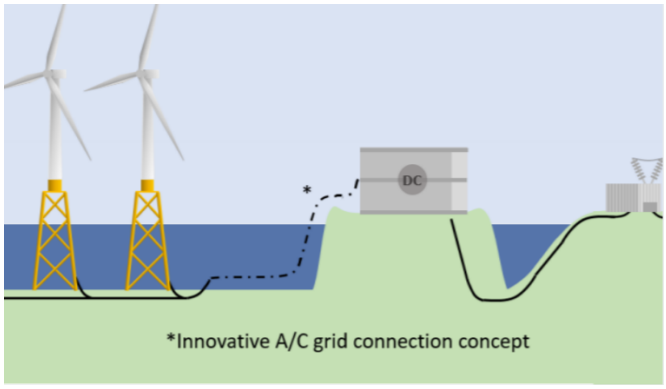

(d) Island with HVDC link

Figure 1.3: Representation of the different grid connection of offshore wind to onshore network [8].

platform. This type of platform increases significantly to the cost of this kind of project. The architecture is illustrated in Figure 1.3b. This architecture is really similar to the one use in this work. However, several differences are important between both configurations.

HVDC platform

This architecture consist in DC current and voltage directly provided by the wind turbines. The connection with the onshore network is also ensured by DC cables. This architecture is represented in Figure 1.3c. The main obstacle of this technique is to obtain DC current at the output of the wind turbine as well as the DC breakers needed in case of fault. For these technical reasons, this architecture is not used in this work.

Island with HVDC link

The principle is almost the same than HVAC collector plateform with HVDC connection to onshore network.However, not only one HVDC connection is considered but several links with the onshore network are used.Moreover, the use of an island allows to use it as a Hub and spoke. The island also enables to create facilities for employees, harbour and power to gas infrastructure, to cite a few. This architecture is represented in Figure 1.3d. This last architecture is the one used in this work [1].

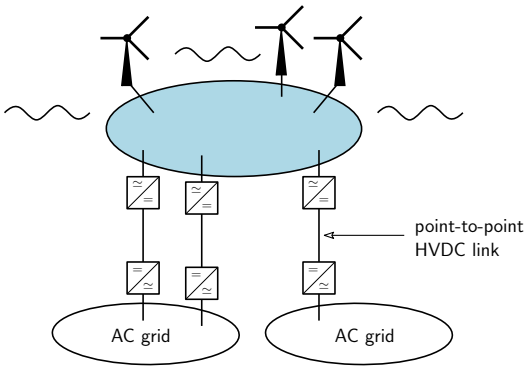

Figure 1.4: Multiple point-to point HVDC links configuration

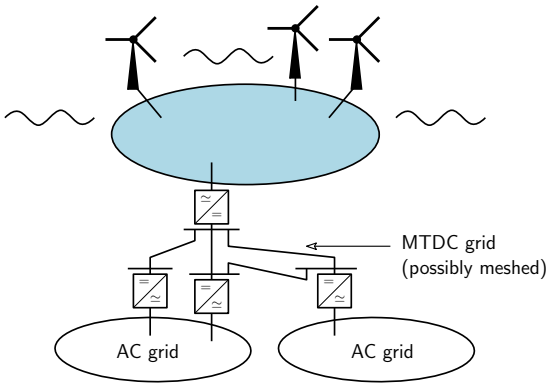

Figure 1.5: Multi-terminal HVDC grid configuration

1.1.3 Connection of wind farms to the Hub

The final architecture exploited for the project is an island/Hub. However, a combination of architectures are developed to connect the wind farms to this island. Some wind farms are connected to the AC collector platform with a 66-kV cable. The AC collector platform are connected to the Hub by a 380-kV cable. Other wind farms are directly connected to the island via a 66-kV cable thanks to transformer.

1.2 HVDC technologies

This section concerns the options available for the decision maker of the project regarding the HVDC technologies such as the converter used and the HVDC connections.

Converters

There are two kinds of converters mostly used: the Thyristor-based Line-Commutated-Converter (LCC) and IGBT-based Voltage-Source-Converter (VSC). The first one is based on Thyristor technology and has been used for many years [42]. The technology associated to LCC is well known. The VSC is more recent due to quite new advances in high-power electronics, specifically the development of insulated gate bipolar transistor (IGBT) [11, 13]. In this project, an IGBT-based VSC model has been considered for two main reasons: [11, 12, 13]:

- A VSC-based HVDC link does not require a strong offshore or onshore AC network. It can even start up against a non-loaded network.
- The LCC requires an important amount of reactive power, which can be hardly made available on the island.It also requires a strong AC network which is not the casse of the island.

HVDC terminal

There are several methods allowing the DC connection between the onshore network and the island. The first one consists in distinguishing clearly each connection from the island to the onshore networks, as shown in Figure 1.4.

This configuration is called multiple point-to-point HVDC links. In case of fault in an HVDC link, it is straightforward to trip it thanks to its converters without shutting down the whole system, which is a big advantage. All the lines are fully controllable [43, 44]. However, a coordination is required between the lines, in order to manage the parallel operations of the multiple links system [46].

Another available architecture is the Multi-terminal HVDC grid, represented in Figure 1.5. In this case, the grid can be meshed, and this gives more flexibility to the system. However, the availability of DC breakers is required to trip a single DC cable in case of fault. Another disadvantage of this configuration is the design of the offshore VSC. Indeed, in this second case, the single offshore VSC has to carry as much power as all the other VSC in the Multiple point-to-point configuration. Moreover, research about this kind of architecture is still in progress [45, 26]. For those reasons, the multiple point-to-point HVDC links architecture has be selected in this work. However, this choice could not reflect the future choice for the real NSWPH project.

Grid forming VS grid following

There exists several techniques for the control of the VSC. The two mains techniques are called "grid following" and "grid forming", and differ from their control strategies [47].

The grid following technique is used in almost all the VSC systems for now. In this case, the network is fed by synchronous machines that dictate the frequency and the voltage of the network. In this case, the VSC measures the amplitude, the phase and the frequency of its terminal grid voltage. The goal is to adapt their injected current in order to meet the active and reactive power set-points [48]. This control has been used for many years and its operation is well known, but it requires the use of a synchronous machine to set up the voltage and the frequency. The main characteristics of the grid-following are as follow [49]:

- Regulates its currents in order to inject a defined amount of active and reactive power.
- Current setpoints are calculated with respect to the angle of the grid voltage at the point of connection.

In the case of a power system 100%-based on converters i.e. without synchronous machines, grid following cannot be considered anymore. Indeed, there is no more voltage and frequency to synchronise to[48]. The new control strategy is called grid forming. In this case, some converters have to operate such as a synchronised voltage source. The VSC has to manage the frequency and the voltage, and is the reference for the system. The VSC still controls the active and reactive power (as a grid following VSC) by controlling the magnitude and the phase of its voltage. This leads to two main disadvantages comparing to the use of synchronous machines: the limited overload capability and the increased sensitive control to grid variations [48]. This adds to the fact that this technology is still in progress.

The following provides the main characteristics of the grid forming converters, as defined by M. Liserre (2019) [49]:

- The converter controls the voltage at the point of connection while respecting its internal physical limitations in terms of converter voltage and current and within the energy balance at system level, independently from the characteristics of the network where it is connected

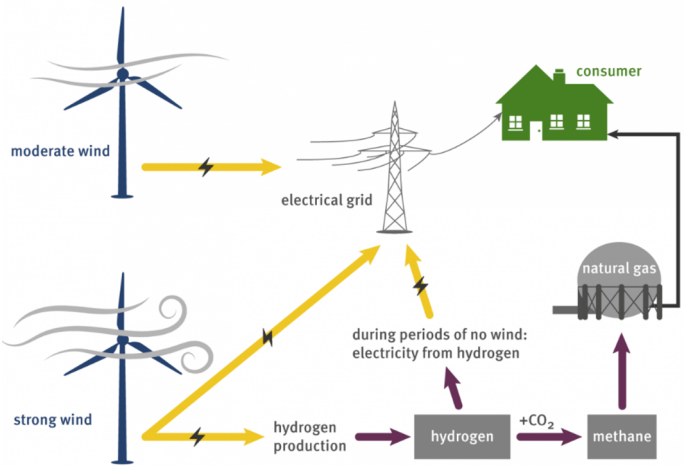

Figure 1.6: Principle of power to gas

- Regulates active and reactive power injection by controlling amplitude and phase of the voltage at the connection point.
- According to the implementation, the knowledge of the grid voltage angle might be needed or not.
- The converter is controlled so as to show an equivalent converter output impedance, whose characteristics can be arbitrarily modified within defined ranges, while respecting hardware constrains.
- If the physical limitations of the converter are violated, the converter is allowed temporarily to switch to another control strategy (e.g. Grid following operating mode) to prevent the hardware from damages.

Even though the grid forming technique is a "hot topic" due to its attractiveness and its potential, a grid following strategy is considered in this work for the sake of ease and well known behaviour. However, this requires forming a voltage to synchronise to. This is provided by a Synchronous Condenser, as explained in section 1.5

1.3 Power to gas

With a mass scale wind power roll-out and one or several Hubs in the North Sea, conversion and storage solutions for electricity are essential. Unfortunately, most of the existing batteries suffer from self-discharge and consequently can only be used for short-term energy storage. Moreover, the limited charge rates, the high maintenance requirements and the short lifetime make Power to Gas (P2G) more suitable to store and convert electrical energy produced on the island [15, 16]. It could be one of the solutions to bring synergies to the project and consequently strengthen its business case. Power to gas conversion could help balance and stabilise power transmission to the onshore market. The principle of P2G is shown in Figure 1.6.

During periods of peak power production, P2G could be exploited to convert and store energy instead of selling it at a low market price or to curtail wind due to possible interconnectors constraints. This possibility strengthen the flexibility of the project. The gas obtained could be used during low power production or to stabilise the system in case of fault. The transformation of hydrogen into electricity is achievable thanks to fuel cell [32].

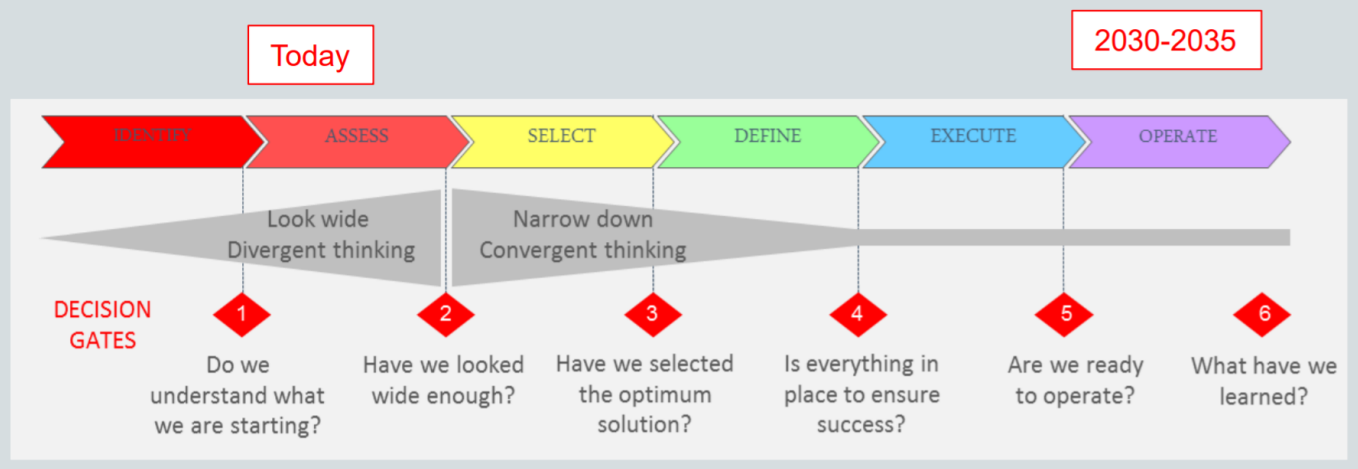

Figure 1.7: Time-line of the project [7].

In this case, the power created by the Hub could be brought onshore through electricity, gas, or both. Due to the already existing north sea gas network, the island could be linked to the onshore gas network. This is another argument for the creation of an island.

The last argument provided for the development of P2G on the island refers to the inability to use electricity as only energy source and how much hydrogen is required to decarbonise our society [17]. Indeed, electrification can not be systematically requested and can not sustain decarbonisation on its own. Hydrogen produced through electricity provides another energy type that could represent one efficient way to help decarbonising our consumption mode. Moreover, the particular case of NSWPH, very large amounts of electrical power (until 180 GW) cannot be accommodated by ever the most advanced HVDC links and converters.

1.4 Status of the project

1.4.1 History, objectives and time-line

Launched in 2016 by TenneT, the NSWPH project has become an international project. Quickly, a general time-line of the project has been set up which is given in Figure 1.7. The term "today" corresponds to the beginning of the project, so approximately the year 2016. The end of the assessment phase is expected for the middle of this current year.

Figure 1.8 represents the expected power production of the project until 2045. Legacy AC refers to currently operational and planned AC radially connected offshore wind farms. Legacy DC stands for currently installed and planned DC connected offshore wind farms. Standalone HVAC refers to the HVAC platform explained previously and standalone HVDC to the HVDC platform. The final power expected corresponds to 181 GW.

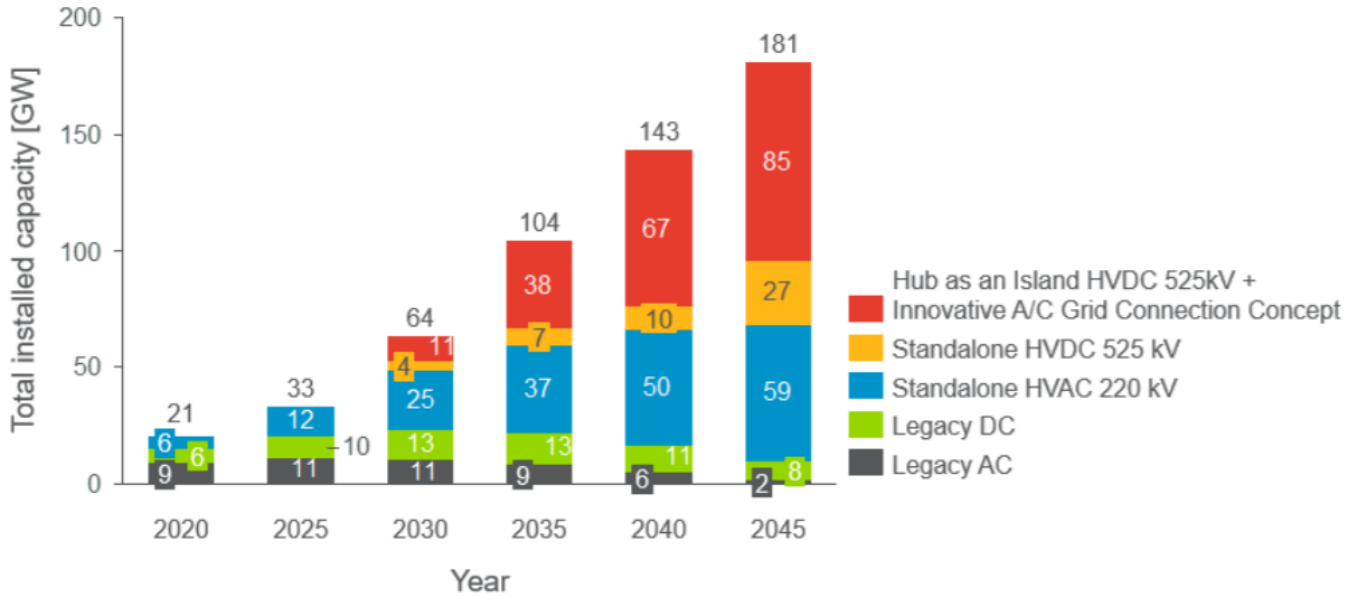

Figure 1.8: Expected power production until 2045 [8]

For now, specific studies of technical, environmental and market perspectives are still in progress. The purpose is to study separately the island, the wind farm and the Hub to understand the global feasibility, the environmental impacts and the economical perspectives for each part.

1.4.2 Internationally coordinated

This project is the collaboration of several countries. Comprised of five main actors, this project involves several countries connected to the Hub, of which Norway, Belgium and Netherlands to cite a few. The five mains actors of this project are the following [1]:

- "TenneT Germany and Netherland: TenneT is a European electricity Transmission System Operator (TSO), with main activities in the Netherlands and Germany."
- "Energinet: Energinet is an independent public enterprise owned by the Danish Ministry of Climate and Energy. They own, operate and develop the transmission systems for electricity and natural gas in Denmark."
- "Gasunie: Gasunie is a European gas infrastructure company. They provide the transport of natural gas and green gas in the Netherlands and the Northern part of Germany."
- "Port of Rotterdam: The objective of the Port of Rotterdam Authority is to enhance the port's competitive position as a logistics Hub and world-class industrial complex. It is the Port Authority's ambition to play a pioneering role in the global energy transition, making this area a frontrunner, fieldlab and flagship of the energy transition."

1.5 Contribution of this master thesis

In order to help the implementation of NSWPH and the integration of renewable energy in the electricity market, the main aim of this master thesis is to investigate a solution to collect variable wind power and use the island as a Hub, while maintaining power balance even after large disturbance (such as the outage of an HVDC link). The solution investigated relies on a Synchronous Condenser (SC).

1.5.1 The new interest for Synchronous Condenser

The SC is an old tool. Originally used to provide or absorb reactive power to control the voltage at one bus of its internal transmission grid, the Synchronous Condenser actually offers new advantages to face challenges of the new electricity network [18]. Simply stated it is a DC-excited synchronous machine with no prime mover. Besides voltage control, the SC has kinetic energy stored in the rotating mass. These two features make it suitable to control the wind power Hub.

The demand for SC is significantly starting to increase nowadays due to the penetration of renewable energies in the electricity mix. Energy sources like solar or winds use power-electronic inverters. Moreover, the expansion of renewable energies leads to a decrease of conventional power plants and consequently reduces total inertia stored in rotating masses throughout the system.This leads to the inability to support the network in case of fault or disturbance. As a result, the resilience and the stability of the network decrease. SC could be a solution to those issues [19, 20]. Indeed, SC could provide some short-circuit power to strengthen the network, help controlling voltage and to some extent provide inertia.

Some studies have already shown the usefullness of SC. For example, Nguyen & al (2018) [9] proves the benefits linked to the use of SC regarding frequency stability enhancement in a low inertia system. Yan, R. & al (2015)[10] studies the same effect in the specific case of wind penetration, which is closer to the project of this thesis. The conclusions of these papers agree with other studies on the Synchronous Condenser [22, 23]. Almost all of those papers date from the last 5 years, which shows that there is an emerging and recent revival of in the SC.

1.5.2 SC application in this project

A first representation of the island is given in Figure 1.9 with two different case: with and without SC. In case without SC, the VSCs has to be in "grid forming" mode. In this case, some power arrives from each HVDC link and from wind farms. In case of sudden wind power production or outage of one link, a power imbalance appears.Immediately this power imbalance is compensated by HVDC capacitors that have small energy storage capacity.Soon after, the imbalance is compensated by the onshore converters. The operation of the VSCs are significantly impacted. With grid forming VSCs on the island there is a risk to have then switched under current limit, in which case the operation of the island grid is still a question in research [36, 37].

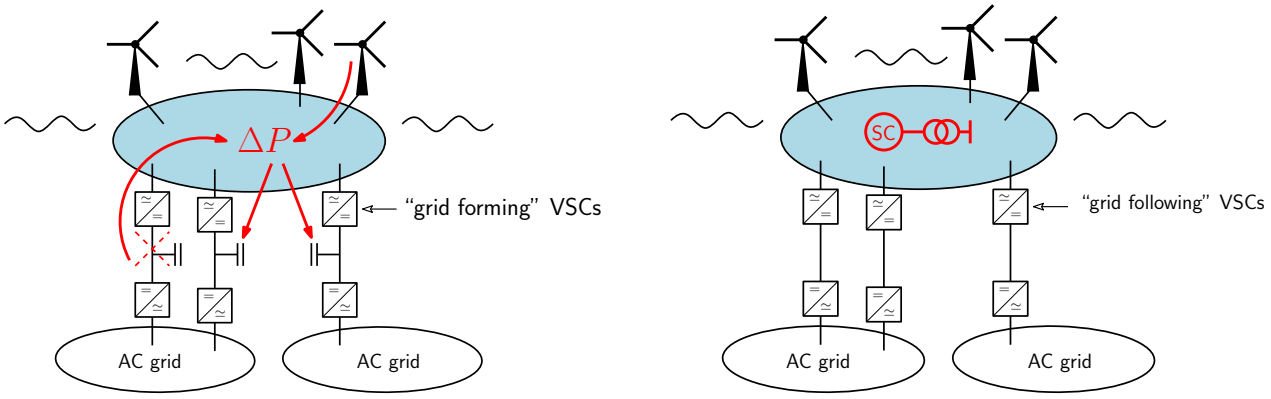

(a) Grid forming **(b)** Grid following

Figure 1.9: Power balance on grid forming and grid following system

To prevent this, a solution is to have some energy storage located on the island. An electrical battery is not large enough, highly expensive and too environmentally nasty to be considered as an effective solution [15]. The alternative explored in this work is to use Synchronous Condenser that brings inertia on the island from zero to low value [9, 10]. This solution allows also to produce an almost constant AC voltage of the island, thanks to the automatic voltage controller installed on the SC. This also gives the references to allows the converters to work in grid following as showed in Figure 1.9b.

In case of imbalance, the rotor speed of the SC changes. This change is counteracted by a prompt adjustment of the power flows through the VSC until the speed of the SC is brought back to its nominal value. This is done to restore the stock of kinetic energy and to be prepared to face another power imbalance.Large speed excursions should be avoided since this results in corresponding frequency deviations of the offshore grid. This correction has to be performed in a specific response time: not too slow, to avoid excessively large deviations of the rotor speed but not too fast either, to avoid that the DC capacitor compensates too much the imbalance and disturb the DC voltage. The participation of each HVDC link to the imbalance correction has to be defined beforehand and needs to be updated in case of link outage.

• Outline of the report

Chapter 2 of this report aims at presenting the modelling of each part of the system. The third chapter is dedicated to the study of one DC link system with linear and nonlinear tools. The purpose is to study a first simple system and propose a first tuning of the parameters involved in the VSC controllers. The fourth chapter presents a five DC-link system and various disturbances are investigated.

Chapter 2

Modelling

The purpose of this chapter is to describe the different components that can interact in the modelling of the island's system. This system is illustrated in Figure 2.1

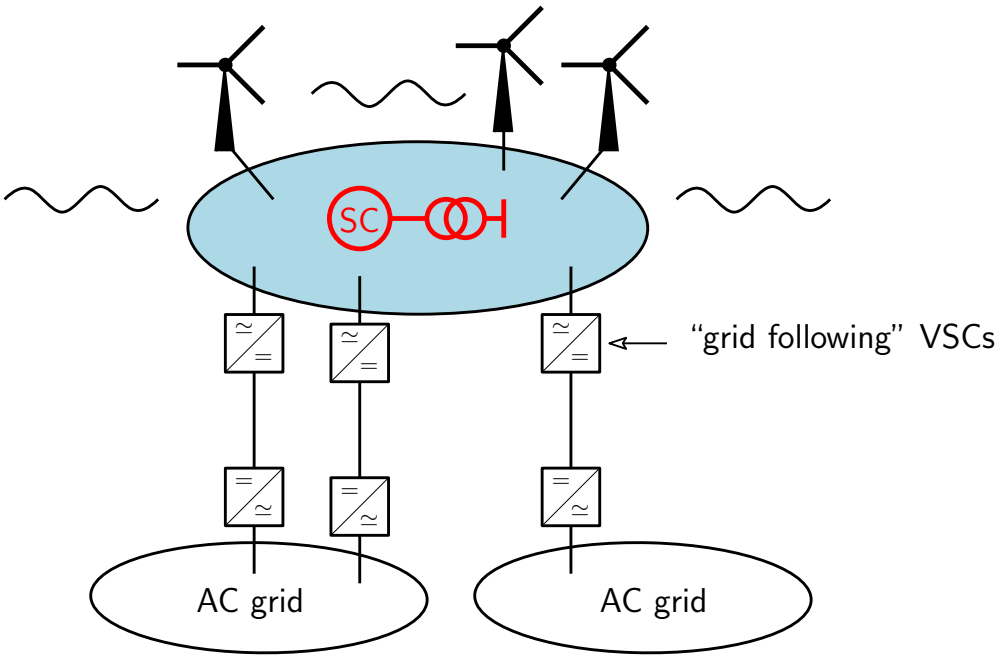

Figure 2.1: General representation of the system

The system exploited in this project has been defined as composed of four parts. First part represents the wind farms that are considered only as a power source to the island. The second part relates the SC, and the VSC with the HVDC links composes another one. Finally, the AC onshore networks are considered, as illustrated with two of them in Figure 2.1. In the following sections, after a short description of the reference frames, the last three specific parts are described more accurately in order to provide a global understanding of the dynamics of the system.

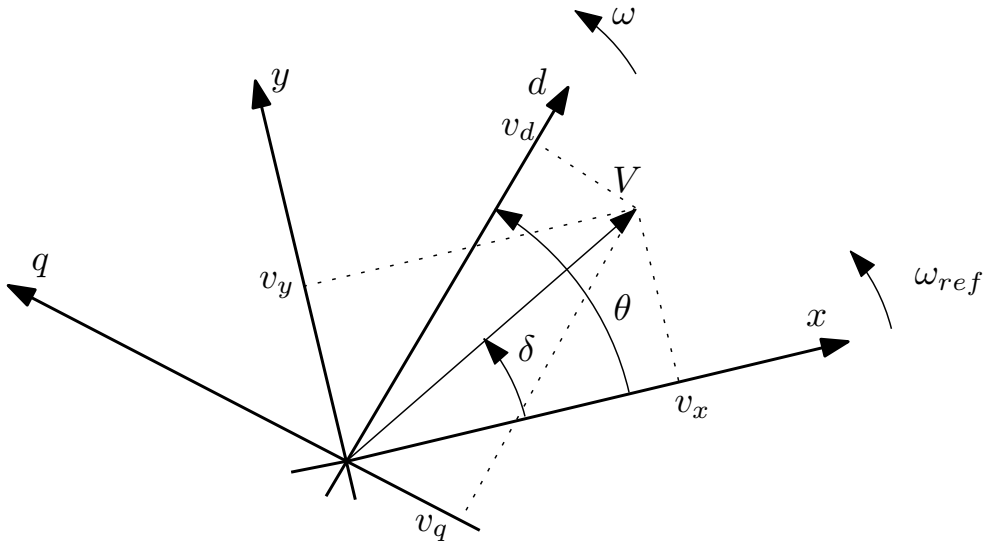

Figure 2.2: Reference frames

2.1 Reference frames

Before developing the equations of the specific parts, the choice of the reference frames need to be specified. These frames are represented in Figure 2.2 [21, 25].

Due to the ease of representation and conciseness of equations in the (d, q) frame, this plan is used often. However, several equations are defined in (x, y) plan, which is more general. That explains the necessity to establish the relations between those two. (x, y) are the orthogonal axes that rotate at the angular speed ω_{ref}. This reference frame is the same for all the elements of the system. On the other hand, the reference frame (d, q) corresponds to axes that can be specific for each element of the system, such as the synchronous machine. These axes rotate at the angular speed ω. In order to simplify the model, in the following, one assumes $\omega = \omega_{ref}$ in steady state, which means that the angle θ between both frames remains constant. In this specific configuration, voltages $\overline{V}$ and currents $\overline{I}$ can be easily expressed in both reference frames:

$$\overline{V} = v_x + j\ v_y = e^{j\theta}(v_d + j\ v_q) \qquad \overline{I} = i_x + j\ i_y = e^{j\theta}(i_d + j\ i_q)$$

2.2 Modelling of the VSC

The generic model of the VSC is made up of several components [12, 25], as shown in figure 2.3. Schematically, it is composed of a phase reactor, the converter itself and a DC capacitor. The subsequent subsections aim at describing more precisely the phase reactor and the converter. Specifically, the converter is presented through its sub-components: the Phase Locked loop, the current controller as well as the active and reactive power control.

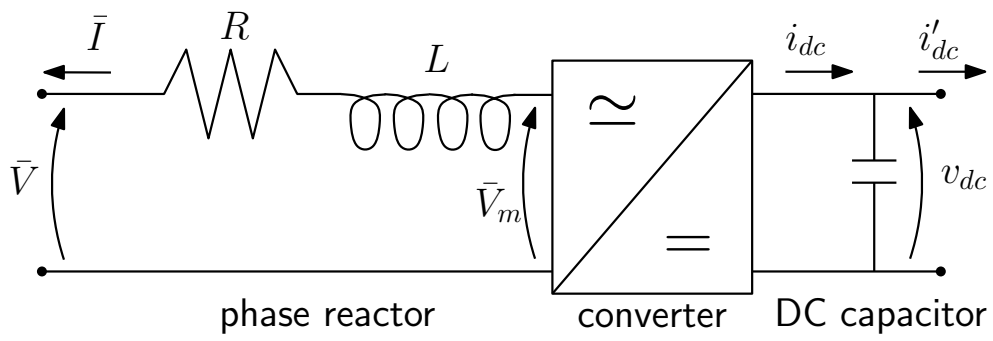

Figure 2.3: General modelling of the VSC. v_{dc} represents the output DC voltage of the VSC. $\overline{V}_m$ is the tension at the output of the converter and $\overline{V}$ is the voltage of the AC network connected to the VSC.

2.2.1 Phase reactor

The phase reactor corresponds to the left part of Figure 2.3. However, for the sake of conciseness, equations of the dynamics of the phase reactor are not be developed here. The complete set can be found in Appendix B.1. Thanks to those detailed equations, one can build a block diagram representation of the phase reactor as shown in Figure 2.4.

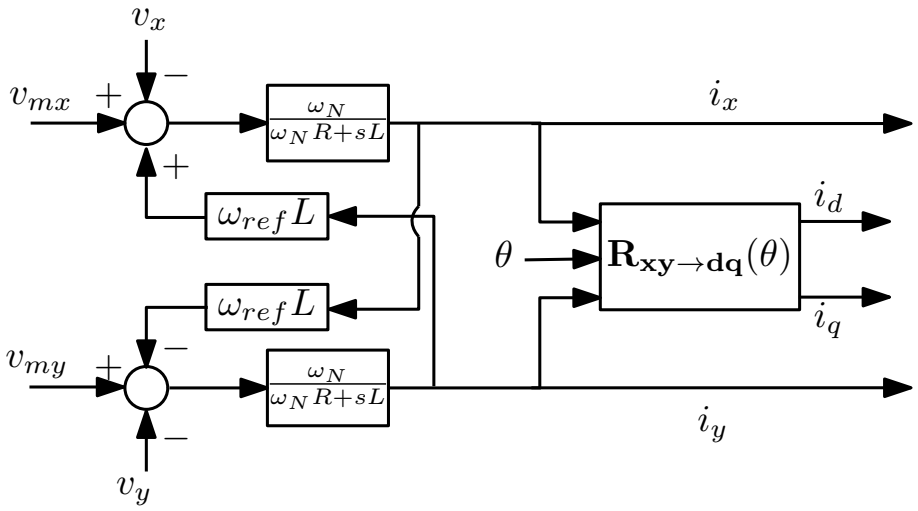

Figure 2.4: Block diagram of the phase reactor.The block $\mathbf{R_{xy\to\,dq}}$ represents the change of reference frame, which is computed using the transformation presented in the previous subsection.

2.2.2 Phase Locked Loop

The representation of the Phase Locked Loop (PLL) used in this project is provided in Figure 2.5 [24]. Notice that in what follows, w_N stands for the nominal angular speed. The PLL of the VSC sets the reference frame and has a single main purpose: align the voltage $\overline{V}$ with the direct d-axis. This means imposing a q-part null, with $v_d = V$. According to Figure 2.2, this means, in steady state, to have an angle $\delta = \theta$. Therefore, in the event of any instabilities, the PLL

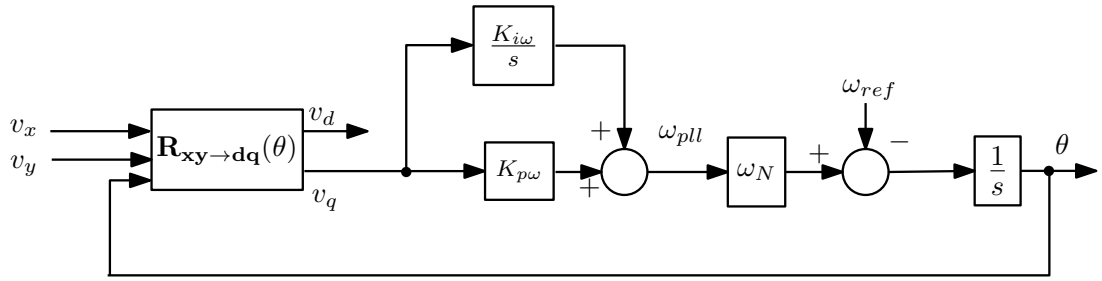

Figure 2.5: Representation of the Phase Locked Loop (PLL). The block $\mathbf{R_{xy\to\ dq}}$ represents the change of reference frame, which is computed using the transformation presented in the previous subsection.

estimates the value of θ, which is therefore not equal to δ. This value of θ is used by the current controllers to adjust the current phasor. This current phasor has to be determined with respect to the voltage phasor in order to obtain the desired active and reactive power. Moreover, during transient, the PLL needs to adjust its angular speed ω_{pll} in order to align the d-axis and the voltage phasor. As the angular speed corresponds to the one of the (d, q) axis, during steady state, $\omega_{pll} = \omega_{ref}$.

2.2.3 Current controllers

The current controllers are intended to force the currents in the system to reach their specified reference value (i_d^{ref} and i_q^{ref}). The specific values for i_d^{ref} and i_q^{ref} are deduced based on the power required in the VSC. This part of the control is discussed in subsections 1.2.4 and 1.2.5.

The current controllers are represented in Figure 2.6. To establish the equations governing those controllers, the principle of the phase reactor has been reversed to determine the voltage based on a current reference value. The current controllers allow to control each current separately [12, 26], which means two separated controls for the active and the reactive power. Indeed, active and reactive power are given by:

$$\begin{cases} P_i = v_d\, i_d + v_q\, i_q \\ Q_i = v_q\, i_d - v_d\, i_q \end{cases}$$

In steady state, $v_q = 0$ thanks to the PLL. This means that if i_d and i_q are controlled separately, it is also the case for both powers.

From Figure 2.6, the equations allowing the control of each current can be deduced:

$$v_{md} = v_d - L\,\omega_{pll}^{pu}\, i_q + C_d(s)\,(i_d^{ref} - i_d) \qquad (2.1) \qquad v_{mq} = v_q - L\,\omega_{pll}^{pu}\, i_d + C_q(s)\,(i_q^{ref} - i_q) \qquad (2.2)$$

Where $C_d(s)$ and $C_q(s)$ can represent any type of controller. By using equation 2.1 in equation B.1, the transfer function $\frac{i_d}{i_d^{ref}}$ can be determined. In equation B.1, the terms v_d and $L\omega_{pll}^{pu} i_q$ are cancelled by the expression of v_{md}.

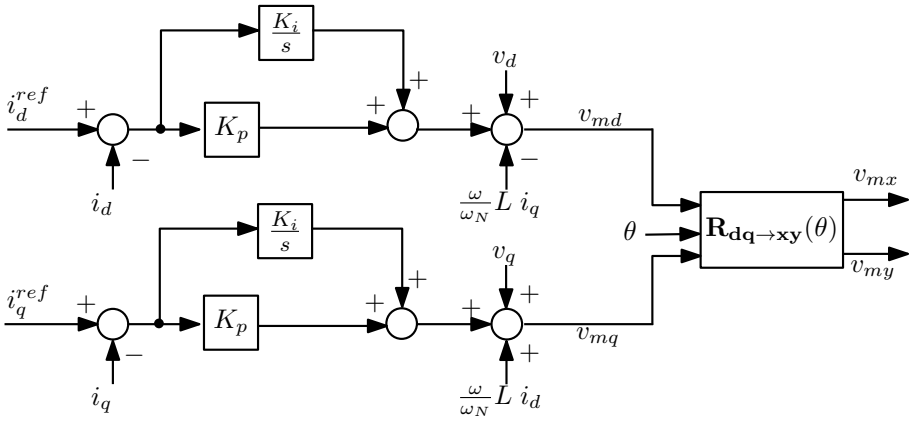

Figure 2.6: Current controllers

By using the same process for equation 2.2 in equation B.2, one can similarly deduce the transfer function $\frac{i_q}{i_q^{ref}}$.

$$\frac{i_d}{i_d^{ref}} = \frac{C_d(s)}{R + \frac{s\,L}{\omega_N} + C_d(s)} \qquad (2.3) \qquad \frac{i_q}{i_q^{ref}} = \frac{C_q(s)}{R + \frac{s\,L}{\omega_N} + C_q(s)} \qquad (2.4)$$

In this project, both current controllers includes PI controllers, according to Figure 2.6. Moreover, the gain in both controllers are the same. According to equations 2.3 and 2.4, this means that both transfer functions are the same and can be renamed $H(s)$. By adding the transfer function of the PI ($K_p + K_i/s$) and by arranging the terms the final transfer function is given by:

$$H(s) = \frac{1 + \frac{K_p}{K_i} s}{1 + \frac{R + K_p}{K_i} s + \frac{L}{\omega_N\, K_i} s^2} \qquad (2.5)$$

This transfer function is used to design the control gain of the current loop. This design is described in the Appendix B.2.

2.2.4 Active power control

In this project, the control of the voltage and the power are spread between the converters of the same DC link. This means that one of the VSC controls the voltage at one point and the other controls the power. The VSC on the island side is considered as the power controller and consequently, the onshore VSC as the voltage controller. Because the control of the power by the offshore-VSC has to depend on the Synchronous Condenser, a special design is considered. This means that both converters of a DC-link use a different power control loop.

Offshore-VSC

The voltage at the offshore-VSC is directed by the voltage controlled by the onshore VSC. This means that the offshore-VSC has to control current in order to control the power. As mentioned previously, the reference value of the current i_d^{ref} is computed based on the power desired in the DC link. The power control loop used on the island is represented in Figure 2.7. In this scheme, P_i is the actual active power in the ith VSC. P_i^o corresponds to the set-point

of the active power in the ith VSC. It is initialised to P_i at $t = 0$. Finally, P_i^{hc} is the active power correction sent by the Hub Coordinator, initialised to zero at $t = 0$.

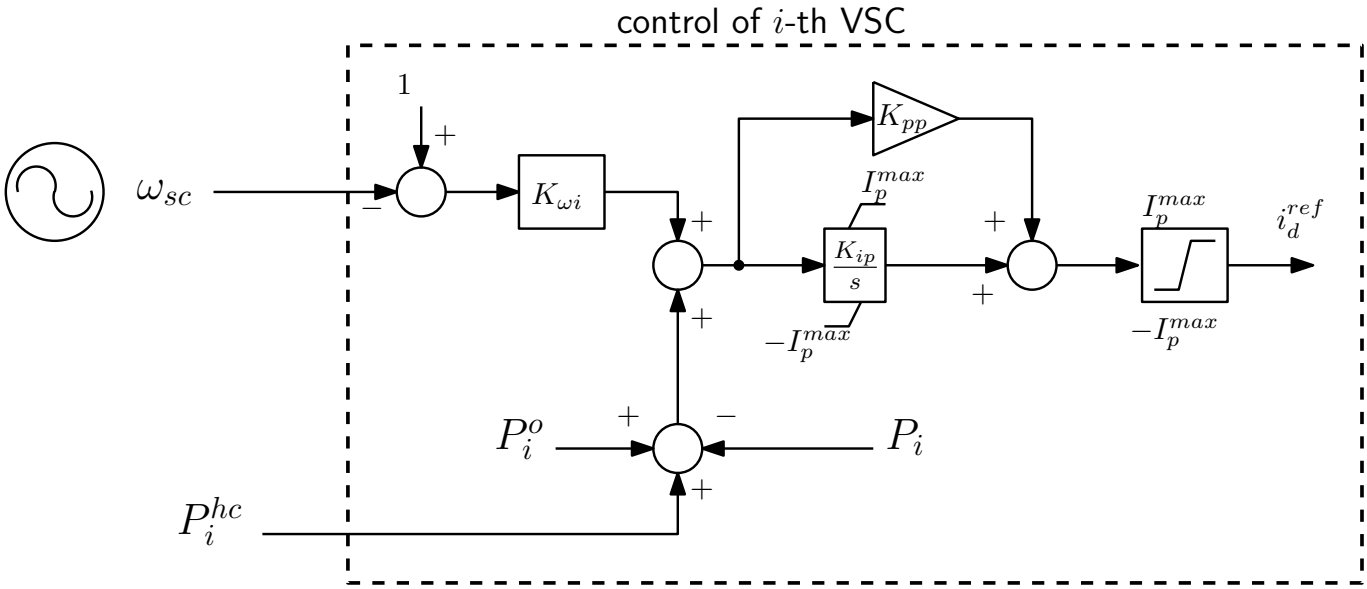

Figure 2.7: Active power control

The principle of the Hub Coordinator is represented in Figure 2.8. This one takes as input the Synchronous Condenser's rotor speed. The output is the active power correction for each VSC. Thanks to these corrections, the Hub Coordinator controls the rotor speed of the SC around its nominal value.

Based on the rotor speed deviation, the HC computes a total power changes P_{tot}^{hc} thanks to the following formulas:

- In case of a continuous time control, the controller used is only composed of an integral term:

$$P_{tot}^{hc} = \frac{K_{hc}}{s}(1 - \omega_{sc}) \tag{2.6}$$

  This gives, in the time domain:

$$\dot{P}_{tot}^{hc} = K_{hc}(1 - \omega_{sc}) \tag{2.7}$$

- In case of a discrete time control, the Backward Euler method is exploited:

$$P_{tot}^{hc}(k) = P_{tot}^{hc}(k-1) + h\ \dot{P}_{tot}^{hc}(k) = P_{tot}^{hc}(k-1) + h\ K_{hc}(1 - \omega_{sc}(k)) \tag{2.8}$$

  Where h is the integration time step. The implicit Euler method is a straightforward method to solve differential equations of the first order. Moreover, the implicit method is more stable than the explicit method [39, 40]. That explains the use of this method in case of a discrete time control.

Once the total power change has been computed, it is distributed among the DC-links. This gives, in the general case of c links:

$$P_{tot}^{hc} = \sum_{i=1}^{c} P_i^{hc} \tag{2.9}$$

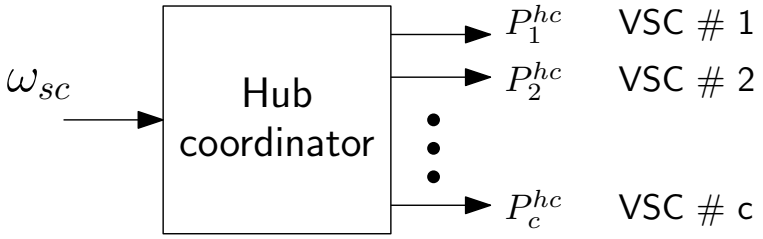

Figure 2.8: Hub Coordinator

The components of each VSC are defined by participation factors μ_i such that:

$$P_i^{hc} = \mu_i \, P_{tot}^{hc} \quad \text{with} \quad 0 \leq \mu_i \leq 1 \quad \text{and} \quad \sum_{i=1}^{c} \mu_i = 1 \tag{2.10}$$

This participation factor reflects the percentage of participation of the ith VSC to a disturbance. Specifically, if $\mu_i = 0$, the VSC does not help the system at all in the event of a fault or disturbance. Therefore, the main purpose of the Hub Coordinator is to ensure the coordination between among the VSCs and their respective factors.

Onshore VSC

In this case, the term "outer controllers" is more adapted. As for the offshore-VSC, the outer control loop starts by computing the current reference values i_d^{ref} and i_q^{ref} [25]. However, in this case, the DC voltage is controlled and no more the power. The outer control loops are represented in Figure 2.9. The outer control loops are more generic in this case than for the offshore-VSC. In the offshore-VSC, it is necessarily the power than controls the current reference values. In these control loops, several options are allowed, such as active and reactive power of the VSC, AC voltage and DC voltage.

The parameters α and β allow to design the desired strategy. In our case, the purpose of the onshore VSC is to stabilise the DC voltage. Therefore, one may choose $\alpha_1 = 0$ and $\beta_1 = -1$. In this case, the active power is controlled by the VSC to reach the reference value v_{dc}^{ref} for the DC voltage [26, 25]. The purpose of this work is not to investigate all the possible combinations of this control loop: the other values of the parameters are not covered here.The second outer control loop controls the reactive power. This is done by taking $\alpha_2 = -1$ and $\beta_2 = 0$.

2.2.5 Reactive power control

The reactive power control described here is applicable only for the offshore-VSC. The reactive power control of the onshore VSC has been already explained in the previous point. As for the active power, a PI controller is used to determine i_q^{ref} as a function of Q_i^{set}. The control of the reactive power is represented in Figure 2.10, where Q_i^{set} represents the reactive power desired in the ith VSC. In steady state, $Q_i = Q_i^{set}$ and Q_i^{set} could be adjusted to allow a comfortable reactive power margin at the Synchronous Condenser.

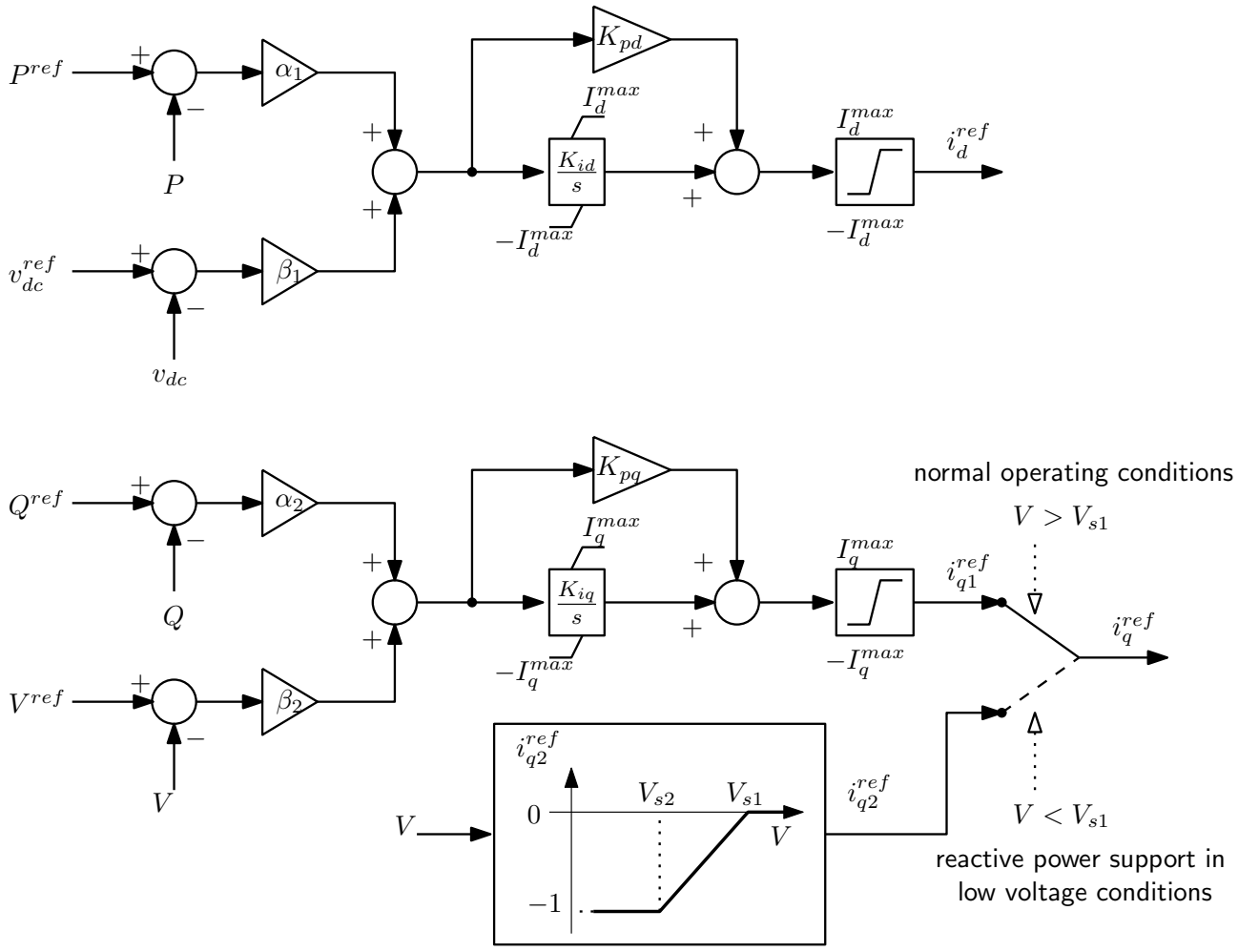

Figure 2.9: Outer control loop

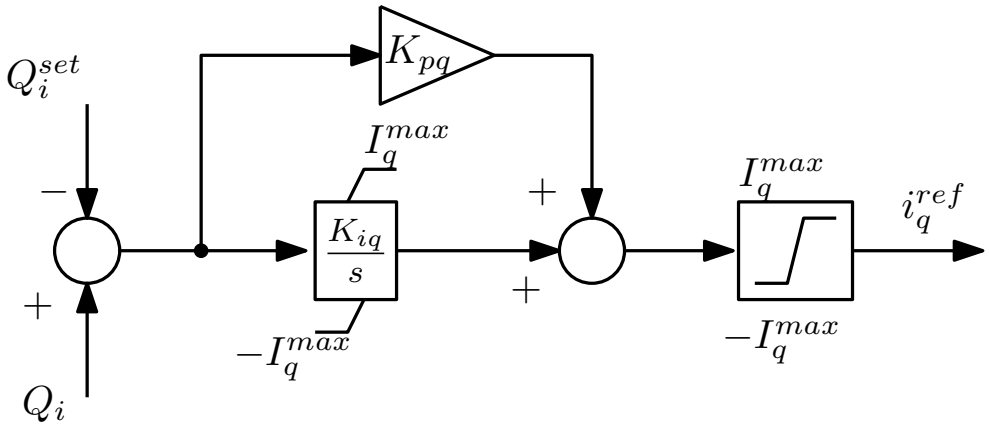

Figure 2.10: Reactive power control

2.3 HVDC link

The connection between the offshore system and the onshore network is ensured by the DC links. The scheme of a single DC link is provided in Figure 2.11. In this representation, the DC branch consists in a resistance only. This is assumed thanks to the fact that the dynamics of the DC link is much faster than the other dynamics of the system. Therefore, the inductances are neglected and capacitances considered as comprised in the VSC capacitors [25, 26].

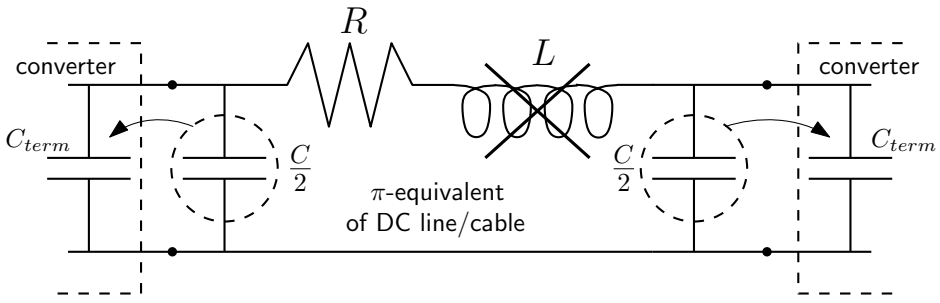

Figure 2.11: Representation of a DC link

2.4 Synchronous Condenser

This section does not aim at developing the complete model of a synchronous machine. However, the main characteristics are described. The model of the synchronous machine correspond to the detailed model presented in the course of "Electric power system analysis" [41]. The model used for the synchronous machine is represented in Figure 2.12.

The stator contains three windings: a, b and c for the three phases. There is 4 rotor windings, 2 for each axis. In the direct axis, there are the field winding (f) and the other winding that represents the dampers (d_1). In the quadrature axis, the first winding represents also the dampers (q_1) and the second one simulates the eddy currents (q_2).

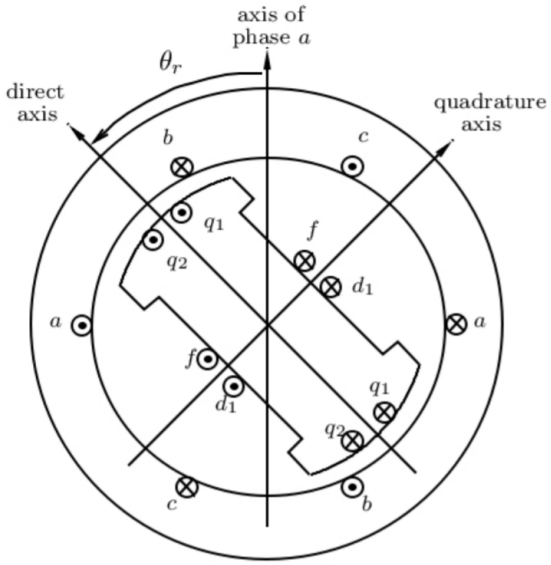

Figure 2.12: Model of the synchronous machine.

All the equations and transformations that characterise the synchronous machine are not developed here. However, one can say that the Synchronous Condenser is characterised by the equation of its power. Indeed, in steady state, there is no active power provided by the SC. This means that the equations of the torque has to change. In a synchronous machine, the equation that assesses the variation of kinetic energy is given by:

$$\frac{dW_c}{dt} = P_m - \dot{\theta}_r \, T_e$$

Where P_m is the mechanical power provided by the turbine, θ_r is the rotor position and T_e the electromagnetic torque applied by the generator to the rotor. In the case of the Synchronous Condenser, there is no mechanical power provided by the turbine. In this case the equation can be rewritten:

$$\frac{dW_c}{dt} = -\dot{\theta}_r T_e = -\dot{\theta}_r(\psi_d \, i_{qsc} - \psi_q \, i_{dsc})$$

Therefore, the variation of kinetic energy depends directly on the reactive and the active power required from the Synchronous Condenser through i_{dsc} and i_{qsc}.

The previous equation can also be considered as the variation of the rotor speed (ω) as a function of the electromagnetic torque developed by the Synchronous Condenser (T_e):

$$2H \frac{d\omega_{pu}}{dt} = -T_{epu} \tag{2.11}$$

Where the rotor speed is given by:

$$\omega = \frac{d\theta_r}{dt} \tag{2.12}$$

The parameter H is highly impacting for the following. Indeed, it is called the specific energy of the Synchronous Condenser and is computed by the ratio between the kinetic energy of rotating masses at nominal speed and apparent nominal power of machine. Therefore, it characterises the robustness of the SC in case of an output power change. It is interesting to notice that H has the dimension of a time.

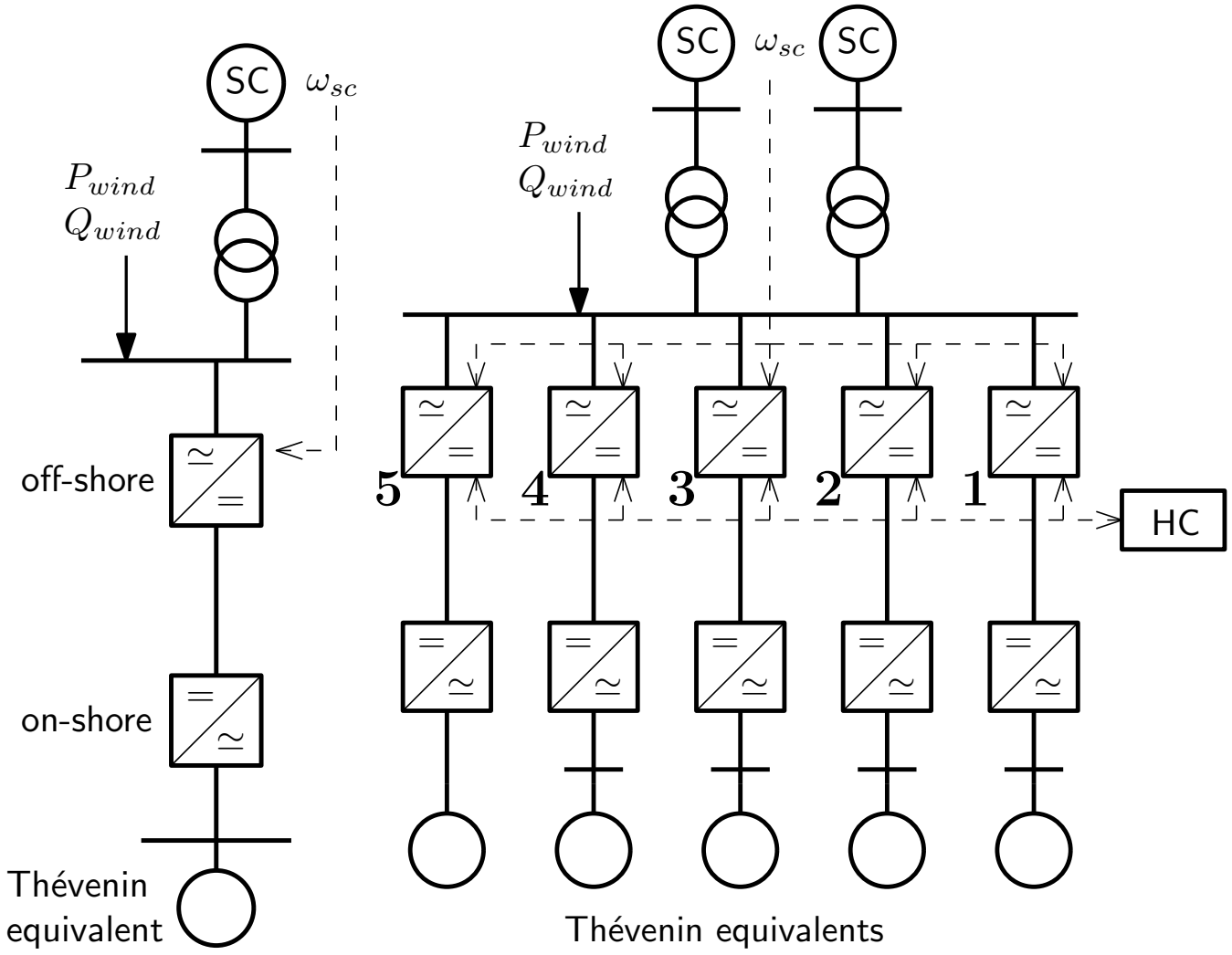

(a) one link system

(b) five link system

Figure 2.13: Modelling of the system studied on Ramses

2.5 Onshore network

For this project, the onshore network is represented by a Thevenin equivalent. So it is simply represented by a generator that provided or absorb what is necessary with an important nominal power.

2.6 Complete system

Now, the complete systems studied in the following are described. There is two different systems represented in Figure 2.13a and 2.13b.

The first system exploited in this project is composed of a single DC line in order to model the connection of the offshore island to the onshore network. The second system aims at representing a more realistic situation. To do so,

5 DC lines have been implemented and 2 Synchronous Condenser are used. The five links represent the connections to different countries/network. A second SC is also necessary in case of fault or maintenance in one of the two SC.

There are different aspects in the first simplified system warranting the necessity to investigate it instead of studying the more realistic model directly. The first advantage is the possibility to deny the Hub Coordinator and focus on other components of the system. The other main advantage is the complementary information provided by the linear and nonlinear study. One has no idea of what should be the value of K_{ip}, K_{pp}, K_{ω}, K_{iq}, K_{pq} and K_{hc}. Thanks to a linear study, an overview of the acceptable range of values for each gain can be assessed. Due to the complexity of a five link system, a linear study is not adapted. Therefore, the one link system is exploited to make the primary work thanks to a linear analysis and then Ramses is used to give more accuracy to the design.So, first a linear analysis is computed for the one link system. This one is completed by a nonlinear study of the one link system and finally, the design found is tested on the five link system. Finally, different events and disturbance are tested on the final five link design.

To give some consistency to the one link system, the single VSC of the first system is adapted to "look like" five VSCs. This means that the nominal power in the VSC in the first system is five times bigger than the nominal power of a single VSC in the second system. Moreover, the nominal power of the SC is adapted. In the five link system, the nominal power for both SC is equal to 250 MVA with a H equal to 2. In the first system, H is still the same but the nominal power of the single VSC is equal to 500 MVA.

Chapter 3

Dynamic analysis of one link system

This chapter is dedicated to the investigation of the stability of a single DC link system with linear and nonlinear tools. The linear study is made thanks to poles analysis and the nonlinear one thanks to Ramses. The first part of this chapter focuses on the linear model and the adaptation of the modelling to a small-signal analysis. Afterwards, a comparison between the linear and the nonlinear model is drawn. The final aim of this study is to design the gains required to allow an efficient control of the system by providing a range of acceptable values for these gains. Two cases are considered: with and without the additional intervention of the Hub Coordinator. The design of the reactive power control is also subjected to a linear and nonlinear analysis but not simultaneously with the active power control design. This choice, as well as the initial denial of the HC, is motivated by a segmentation technique and a progressive inclusion of components allowing an easier design of the gains. All the gains described in the previous chapter are given in Table 3.1 with which part of this chapter analysed them.The final Table 3.4 summarise the steps followed to design the parameters necessary to control efficiently the VSCs.

3.1 Linear study

The model analysed in this linear study is represented in Figure 3.1. Several hypotheses have been set in order to simplify the system:

- Only one HVDC link is modelled.
- For the purpose of the linearisation, one considers the classical model for the Synchronous Condenser. Therefore, it is represented by a voltage source in series with a reactance, connected to the transformer.
- V_{dc} is presumed to be constant. Indeed, it is assumed that the onshore VSC is fast enough to maintain the voltage constant. Consequently, the onshore VSC and the onshore Thevenin are not included in this analysis.
- The purpose here is to investigate small disturbances stability. Any threshold or limitation that could appear in the system and constraint the values due to disturbance is not taken into account in the equations.

The linear analysis is divided in several parts. First, the basics tools necessary to understand the results are presented such as the set of equations or the constraints on the behaviour of the system. Secondly, the linear analysis of the active power without the Hub Coordinator is performed. The HC is added to the study and a complete analysis of combined effect of K_ω and K_{hc} is undertaken. Finally, the reactive power control is studied to give a first approximation of K_{iq} and K_{pq}.

Gain	Function	Discussion
K_i	Integral gain of both current control loops	Fixed in the basic tools section of the linear study
K_p	Proportional gain of both current control loops	Fixed in the basic tools section of the linear study
$K_{i\omega}$	Integral gain of the PLL	Fixed in the basic tools section of the linear study
$K_{p\omega}$	Proportional gain of the PLL	Fixed in the basic tools section of the linear study
K_{ip}	Integral gain of active power control loop	Discussed mainly in the linear study and fixed at the beginning of the nonlinear part
K_{pp}	Proportional gain of active power control loop	Discussed mainly in the linear study and fixed at the beginning of the nonlinear part
K_{iq}	Integral gain of the reactive power control loop	Discussed in the linear study and fixed at the beginning of the nonlinear study
K_{pq}	Proportional gain of the reactive power control loop	Discussed in the linear study as well as in the nonlinear study
K_ω	Gain that link the rotor speed variation to the active power control	Discussed in the linear study as well as the nonlinear study
K_{hc}	Integral gain used by the Hub Coordinator	Discussed in the linear study as well as the nonlinear study

Table 3.1: Summary of function and study of each gain used in all control loops

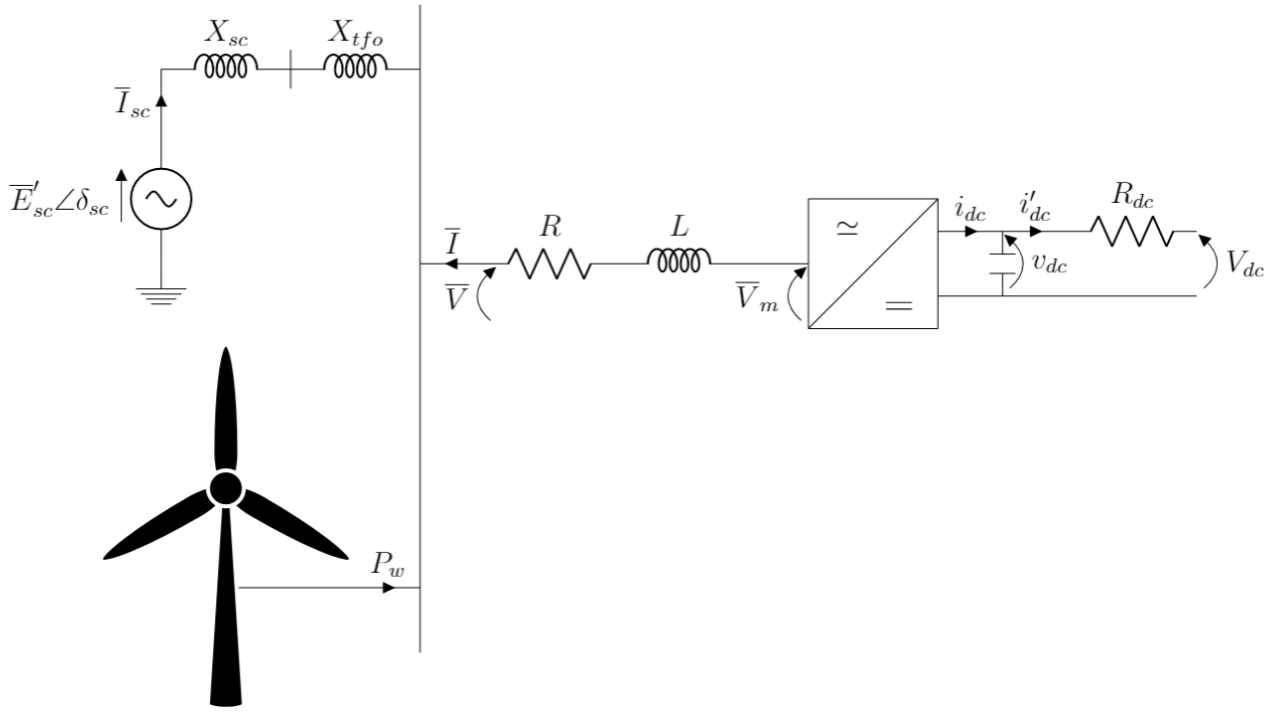

Figure 3.1: Representation of the system used to study the linear behaviour

3.1.1 Basic tools for the linear analysis

This introductory subsection aims at providing tools required for the linear analysis before presenting the results. Therefore, the set of equations exploited is first presented. Then, the general linear representation of the equations is introduced and the concept of the operating point is explained. The values of some gains and parameters are provided and finally, the dynamic constraints applied on the analysis of the system are described.

• Set of equations

Thanks to the hereabove presented hypotheses, the equations based on the model introduced in the previous chapter can be established. This set of equations is the one exploited in the linear study.

Reference frame conversion

These equations originate from the reference frames (Figure 2.2) and allow to express a state from the (x, y) frame to the (d, q) frame:

$$v_d = v_x \cos\theta + v_y \sin\theta \tag{3.1}$$

$$v_q = v_y \cos\theta - v_x \sin\theta \tag{3.2}$$

$$i_d = i_x \cos\theta + i_y \sin\theta \tag{3.3}$$

$$i_q = i_y \cos\theta - i_x \sin\theta \tag{3.4}$$

Phase Locked Loop

Based on Figure 2.5, the equations that express the dynamics of the PLL can be derived such that:

$$\frac{d\theta}{dt} = \omega_{pll}\,\omega_N - \omega_N \tag{3.5}$$

$$\omega_{pll} = K_{pw}\,v_q + M_{pll} \tag{3.6}$$

$$\frac{dM_{pll}}{dt} = K_{iw}\,v_q\,\omega_N \tag{3.7}$$

Phase reactor

The equations of the phase reactor dynamics are computed in Appendix B.1 and are represented in Figure 2.4:

$$\frac{di_d}{dt} = \frac{\omega_N}{L}(-R\,i_d + v_{md} - v_d + \omega_{pll}^{pu}\,L\,i_q) \tag{3.8}$$

$$\frac{di_q}{dt} = \frac{\omega_N}{L}(-R\,i_q + v_{mq} - v_q - \omega_{pll}^{pu}\,L\,i_d) \tag{3.9}$$

The active and reactive power in the phase reactor are expressed by:

$$P_i = v_d\,i_d + v_q\,i_q \tag{3.10}$$

$$Q_i = v_q\,i_d - v_d\,i_q \tag{3.11}$$

Current controllers

The equations of the dynamics of the current controllers are based on Figure 2.6:

$$v_{md} = v_d - \omega_{pll}\,L\,i_q + K_p(i_d^{ref} - i_d) + M_d \tag{3.12}$$

$$\frac{dM_d}{dt} = K_i\,(i_d^{ref} - i_d) \tag{3.13}$$

$$v_{mq} = v_q + \omega_{pll}\,L\,i_d + K_p(i_q^{ref} - i_q) + M_q \tag{3.14}$$

$$\frac{dM_q}{dt} = K_i\,(i_q^{ref} - i_q) \tag{3.15}$$

Active power control

From Figure 2.7, one can establish the equations that give the dynamics of the power control. In order to avoid any confusion between $K_{i\omega}$ and $K_{\omega i}$, in the following, due to the single link hypothesis, $K_{\omega i}$ is replaced by K_ω:

$$i_d^{ref} = K_{pp}\,(P_i^o + P^{hc} - P_i + K_\omega\,(1 - \omega_{sc})) + M_p \tag{3.16}$$

$$\frac{dM_p}{dt} = K_{ip}\,(P_i^o + P^{hc} - P_i + K_\omega\,(1 - \omega_{sc})) \tag{3.17}$$

Indeed, due to the first hypothesis, $\mu_i = 1$. Consequently, $P_i^{hc} = P_{tot}^{hc}$ and is shortened as P^{hc} in the equations.

Hub Coordinator

The analysis is conducted in continuous time. Consequently, the equations used for the Hub Coordinator are the ones in case of continuous time control:

$$\frac{dP^{hc}}{dt} = K_{hc}\,(1 - \omega_{sc}) \tag{3.18}$$

In case of no Hub Coordinator, the gain K_{hc} is equal to zero. In this case, the second equation of the active power dynamics becomes:

$$\frac{dM_p}{dt} = K_{ip}\,(P_i^o - P_i + K_\omega\,(1 - \omega_{sc}))$$

And, in steady state, the derivative is null, which means:

$$P_i^o - P_i + K_\omega\,(1 - \omega_{sc}) = 0$$

Due to the initialisation of P_i^o, if P_i does not change, the rotor speed remains the same. However, if the active power changes, due to extra wind for example, the rotor speed changes as well and stabilise around a new value. The term $K_\omega\ (1 - \omega_{sc})$ has to be equal to this change. Therefore, bigger the gain K_ω, smaller the change of the rotor speed. An analogy with the primary and secondary reserve for the frequency control in a power network can be established. The SC and the gain K_ω act as the primary reserve to buffer the frequency changes. The Hub Coordinator acts as the secondary reserve to restore the primary reserve and to bring the states at their nominal value in prevention to face another event. However, in this particular case, one wants a faster secondary control. Thus the gain K_{hc} is designed to help the Synchronous Condenser faster than the secondary reserve in a conventional AC network.

Reactive power control

The two equations that give the dynamics of the reactive power control are computed based on Figure 2.10:

$$i_q^{ref} = K_{pq}\ (Q_i - Q_i^{set}) + M_{qc} \qquad (3.19) \qquad \frac{dM_{qc}}{dt} = K_{iq}\ (Q_i - Q_i^{set}) \qquad (3.20)$$

DC link

Based on Figure 2.11, three equations that govern the dynamics of the DC link can be established. First, the variation of the voltage v_{dc} can be expressed as a function of the current that flows through the capacitor:

$$\frac{dv_{dc}}{dt} = \frac{i_{dc} - i'_{dc}}{2H_{dc}} \qquad (3.21)$$

Thanks to the power balance on the VSC, it is also possible to link the DC part to the AC part through:

$$v_{dc}\ i_{dc}\ P_d + (i_d v_{md} + i_q v_{mq})\ S_n = 0 \qquad (3.22)$$

Where P_d and S_n represent respectively the nominal active power of the DC part and the nominal complex power of the AC part of the VSC. And finally, the second Kirchhoff law applied on the link gives, according to Figure 3.1:

$$v_{dc} = V_{dc} + i'_{dc}\ R_{dc} \qquad (3.23)$$

Synchronous Condenser

The Synchronous Condenser is assumed to be represented by the classical model. That explains why there is no internal resistance. Therefore, it is represented by a voltage source $\overline{E}'_{sc}$ and a reactance X_{sc}. The second reactance X_{tfo} represents the reactance of the transformer between the Synchronous Condenser and the general bus. In the following equations, X_e corresponds to the sum of X_{sc} and X_{tfo}.

Due to the internal controller in the Synchronous Condenser, the voltage $\overline{E}'_{sc}$ is assumed to be constant. This makes feasible to easily define v_{xsc} and v_{ysc}:

$$v_{xsc} = E'_{sc} \cos\delta_{sc} \qquad (3.24) \qquad v_{ysc} = E'_{sc} \sin\delta_{sc} \qquad (3.25)$$

It is also possible to express the active and the reactive power of the Synchronous Condenser thanks to the current $\overline{I}_{sc}$:

$$P_{sc} = v_{xsc}\ i_{xsc} + v_{ysc}\ i_{ysc} \qquad (3.26) \qquad Q_{sc} = v_{ysc}\ i_{xsc} - v_{xsc}\ i_{ysc} \qquad (3.27)$$

Due to the hypothesis of no internal resistance, the active power can be directly linked to the rotor speed:

$$\frac{d\omega_{sc}}{dt} = \frac{-P_{sc}}{2H} \tag{3.28}$$

And finally the variation of the angle δ_{sc} is linked to the rotor speed by:

$$\frac{1}{\omega_N}\frac{d\delta_{sc}}{dt} = \omega_{sc} - 1 \tag{3.29}$$

Kirchhoff law and power balance

The law of Kirchhoff may be applied between the general bus and the Synchronous Condenser. After segmenting equations for each axis x and y, one can write:

$$v_{xsc} = v_x - X_e\, i_{ysc} \tag{3.30}$$

$$v_{ysc} = v_y + X_e\, i_{xsc} \tag{3.31}$$

Finally, the active and the reactive power balance at the general bus provide two additional equations:

$$P_i + P_{sc} + P_w = 0 \tag{3.32}$$

$$Q_i + Q_{sc} + Q_w = 0 \tag{3.33}$$

• General representation

The complete set of equations can be represented in the following general form:

$$\begin{cases} \dot{\mathbf{x}} = \mathbf{f}(\mathbf{x}, \mathbf{y}, \mathbf{p}) \\ 0 = \mathbf{g}(\mathbf{x}, \mathbf{y}, \mathbf{p}) \end{cases}$$

The function **f** refers to the set of differential equations provided in equations 3.5, 3.7, 3.8, 3.9, 3.13, 3.15, 3.17, 3.18, 3.20, 3.21, 3.28 and 3.29. Second function **g** is composed of the remaining 21 algebraic equations from equation 3.1 to equation 3.33. That being said, one can deduce expressions of **x**, **y** and **p**:

- **p** = [R, L, $K_{p\omega}$, $K_{i\omega}$, H_{dc}, R_{dc}, P_d, S_B, H, P_w, X_e, K_{pp}, K_{ip}, ω_N, K_{pq}, K_{iq}, K_i, K_p, K_ω, Q_i^{set}, V_{dc}, K_{hc}]
- **x** = [θ, M_{pll}, i_d, i_q, M_d, M_q, M_p, M_{qc}, v_{dc}, δ_{sc}, ω_{sc}, P^{hc}]
- **y** = [v_d, v_q, v_x, v_y, i_x, i_y, P_i, Q_i, ω_{pll}, v_{md}, v_{mq}, i_d^{ref}, i_q^{ref}, i_{dc}, i'_{dc}, v_{xsc}, v_{ysc}, P_{sc}, i_{ysc}, i_{xsc},P_{sc}]

Where **p** is the set of parameters considered as constant in the equations. By combining **x** and **y**, there is a total of 33 unknowns for 33 equations (equation 3.1 to 3.33). Linearisation of this set of equation as described in the Appendix C.1 and exploitation of the Jacobian allow to investigate the poles of the whole system. As it is described in the following paragraph, the 12 differential equation lead to 12 poles which can be exploited to fit constraints on the system.

• Operating point

Equations being linearised, the definition of an operating point is required if one desires to study the small disturbance stability. To be able to do so, initial values of all the states of the system should be assessed. Several states can be fixed thanks to steady-state values:

$$\begin{cases} V_{sc} = 1 \text{ p.u.} \\ \delta_{sc}^{o} = 0 \text{ rad} \\ V_{dc} = 1 \text{ p.u.} \\ P_w = 25 \text{ p.u.} \\ Q_w = 2.5 \text{ p.u.} \\ P_{sc}^{o} = 0 \text{ p.u.} \\ Q_{sc}^{o} = 0.25 \text{ p.u.} \end{cases}$$

The operating point is fulfilled based on the previously established equations ruling the system. The complete set of initial states is provided in Appendix C.2. Notice that initial P_w is considered at the half of the nominal active power of the DC line. This value is a bit arbitrary but allows to simulate a large deviation in the wind power production without overloading the cables. Moreover, the value chosen for δ_{sc}^{o} permits to consider the Synchronous Condenser as the slack bus of the system.

• Gains and parameters

Before studying the stability of the system, some of the parameters have to be determined. The value of R, L, H, H_{dc}, P_d, S_B, R_{dc} and X_e are given in Table 3.2. The specific values chosen for those parameters are explained in Appendix D.

R	0.01 p.u.	L	0.2 p.u.	H	2 p.u.	H_{dc}	0.0102 p.u.	R_{dc}	0.094 p.u.
P_d	5000 MW	S_B	100 MVA	S_n	5500 MVA	ω_N	100 rad/s	X_e	0.09 p.u.

Table 3.2: Value of some parameters required for the small disturbance stability analysis

To avoid having to deal with an excessive number of degrees of freedom, some values of the gains have to be fixed before studying the poles. Therefore, four gains are set in the following paragraphs: K_i and K_p, as well as $K_{p\omega}$ and $K_{i\omega}$. Their values are determined thanks to the desired dynamics constraints for the two corresponding control loops.

K_i and K_p

The method followed to compute the value of K_i and K_p is provided in Appendix B.2. Because the current control relates to the inner loop of the control, it has to be faster than the power control one. By considering a settling time

of 0.01 s, one gets rid of the risk to have interference between inner and outer control loops. Indeed, to have an interference, the settling time of the outer loop should be smaller than 0.1 s ([28]). As it is explained later thanks to the nonlinear study, this is much faster than the expected behaviour of the system. A damping ratio of 0.7 and a tolerance of 5% are chosen [12]. This gives the following values for the gains of the current control:

$$\begin{cases} K_p = 0.0371 \text{ p.u.} \\ K_i = 10.6 \text{s}^{-1} \end{cases}$$

Notice that the units of the integral gain are s^{-1} in order to match with the units of the differential equations.

$K_{p\omega}$ and $K_{i\omega}$

To determine the values of $K_{p\omega}$ and $K_{i\omega}$, another method entirely based on the time response is used. Based on the latter, both gains can be computed with the following equations [26]:

$$\begin{cases} K_{p\omega} = \dfrac{10}{t_\omega \, \omega_N} \\ K_{i\omega} = \dfrac{25}{t_\omega^2 \, \omega_N} \end{cases}$$

Where t_ω corresponds to the time response of the PLL. For now, a value of 0.05 s is considered according to Papangelis & al (2018) [29]. Finally, the following gains are set: $K_{p\omega} = 0.6366$ p.u. and $K_{i\omega} = 31.83 \text{ s}^{-1}$.

• Dynamic constraints

The last step before designing the gains is the introduction of the constraints. First, from the linearisation and the Jacobian, the state matrix A can be computed. This one is constructed from the following general representation of a MIMO system [28]:

$$\begin{cases} \dot{x} = Ax + Bu \\ y = Cx + Du \end{cases} \tag{3.34}$$

The poles of the system can be deduced from the state matrix. Then, dynamic constraints are checked on these poles. Except for the fact that poles should have a negative real part for the system to be stable, the first specific constraint is linked to the response time of the system. As this one is limited by the slowest part, only the pole linked to the slowest behaviour is considered for this analysis. This corresponds to the pole with the smallest real part in absolute value (meaning the closest to the imaginary axis). Indeed, the response time τ of the system is given by:

$$\tau = \frac{-1}{\text{Re}(\lambda_i)} \tag{3.35}$$

Where λ_i represents the "slowest" pole of the system. The aim of the first constraint is to allow the system to reach the 5% band after a specific (parametrised) settling time that should be as small as possible. As this band is reached after

three times the response time, the settling time itself should be kept as three times the response time. This relation is therefore constraining the pole. For example, to begin with, a value of 20 s is considered, which means 6.67 s of response time. Consequently, the corresponding real part of the analysed pole is constrained to be smaller or equal to -0.15:

$$\mathrm{Re}(\lambda_i) \leq \frac{-1}{6.67} = -0.15 \tag{3.36}$$

The second constraint is related to the damping ratios of the system. Indeed, in order to avoid excessive oscillations and overshoot in the event of a disturbance or directive change, the minimum damping ratio should be as high as possible. This criterion is constraining the system because each damping ratio is associated with a pole through its imaginary and real parts:

$$\zeta_i = \frac{-\mathrm{Re}(\lambda_i)}{\sqrt{\mathrm{Re}(\lambda_i)^2 + \mathrm{Im}(\lambda_i)^2}} \tag{3.37}$$

Therefore, imposing a threshold on the smallest damping ratio is constraining the pole as well. To begin with, a first value of 0.7, as for the current control, is chosen.

The settling time and the minimum value for the damping ratio are two parameters that have to be adjusted and optimised in this chapter.

3.1.2 Active power control design without Hub Coordinator

Now that the basics of the analysis have been introduced, the stability of the system to small disturbances can be studied. The purpose here is to design the values for K_{ip}, K_{pp} and K_{ω}. Notice that K_{hc} is initialised to zero in order to simulate the absence of the Hub Coordinator. Moreover, to avoid dealing with a lot of degrees of freedom simultaneously and to segment the analysis, K_{iq} and K_{pq} are arbitrarily fixed to 100 s^{-1} and 100, respectively. Their values are adjusted later. This allows to focus on K_{ip}, K_{pp} and K_{ω} as a first step.

To analyse the effect of each gain on the behaviour of the system, a triple loop is computed in which each gain is varied between 0 and 100. The expected values of the gains are a priori unknown which is why the covered panel is so large. For each threesome of values for the gains, the poles are deduced. Then, both criteria described hereabove are checked: that is, the smallest damping ratio bigger than 0.7 and the smallest absolute real part bigger than 0.15 (the real part has still to have negative to ensure stability). To do so, the damping ratio of each pole is analysed and the smallest one is recorded into a 3D matrix. The same thing is done for the real part of each pole. Figures 3.2a to 3.2d represent the combination of those two matrices. Indeed, K_{pp} evolves along the x-axis, K_{ip} along the y-axis and each figure corresponds to a different K_{ω}. Finally, the green dots correspond to the set of gains that satisfied both criterion. Consequently, red dots mean one of the criterion is not satisfied for the corresponding threesomes.

Several remarks can be deduced from these graphs. First, one can notice that the intervals of values that satisfies both criteria are large. This proves that the system is strongly stable especially considering the rather strict constraints applied to find the green dots. The minimal required value for K_{pp} is easily identifiable. It is also shown that small

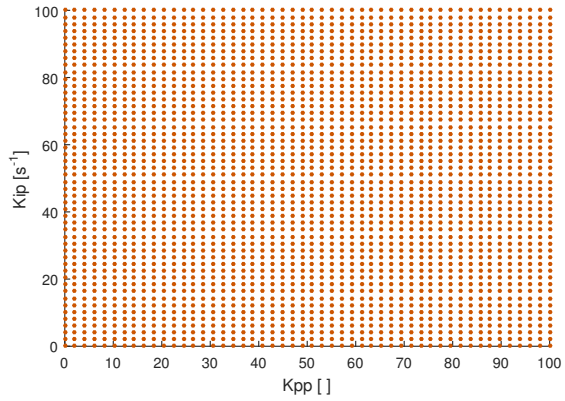

(a) $K_\omega = 0.01$

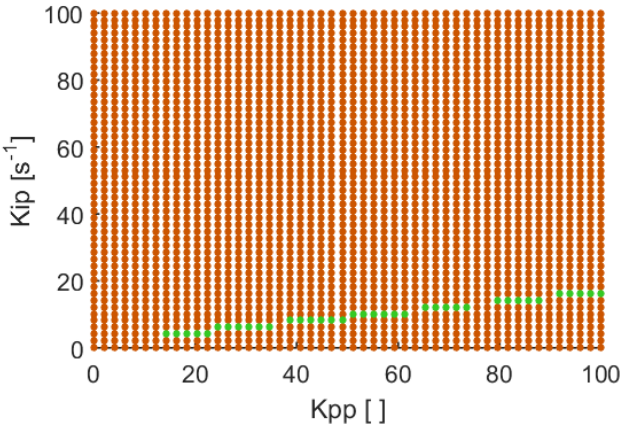

(b) $K_\omega = 0.05$

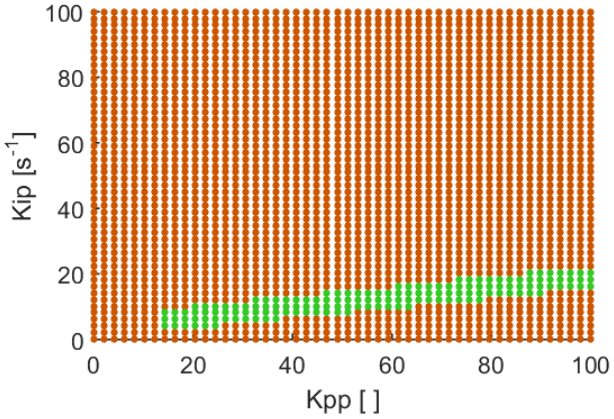

(c) $K_\omega = 0.1$

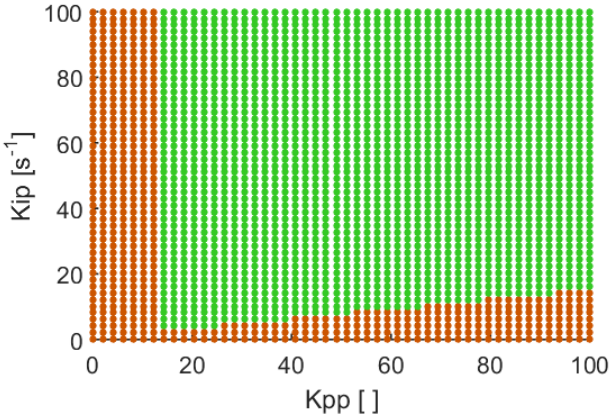

(d) $K_\omega = 0.2$

Figure 3.2: Variation of acceptable threesome for variyng K_{ip}, K_{pp} and K_ω

values of K_ω are sufficient to generate a considerable amount of accepted threesomes. To have a better visibility of the evolution of green dots with K_ω, Figures E.1 to E.4 in Appendix E show additional graphs for increased values of K_ω. On those graphs, it can also be observed that high K_ω may lead to combinations of K_{ip} and K_{pp} that are not acceptable anymore. This is explained in the analysis of the following three paragraphs, showing the effect of one single gain on the poles location. Indeed, each couple of Figure 3.3a to 3.5b illustrates the poles location for a single varying gain. Figures on the left represent the global overview of the poles and the right ones illustrate the pole location in the vicinity of the imaginary axis. The bigger the gain, the lighter the dot. The red dashed lines represent the limit imposed by the desired damping ratio on the system. The orange dashed vertical line represent the threshold on the real part of each pole. Therefore, only the dots on the left part of this line, and within the cone described by the red dashed lines are acceptable. The value of the gains that do not vary are respectively (and based on an acceptable threesome) fixed to $K_{pp} = 40$, $K_{ip} = 20$ and $K_\omega = 10$.

- **K_ω effect**

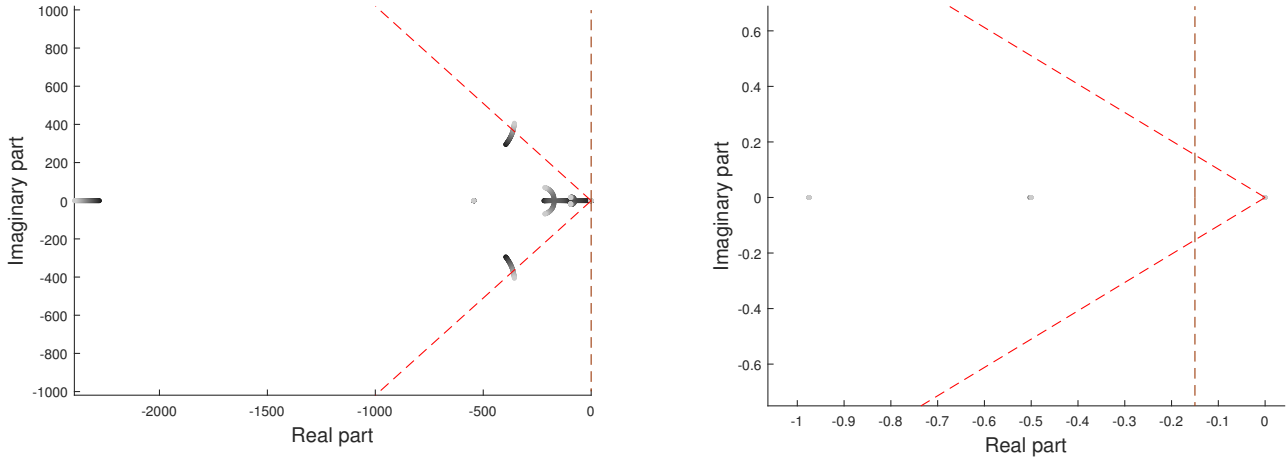

(a) Global view **(b)** Zoom in the vicinity of the imaginary axis

Figure 3.3: Effect of K_ω on poles location

From Figure 3.3, it can be noticed that the main effect of K_ω, near the damping ratio limits, is to increase the absolute value of the imaginary parts of the poles while decreasing the absolute value of the real parts. Consequently, this shows that increasing K_ω decreases the damping ratio until the limit is crossed. This explains why, in Figure E.1 to E.4, the domain of acceptable values decreases when K_ω that increases.

- **K_{ip} effect**

As shown in Figure 3.4a and Figure 3.4b, the effect of K_{ip} is not very significant. In the vicinity of the imaginary axis, it mainly allows to move slightly the pole towards the vertical limit and cross it above a certain value. The effect on the other poles is negligible as seen in the global view.

- **K_{pp} effect**

Finally, the effect of K_{pp} is shown in Figure 3.5. It can be observed that when K_{pp} becomes bigger, the poles outside the damping ratio limits seem to be displaced towards a better damping ratio. However, in the vicinity of the imaginary axis, an increase of K_{pp} reduces the absolute value of the real part of the pole.

In conclusion, one can extract two opposite trends close to each constraint. Near the damping ratio limits, K_w and K_{pp} have opposite effects, whereas near the settling time limit, it is K_{ip} and K_{pp} that have contrary trends. This can help explaining figures of the acceptable threesomes. Indeed, if K_{pp} increases, K_{ip} should also increase to avoid generating a pole on the right side of the limit. It also explains why, for bigger values of K_ω, K_{pp} has to increase to balance the effect of K_ω.

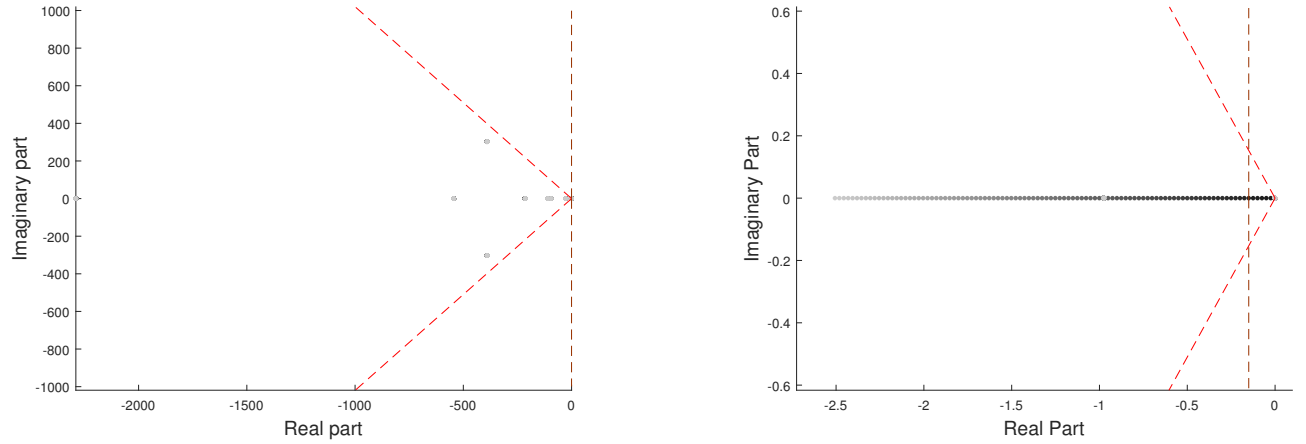

(a) Global view **(b)** Zoom in the vicinity of the imaginary axis

Figure 3.4: Effect of K_{ip} on poles location

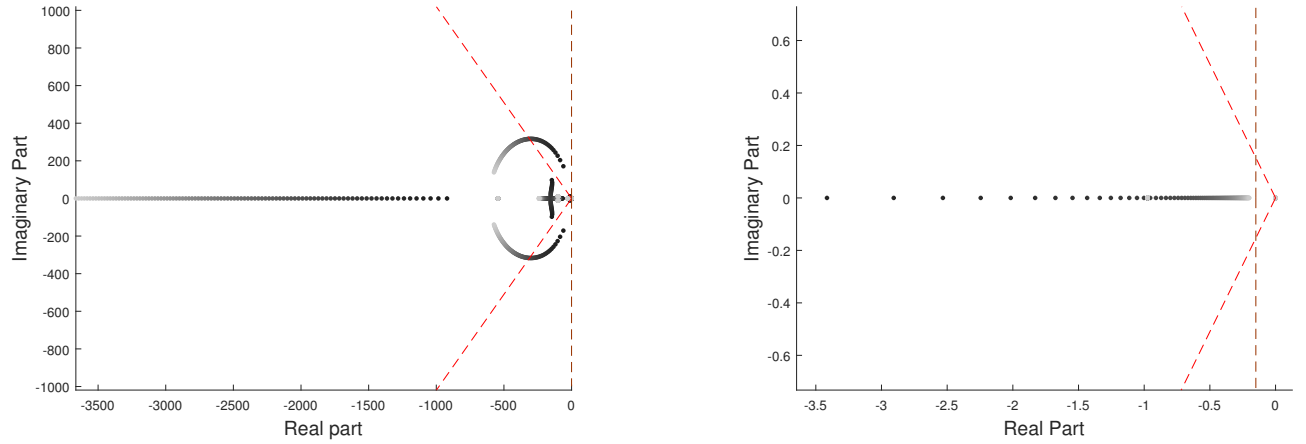

(a) Global view **(b)** Zoom in the vicinity of the imaginary axis

Figure 3.5: Effect of K_{pp} on poles location

- **Final set of values**

Now that the influence of the gains on the poles has been investigated, the final range of values considered as acceptable to control the VSC should be determined. Based on Figure 3.2a to Figure 3.2d, it seems that it requires a minimum amount of K_ω to generate a satisfying amount of acceptable values for K_{ip} and K_{pp}. This value of K_ω is approximately equal to 0.2. To be safe, a value of $K_\omega = 0.5$ is selected. Then, it is straightforward to fix the lower threshold of K_{pp}. This limit is fixed at 20. This allows some freedom on the value of K_ω. It seems also obvious that no upper limit is required for K_{ip}. However, the upper bound for K_{pp} and the lower limit for K_{ip} are more delicate to select. Indeed, as explained before, both gains are linked and have contrary effects. Therefore, the upper limit of K_{pp} depends on the lower limit of K_{ip}. If one wants to have a wide range of value for K_{pp}, the lower limit for K_{ip}

has to increase. Consequently, a trade off is made between both gains. Based on Figure 3.2d, the upper limit for K_{pp} is chosen at 50 and consequently, the lower limit of K_{ip} is fixed at 10.

- **Influence of the constraints**

One may observe that in our study, the final set of gains selected is completely dependent on the limits imposed by the desired behaviour of the system in terms of settling time and damping. Consequently, these dynamic constraints play a crucial role in the computed acceptable range for each gain. This observation being made, it is worthwhile to analyse how restrictive are these constraints on the range of acceptable values.

To do so, the principle is the same as previously: the poles generated by a broad range of threesomes are evaluated and compared to the same conceptual constraints as before, but for other specific values. Previously, a settling time of 20 s had been imposed. Here, a constraint of 7.5 s is evaluated. This means a minimum absolute real part equal to 0.4. Figure 3.6a shows the range of acceptable threesomes for $K_\omega = 10$.

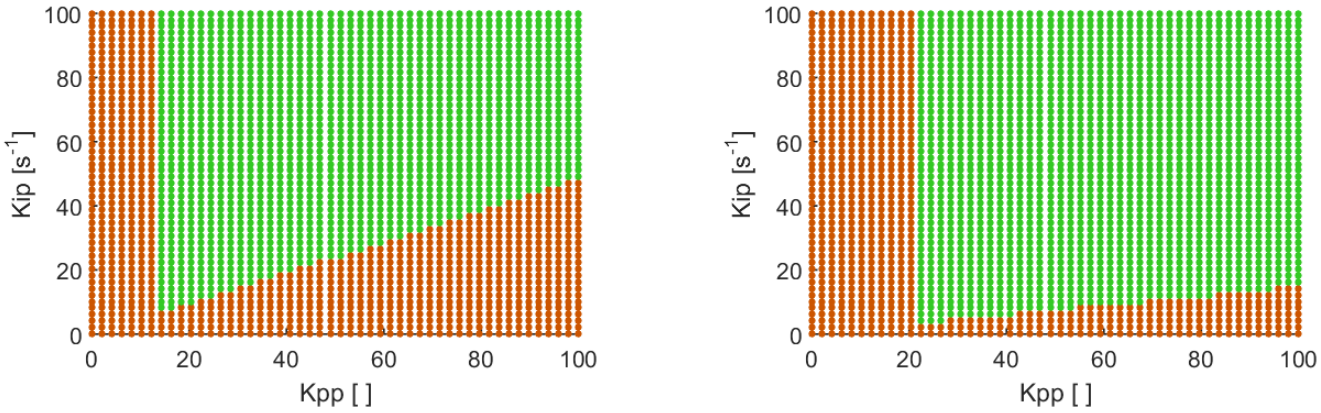

(a) $\zeta(\lambda_i) \geq 0.8$ and $\mathrm{Re}(\lambda_i) \leq -0.15$ **(b)** $\zeta(\lambda_i) \geq 0.7$ and $\mathrm{Re}(\lambda_i) \leq -0.4$

Figure 3.6: Range of acceptable threesomes for $K_\omega = 10$

The second constraint is also modified: the bound on the damping ratio is imposed to be 0.8 instead of 0.7. The settling time is kept equal to 20 s. The results are presented in Figure 3.6b. As for the case of the settling time, the set of acceptable values is slightly impacted (the lower limit of K_{ip} is increased) but it does not change conceptually our conclusions.

It can be concluded that the system seems generally stable. One would probably have to select extremely small values of gains to reach the unstable region. That being said, the acceptable range of value for each gain depends on the imposed desired behaviour of the system. The specific chosen constraints seem to be able to generate satisfying acceptable regions, even though more restrictive limits could have been chosen. However, as new constraints are added in the following, keeping the first general constraints not too restrictive allows to further play more easily with the gains to fit these other constraints.

3.1.3 Active power control design with the Hub Coordinator

The analysis of the active power control without the Hub Coordinator has permitted to enlighten some first behaviours of the system and to define the effect of the constraints on the gains.Moreover, the nonlinear analysis bring to the fore the limited effect of K_{ip} and K_{pp}.For these reasons, as explained in section 3.2.1 and in Table 3.1, K_{ip} and K_{pp} are fixed and considered as constant in the following investigation.

Fixing K_{ip} and K_{pp} allows to restrict our study to the effect of K_ω and K_{hc} on the model. As K_{hc} is not zero anymore, the influence of the Hub Coordinator is included this time. Notice that in this analysis, the range of values considered for K_ω is restricted to [0.3 ; 20] instead of [0.5 ; $+\infty$] that has been set before. Those bounds are justified in the nonlinear study.

The simulations and the constraints are the same as for the previous linear study, except that only two gains are investigated this time. Graph showing acceptable pairs is represented in Figure 3.7a. The number of allowed pairs of gains seems still broad. However, the general trend is that K_ω needs to increase when K_{hc} increases. This means that the HC is not reacting alone whenever the rotor speed changes. If the HC acts quickly to the latter, the power control has to act quickly as well.

Once more, the criteria on the acceptability of the couple of points is modified to visualise the influence of the specific values chosen. Figure 3.7b shows the acceptable pairs for a damping ratio of 0.8 instead of 0.7 and a maximal real value of -0.4, meaning a settling time of 7.5 s. In practise, the constraint on the time response cannot be less restrictive than 20 s: it would not be viable for the system. If the DC link is used by the onshore network to support the frequency variation, the system has to react quickly to provide power to the system. That explains why a smaller settling time is analysed.

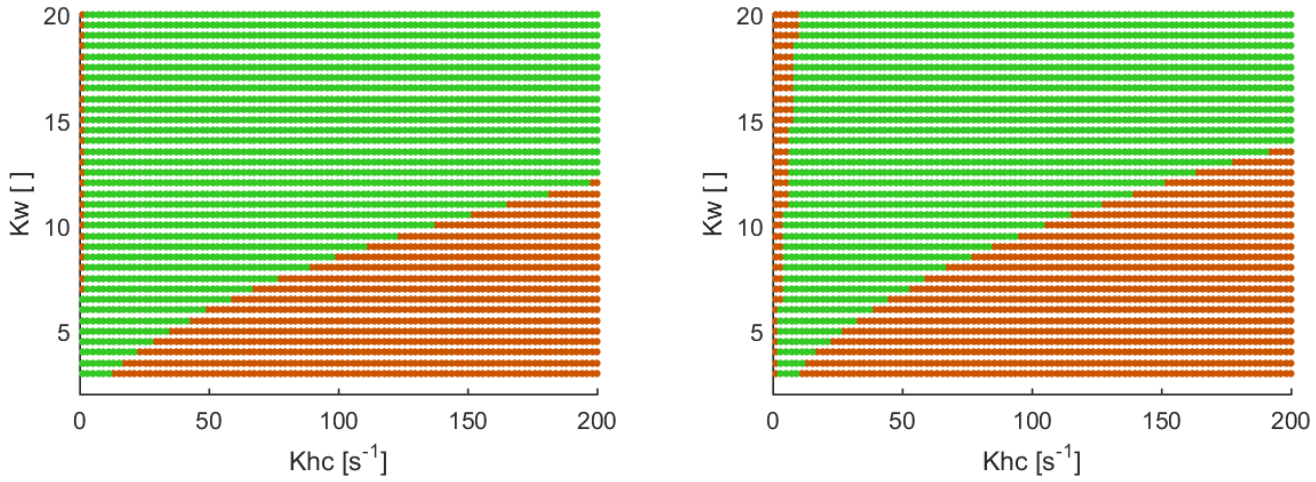

(a) $\zeta(\lambda_i) \geq 0.7$ and $\mathrm{Re}(\lambda_i) \leq -0.15$ **(b)** $\zeta(\lambda_i) \geq 0.8$ and $\mathrm{Re}(\lambda_i) \leq -0.4$

Figure 3.7: Variation of K_ω and K_{hc} for the linear study

It can be observed that the constraints have visible impacts on the acceptable range of gains. However, they still generate a broad range of pairs so the more restrictive set of values could be retained. In conclusion, the designed constraints are viable for the model and generate a satisfying amount of combinations for the gain values.

3.1.4 Reactive power control design

Due to the independent control of the active and reactive power, it is assumed that the design of their associated gains can be made separately. The gains K_{ip} and K_{pp} are fixed to acceptable values thanks to the ranges determined previously and are equal to 20 s^{-1} and 40 respectively. However, to ascertain the independence of the controls, the impact of a change in K_ω and the influence of the Hub Coordinator (through modifications of K_{hc}) are first investigated. Broadly speaking, the principle of analysis regarding the gains is the same as previously, with the same constraints on the poles (settling time of 20 s and damping ratio of 0.7).

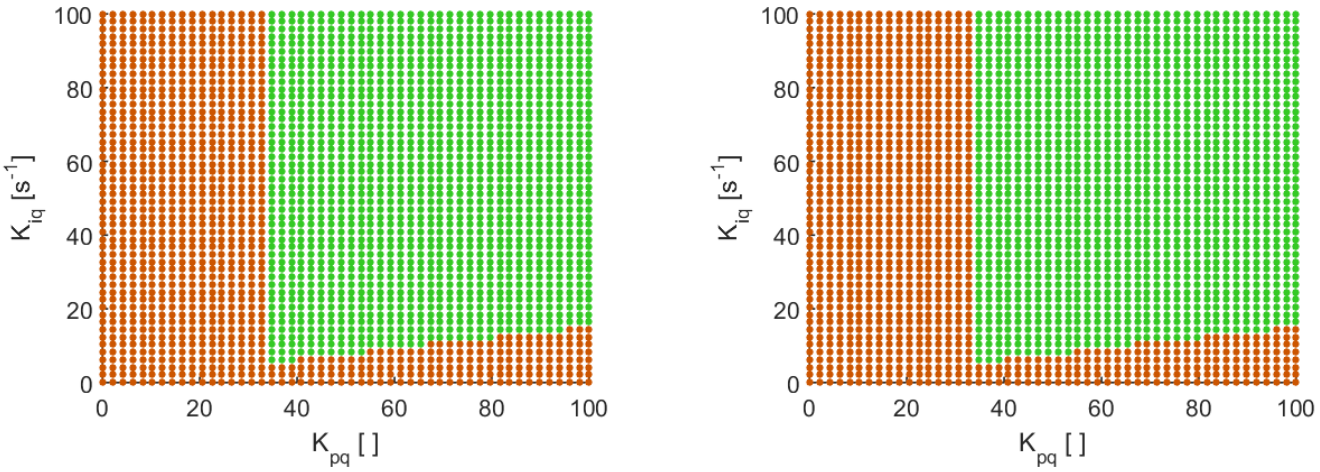

(a) Without HC **(b)** With HC

Figure 3.8: Range of acceptable value for K_{iq} and K_{pq}

Figure 3.8a represents the acceptable pairs of gains without Hub Coordinator ($K_{hc} = 0$), and Figure 3.8b for $K_{hc} = 100$ and $K_\omega = 10$. As expected, changing the gains of the active power control is not affecting the reactive power control due to their independent loops. That being said, the effect of K_{pq} and K_{iq} on the poles seems to be similar to respectively K_{pp} and K_{ip}. This explains the similarity between the graph shapes for the current analysis and the study of K_{pp} and K_{ip}.

Figure 3.9a illustrates the same gains for a constraint on the damping ratio equal to 0.8 and 3.9b is additionally considering a real part smaller than -0.4. The allowed range of pairs becomes really restricted. It seems that big value of both gains are safe (meaning generate allowed pairs), even considering more restrictive constraints. One of the goals of the nonlinear study is to ensure that those high values of the gains do not damage some aspects that have not been covered with linear tools.

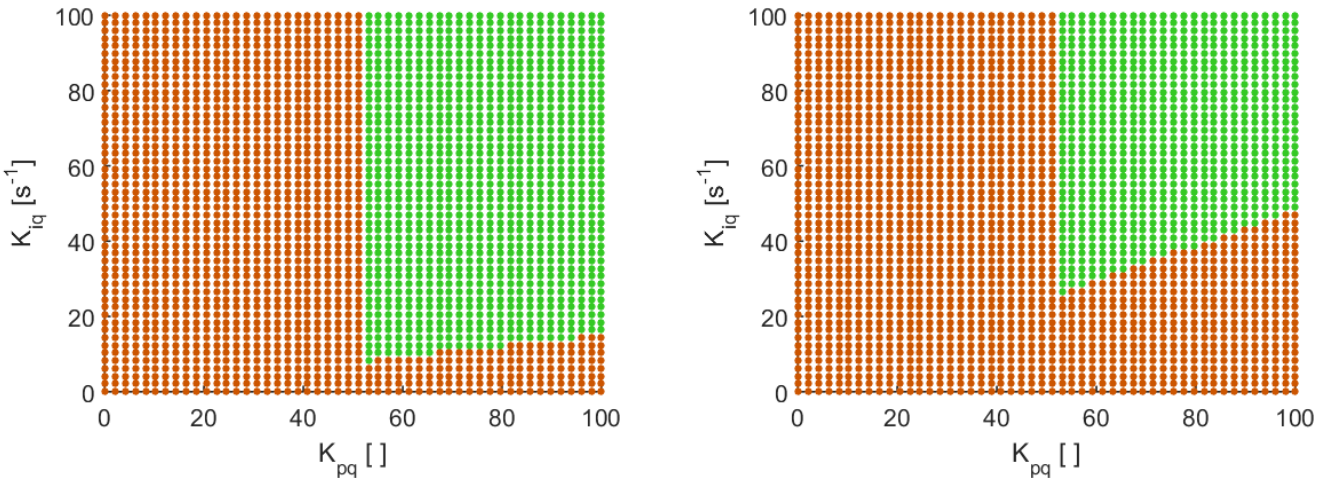

(a) $\zeta(\lambda_i) \geq 0.8$ and $\mathrm{Re}(\lambda_i) \leq -0.15$

(b) $\zeta(\lambda_i) \geq 0.8$ and $\mathrm{Re}(\lambda_i) \leq -0.4$

Figure 3.9: Variations of K_{pq} and K_{iq} with changing constraints

3.2 Nonlinear study

The system exploited with Ramses is conceptually similar to the one studied in the linear analysis. However, the first big change is related to the use of a complete model for the Synchronous Condenser while the linear model used a classical representation of the SC. The other change consists in the incorporation of the onshore VSC and a Thevenin equivalent to represent the onshore network, whereas the linear model was stopped at the constant voltage of the DC line. In order to investigate the impact of a disturbance on the onshore network, this Thevenin equivalent is needed. The complete system is illustrated in Figure 2.13a.

The nonlinear study allows to examine extended aspects of the system in case of disturbance. To bring to light those behaviours, two mains disturbances are simulated. The first one, called D1 in the following, corresponds to a rectangular pulse of 500 MW during 0.2 s. The increase and decrease in wind power production last during 0.05 s. This disturbance is represented in Figure 3.10. The second disturbance, named D2, represents a step of 500 MW, with an increasing time of 0.05 s as well. This disturbance is shown in Figure 3.11.Notice that the value of 500 MW is arbitrarily chosen in order to be able to easily observe the impact of the disturbance without overcoming the potential internal limits in the controllers.

3.2.1 Active power control design without Hub Coordinator

Several specific aspects of the nonlinear model could be used as new constraints to design the gains: the rotor speed deviations, the Hub voltage or the DC voltage, for example. Two aspects have been retained for this analysis: the rotor speed deviation and the onshore active power. In particular, without the help of the Hub Coordinator, the rotor speed deviation during D2 is analysed as well as the onshore active power spike due to D1.

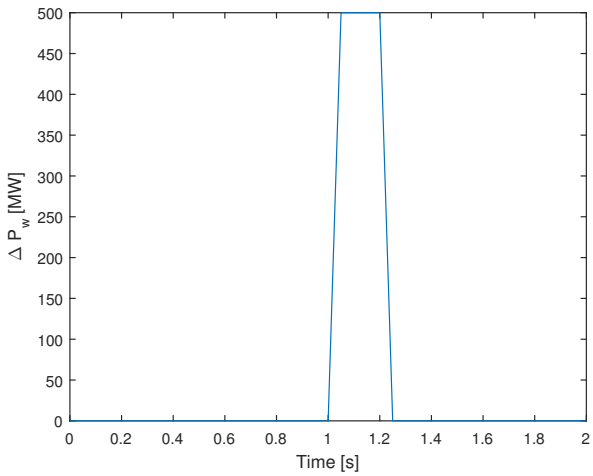

Figure 3.10: Rectangular pulse disturbance D1

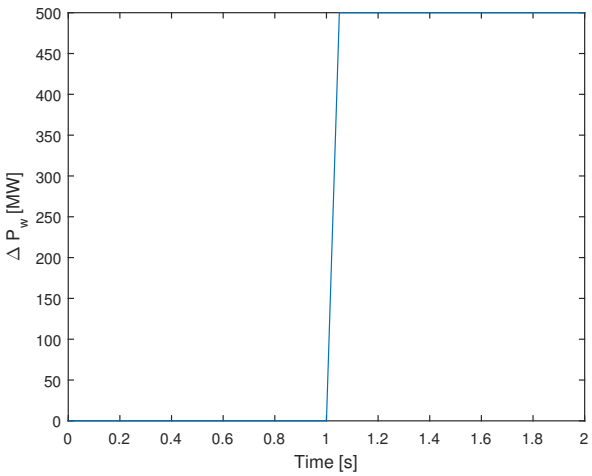

Figure 3.11: Step disturbance D2

Figure 3.12a and 3.12b illustrate the values of the onshore active power spike due to D1. K_{ip} evolves along the x-axis and K_{pp} along the y-axis. Their range of values are fixed based on the linear analysis. Figures differ by the value of K_ω. It seems that the value of the spikes are not highly dependent on K_{ip} and K_{pp}. However, K_ω has a big impact on the values of the spike.

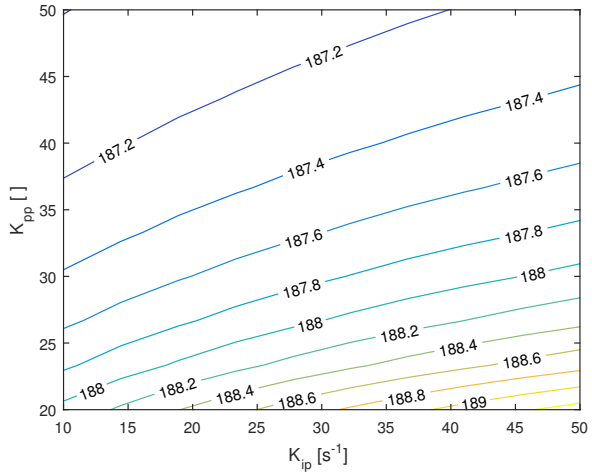

(a) $K_\omega = 1$

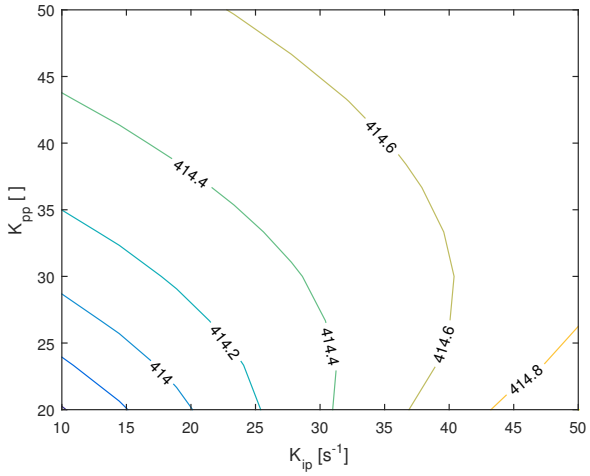

(b) $K_\omega = 5$

Figure 3.12: Variation of onshore active power spike in MW due to D1

Due to the droop characteristic of the active power control (as explained in Hub Coordinator part of the set of equation at the beginning of the chapter), D2 disturbance coerce the rotor speed to stabilise around an updated value. As for D1 disturbance, this value does not depend on K_{ip} and K_{pp} neither. Therefore, for the following, K_{ip} and K_{pp} are arbitrarily fixed to a value within the range studied here: that is, K_{pp} = 40 and K_{ip} = 20. Now that their values are fixed, one can focus on the behaviour of K_ω alone as a first step, and then K_{hc} is included with the HC itself in the next subsection.

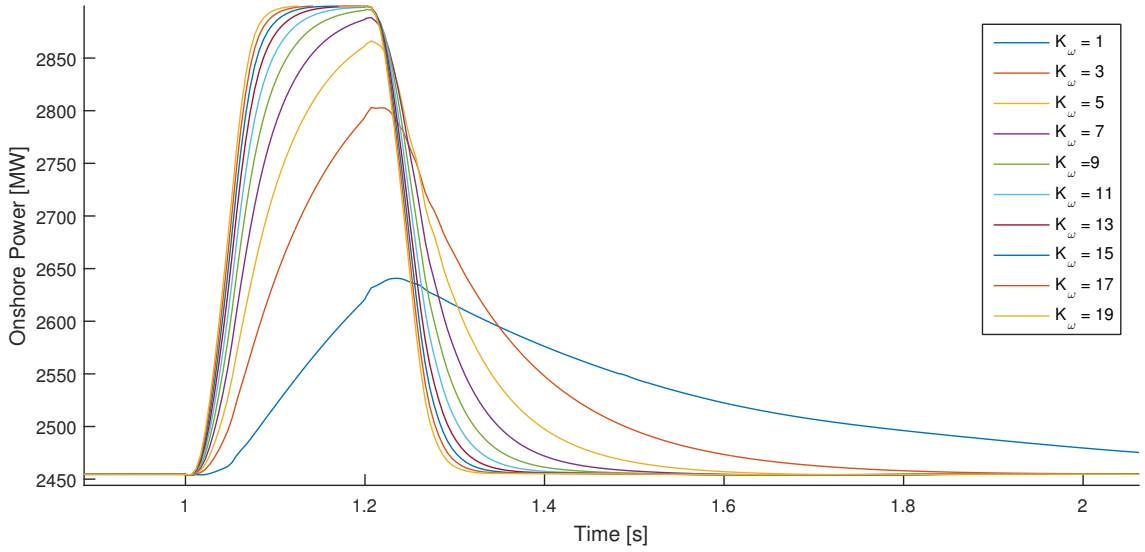

Figure 3.13: Onshore active power evolution due to D1 for different value of K_ω

Figure 3.13 illustrates the spike of the onshore active power with different values of K_ω for disturbance D1. Figure 3.14 represents the rotor speed variations in the event of disturbance D2. These figures provide a more complete and accurate overview of the impact of K_ω in both disturbance situations.

According to the results, increasing K_ω intensifies the onshore spike and decreases the excursion of the rotor speed. When increasing, K_ω enhances the impact of the rotor speed variations on the control. Consequently, the control reacts to any small change and sends the power quickly to the onshore network, and this could disturb it. On the other hand, in the droop characteristic of the active power control, considering a high value of K_ω reduces the rotor speed excursion in steady state.

The steady-state value of the rotor speed deviation, without the HC, represents the maximal excursion of the rotor speed even with the HC. In order to limit the effects of the disturbance on the offshore system, this maximal excursion cannot be too high. Therefore, a minimal value of $K_\omega = 3$ is chosen for the following.

Due to the reactivity of rotor speed changes with high K_ω, the active power received onshore corresponds to the 500 MW minus the losses in the DC line. Therefore, for a value bigger than $K_\omega = 7$, the onshore effect is almost the same. A more complete study with other constraints and the use of the Hub Coordinator is required to determine the best K_ω gain.

3.2.2 Active power control design with Hub Coordinator

The inclusion of the Hub Coordinator in the nonlinear model allows the analysis of K_ω and K_{hc}. This one is based on the optimisation of several characteristics:

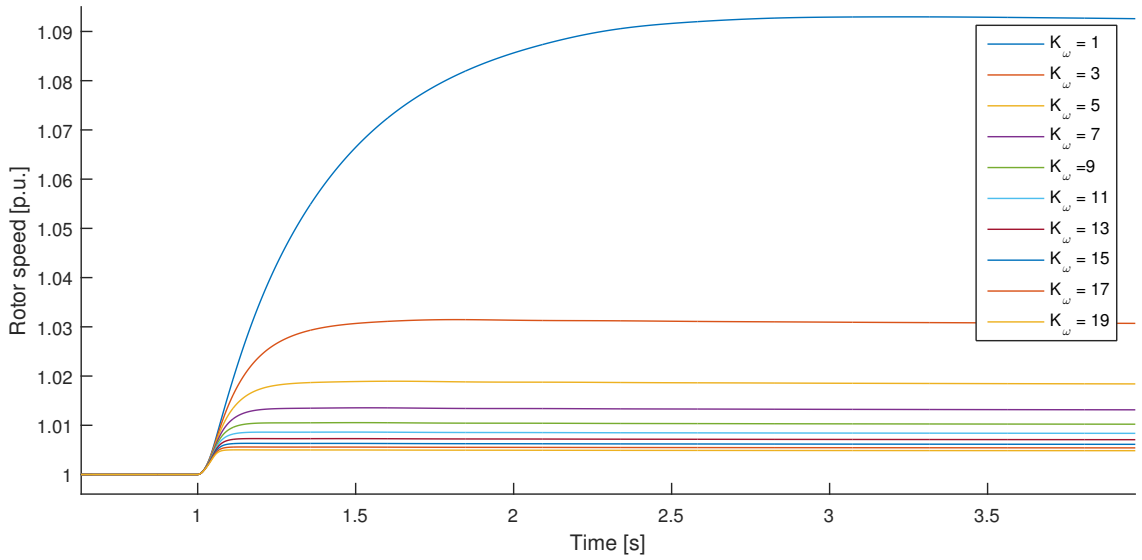

Figure 3.14: Variation of the rotor speed due to D2 for different value of K_ω

- The rotor speed excursion in case of D1 and D2.
- The spike of the onshore active power due to D1 and D2.
- The overshoot of the onshore active power still in case of D2.
- The time required to reach the reference value of ω_{sc} after D2.

The four first criteria bring complementary information to the linear analysis since the power and rotor speed excursion cannot be linked to a poles study. Regarding the last criterion, even though time response has already been investigated in the linear study, it is considered again here in order to potentially refine the ranges of values and compare the outputs of both approaches. No strict value is imposed for all these characteristics. Rather, the purpose is to minimise all of them to ensure the smoothest system in the event of any disturbance or operation change.

Thanks to Ramses, these characteristics are computed for several combinations of K_ω and K_{hc}. The value for each combination are registered in matrices which are represented from Figure 3.15 to Figure 3.18 as a function of K_ω and K_{hc}.

• Rotor speed deviation

As expected, there is still a trade-off between the two gains K_{hc} and K_ω to meet the imposed criteria. Notice that in Figure 3.15, the rotor speed is depicted in p.u. Therefore, a value of 1.025 means that the maximal excursion of the rotor speed for this pair of gains corresponds to 51.25 Hz. In a conventional AC network, such a high value would not be accepted. In this system, this is less problematic even if minimising the rotor speed excursion should be part of the criteria. Indeed, in the event of a bigger increase in the wind power production, the speed variation increases, which could be harmful for some components.

Figures 3.15 suggest that the rotor speed depends essentially on K_ω. However, choosing a bigger value of K_{hc} allows to take a slightly smaller value of K_ω for the same output speed (curves are not perfectly horizontal). Figure 3.15a gives the rotor speed deviation after D1, whereas Figure 3.15b shows the same parameter but after disturbance D2. Even if values are not exactly the same, the general shapes of the graphs are similar.

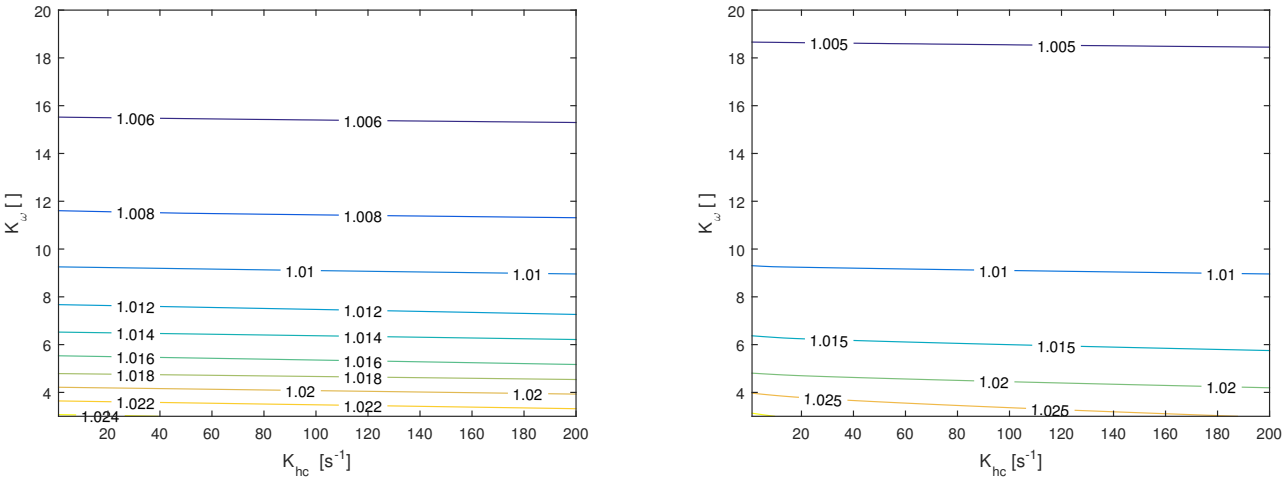

(a) Disturbance D1

(b) Disturbance D2

Figure 3.15: Rotor speed deviation after imposed disturbances

• Spike of the onshore active power

To generate Figure 3.16b, the maximal and the minimal active power in the link have been computed and the difference between both has been divided by the step of 500 MW. For example, an output of 1.02 means that the difference between the maximum and the minimum power equals 510 MW. This measurement is different from the overshoot because of the decreasing power in the event of a disturbance, as illustrated in Figure 3.13. The behaviour related to the relative overshoot and the spike of onshore active power (Figures 3.17 and 3.16b) is the same. In both cases, increasing the value of K_{hc} requires to increase K_ω as well to decrease the overshoot and the spike. Therefore, the best pairs of gains should be a small value of K_{hc} for a high value of K_ω.

Afterwards, Figure 3.16a shows the relative spike of onshore active power due to disturbance D1. As previously, this one is given by the difference between the smaller and the highest power registered in the line divided by the pulse, 500 MW. A value of 0.96 means that the spike of active power equals 480 MW. The spike depends almost only on K_ω. As expected, the behaviour is the contrary of the rotor speed deviation: if K_ω increase, the control is more reactive to ω_{sc} changes. This is logically reducing the rotor speed deviation but increases the spike of onshore power. One can also notice that the effect of increasing K_{hc} is stronger than for the rotor speed deviation. Conceptually, this trend can be explained by the fact that increasing K_{hc} enhances the relative control on the variation of the rotor speed, which allows to reduce the rotor speed variation and increase the spike.

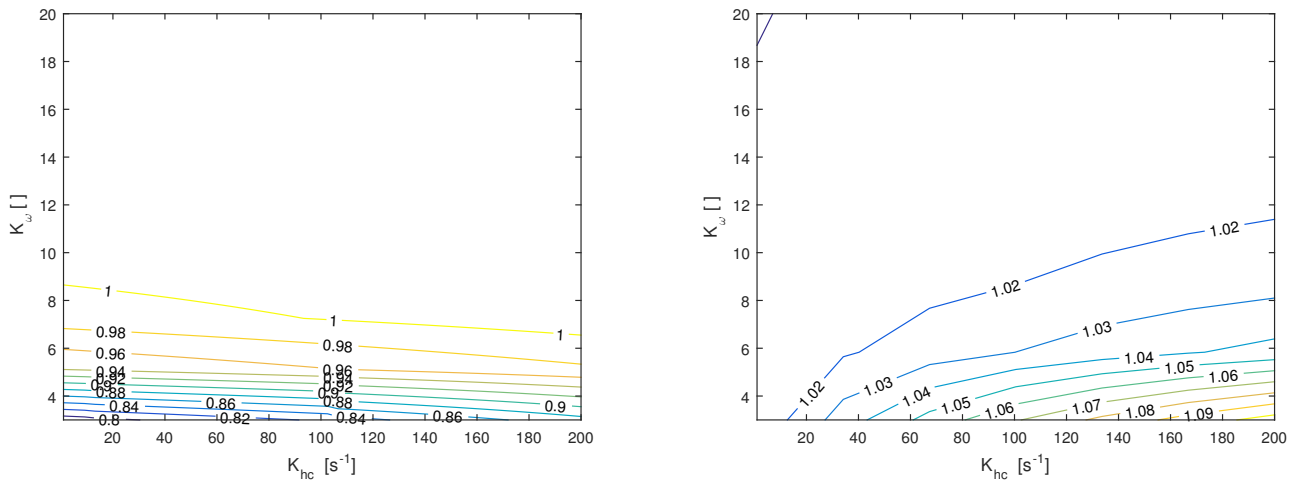

(a) D1 disturbance

(b) D2 disturbance

Figure 3.16: Relative spike of the onshore active power after imposed disturbances

• Overshoot of the onshore active power

Figure 3.17 illustrates the percentage of the overshoot compared to the imposed pulse of 500 MW. Therefore, a value of 0.01 means that the overshoot corresponds to $0.01 * 500 = 5$ MW, and the maximal value that appears here corresponds to 40 MW. This value becomes high for the onshore network, particularly if the step of wind production becomes greater than 500 MW.

• Settling time

Finally, the settling time investigated through Figure 3.18 seems to depend essentially on K_{hc}. This correlates with the results of the linear study. Indeed, in the latter, modifying the constraint on the time response was reducing the range of acceptable values of K_ω for small K_{hc}. The left red side of Figure 3.7b has the same shape as the contour lines in Figure 3.18. In other words, choosing a smaller K_{hc} increases the time response. Even though this message is clearer in the nonlinear analysis, it could have been deduced from the linear one as well. Notice that settling times represented in Figure 3.18 correspond to the time required for the rotor speed response to enter in the 0.1% band of the steady-state value, which is equal to 7 times the time response τ. This means that, for example, if the time shown in Figure 3.18 is equal to 20 s, the time response is equal to 20/7 s and consequently the real part of the associated pole is equal to -0.35.

• Final set of values

As a conclusion, for each criterion, choosing a high value of K_{hc} is not really problematic, it is rather the final value of K_ω that is decisive regarding the behaviour of the system. Therefore, $K_{hc} = 200$ is fixed. Regarding K_ω, both criteria on the rotor speed, as well as the ones regarding the relative spike due to D2 and the overshoot all suggest a high value. However, the impact of K_ω on the outputs is small. On the opposite, criterion based on the spike in

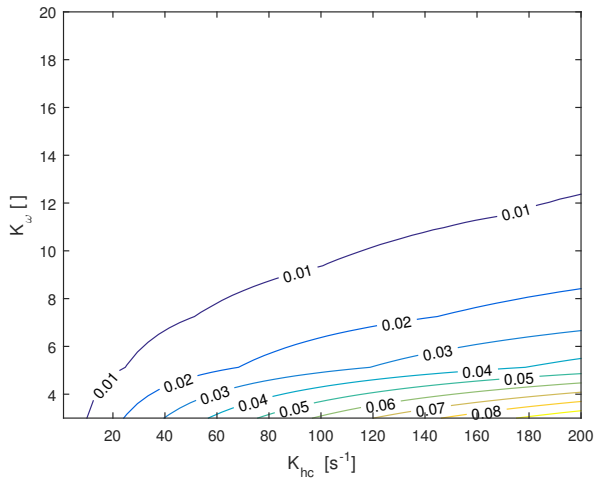

Figure 3.17: Overshoot of onshore active power due to D2

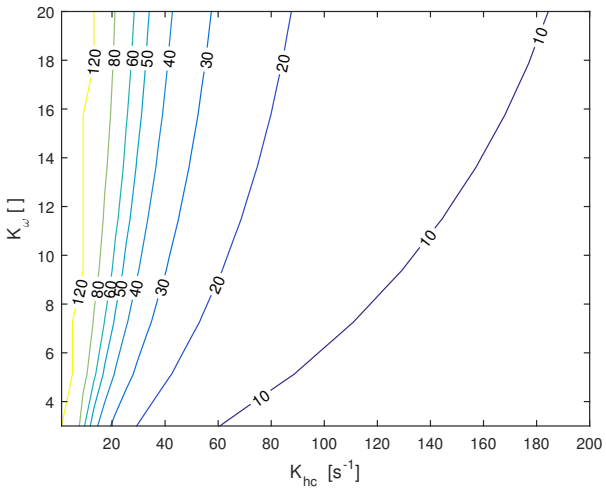

Figure 3.18: Settling time to enter in the 0.1% band after D2

case of D1 would rather suggest a reduced value. However, in this case, to decrease significantly the onshore spike of active power, a really small value should be taken. The criterion on the settling time requires a small value of K_ω.

All in one, a compromise has to be drawn: because a high value of Kw would badly increase the settling time, a value of $K_\omega = 5$ is chosen. In this case, the maximum rotor speed deviation is equal to 0.8 Hz, the overshoot of the onshore active power is equal to 25 MW, the onshore spike after D1 equals 450 MW and the settling time is much smaller than 10 s. Even if the onshore spike after D1 seems quite high, this case is purely a case study and such a situation happens rarely in practise.

3.2.3 Reactive power control design

Regarding the reactive power design, it is not instructive to consider similar constraints as for the active power. Indeed, as we discussed in the linear study, the impact of the reactive power on the onshore power and the rotor speed are negligible due to the independence of the control loops. More interestingly, the control of the voltage at the Hub can be investigated. As a reminder, the Synchronous Condenser has two main purposes: on one hand, ensure the power balance thanks to its power storage in rotating masses, and on the other hand, the control of the voltage on the island. The latter is as important as the power balance to ensure a consistent behaviour of the system.

As previously, the design of the reactive power control focuses on K_{iq} and K_{pq}. Many combinations have been tested on Ramses and for each pair, the maximum and the minimum voltage at the bus have been recorded. If one of them deviates from the initial value of more than 0.10 p.u., the response is considered as unacceptable. Figure 3.19 illustrates the limit between acceptable and unacceptable couples. The combinations on the left of the line are not acceptable. It seems that only a minimal value on K_{pq} is required to reach the allowable zone.

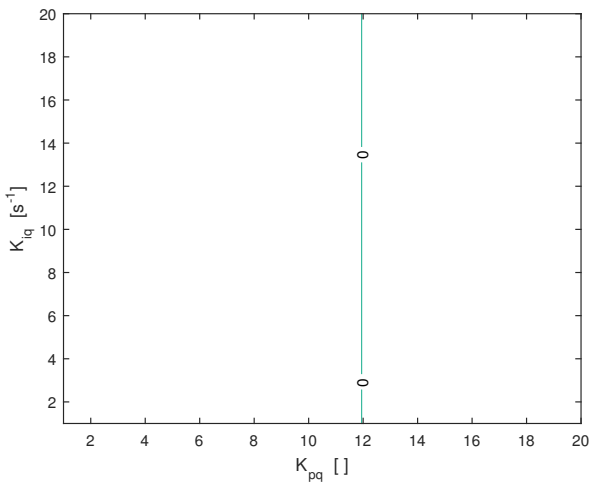

Figure 3.19: Accepted pairs of gains for K_{iq} and K_{pq}

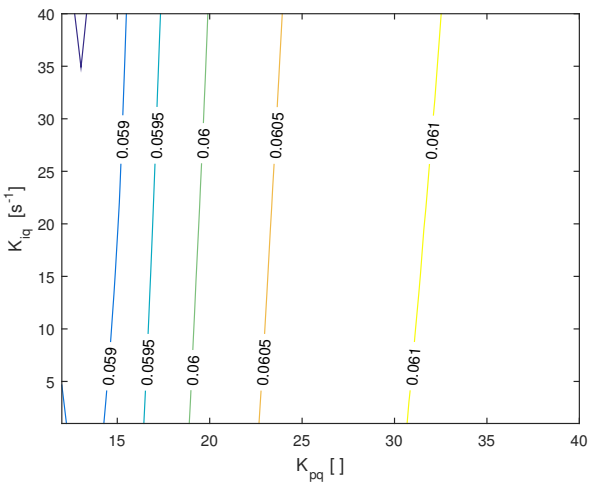

Figure 3.20: Excursion of voltage at the Hub

K_i	10.6	K_p	0.0371	$K_{i\omega}$	31.83	$K_{p\omega}$	0.6366	K_ω	5
K_{ip}	20	K_{pp}	40	K_{iq}	10	K_{pq}	13	K_{hc}	200

Table 3.3: Final values of the gains for the complete control

Figure 3.20 provides the values of the voltage excursion the Hub. The value of this excursion depends mainly on the value of K_{pq}. In addition to that, the value of the excursion varies sparsely with K_{pq}. Therefore, the value of K_{iq} is chosen arbitrarily to 10 and K_{pq} is set to 13 in order to minimise the excursion of the Hub voltage.

3.3 Final design

Thanks to all the constraints established in this chapter, a final design of the gains can be drawn and is provided in Table 3.3. To prove the efficiency of the conceived system, Figure 3.21a and 3.21b respectively depict the onshore active power and the rotor speed deviation due to D2.

The most important conclusion of this chapter is that the system is extremely stable. Only extreme choices of the gains could lead to instability. The gains have been fixed to obtain smooth signals in the event of a disturbance. The graphs 3.21a and 3.21b of the final design illustrate that the model is able to obtain smooth response and successfully bring the power to the onshore network or face important disturbance without destabilising the system.

As a summary, Table 3.4 synthesises the design process of the gains. In other words, this table provides an overview of the discussion of the gain in each section.

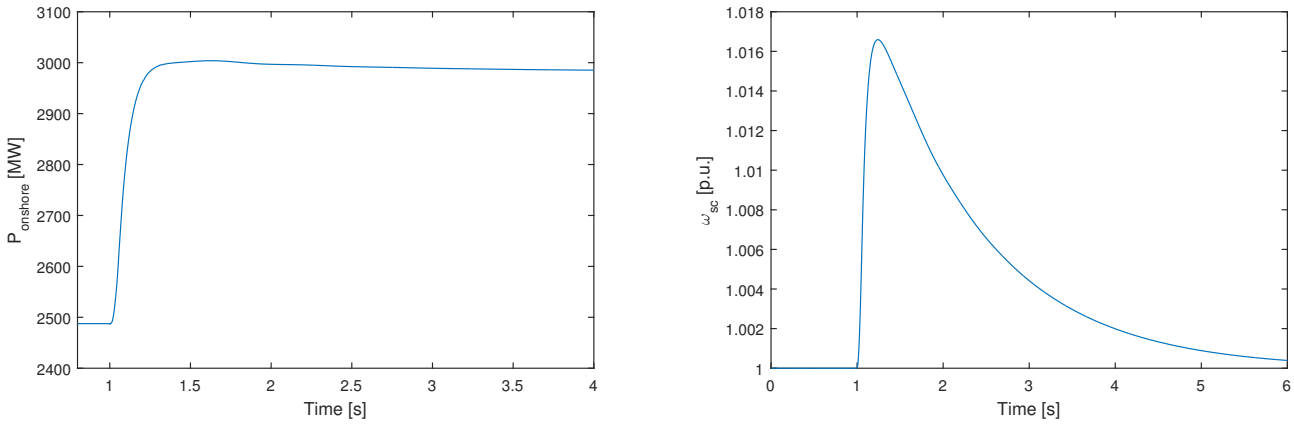

(a) Active power in the DC link

(b) Rotor speed deviation

Figure 3.21: Outputs of the final design of the control

Gains	**Linear study**	**Nonlinear study**
K_{iq}, K_{pq} and K_{ω}	First range provided based on settling time and damping ratio: see section 3.1.2.	Two aspects analysed: spike of onshore active power and rotor speed variations. K_{ip} and K_{pp} fixed definitively due to their limited effect.More restrictive range determined for K_{ω}: see section 3.2.1.
K_{ω} and K_{hc}	Damping ratio and settling time tested on range of K_{ω} determined in 3.2.1 and a large range for K_{hc}: see section 3.1.3.	6 characteristics used: the spike of onshore active power after D1 and D2, the rotor speed variation after D1 and D2, the overshoot of active power due to D2 and the time response after D2. Accurate value of K_{ω} and K_{hc} are fixed definitively: see section 3.2.2.
K_{iq} and K_{pq}	First range provided based on settling time and damping ratio: see section 3.1.4.	Hub voltage used as criteria.K_{iq} is fixed due to limited effect. Minimal value of K_{pp} necessary to stabilise the system is determined: see section 3.2.3

Table 3.4: Summary of process design of the gain

Chapter 4

Dynamic analysis of five link system

After the investigation of the one link system, the realism of the model is increased. To do so, some modifications are introduced. These adjustments are explained in chapter 2 and this new model is illustrated in Figure 2.13b.

The gains determined previously can be exploited for the control of this system as well. Indeed, the gains K_{ip}, K_{pp}, K_{pq} and K_{iq} should remain the same to ensure the behaviour of the power control in each HVDC link. Moreover, the structure of the one link model has been designed to be similar to the second one in terms of power. Therefore, considering the same value for K_ω should generate similar results and at a given variation, ω_{sc} should lead to the same VSC response in both systems. Imposing specific K_ω for each link changes how the power disturbance is spread between the links. K_{hc} does not have to change either. Indeed, K_{hc} operates in the computation of P_{tot}^{hc}. In the one link system, the latter corresponds to P_i^{hc}. In the five link system, a participating factor determines the relative influence of each VSC. If all the participating factors are equal, the situation is the same as dividing the gain K_{hc} by five, for each VSC.

The response of the system to a step variation of the wind power as D2 is shown in Figure 4.1a and 4.1b. The response is exactly the same as the response of the one link system with the final design of the gains. The value for the active power is not the same due to the shared power between the five links. However, the shape is the same as Figure 3.21a. Figure 4.1b is exactly the same as Figure 3.21b. This shows than both SC can be considered as a single Synchronous Condenser with the same capacity as in the one link system.

The purpose of this chapter is to study specific situations on the five link system that could appear in practise such as link outage. After that, further analyses are undertaken to ensure the consistent performance of the system in several operating points.

4.1 Criterion on the system

Considering that the design of the gains has been verified, one can include additional features to be optimised:

- The outage of a DC link.
- The use of the island as a Hub.
- A sudden request of power to support the onshore frequency.

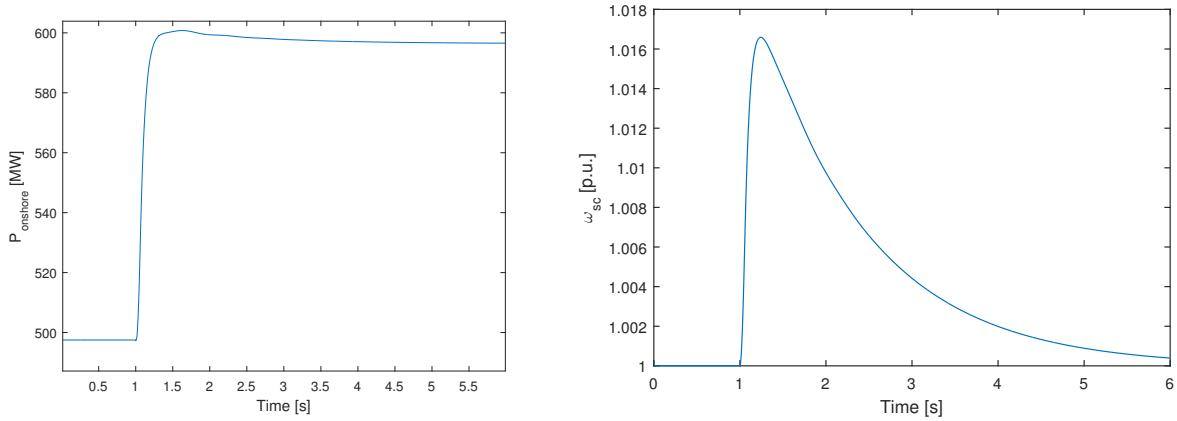

(a) Active power in one of the DC links **(b)** Rotor speed deviation

Figure 4.1: Response of the five link system after D2

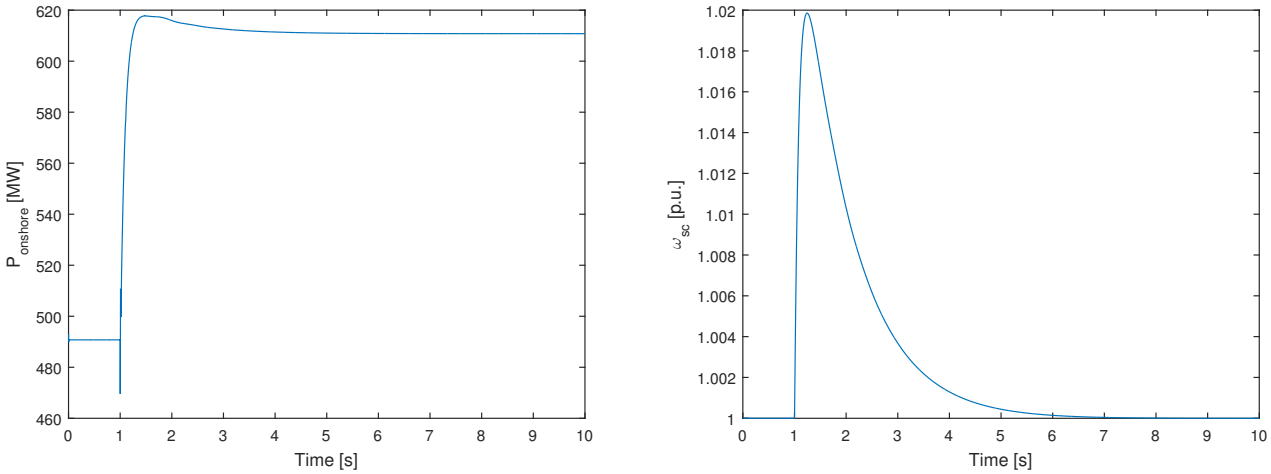

(a) Active power into a DC link **(b)** Rotor speed variation

Figure 4.2: Outage of a DC link

Outage of a DC line

In the event of a link outage, the participating factors determine how the power is spread between the remaining links. With equal coefficients, all the links carry a quarter of the power supported by the tripped link. Because each link holds 500 MW, the added power by link equals 125 MW. Figure 4.2a represents the active power in one of these links and Figure 4.2b illustrates the rotor speed change due to this tripping.

Even if the rotor speed deviation seems high (almost 1 Hz), the system is still stable. Therefore, the system can handle the outage of a link. Figure 4.2a shows that the power is correctly spread between the four remaining links. Due to the losses in the DC line, the final power is not exactly 625 MW (500+125) but more 616 MW per link.

Figure 4.3 illustrates the total power received onshore thanks to the four remaining links. At the tripping time, there is a big overshoot of power, even higher than the missing 500 MW, carried previously by the tripped line. This can also be noticed thanks to Figure 4.2a. Before increasing, the power decreases of almost 20 MW. Finally, thanks to other links, the power stabilise at the initial value.

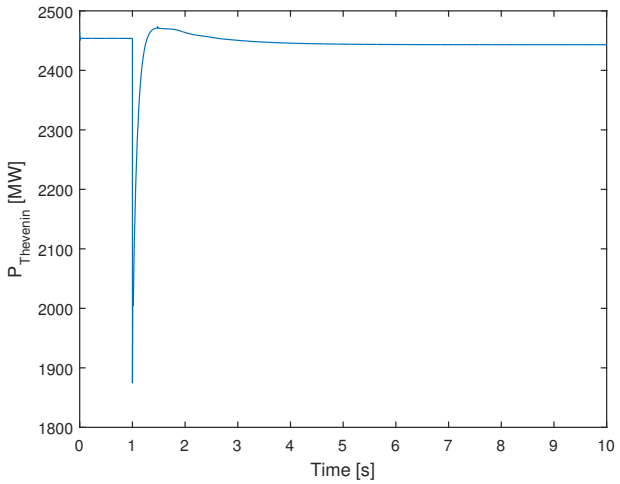

Figure 4.3: Power received by the onshore network

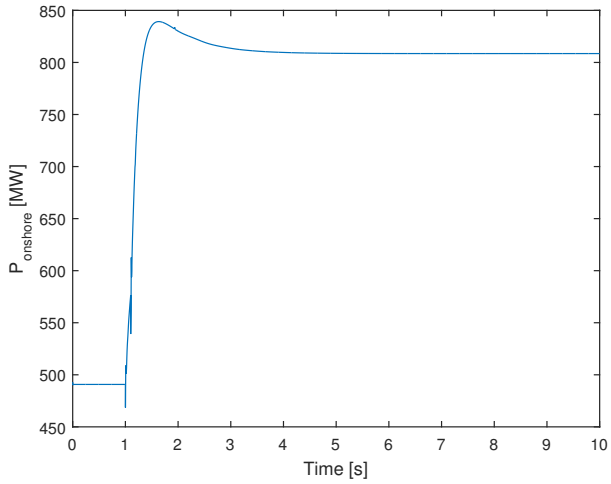

Figure 4.4: Active power into a DC link after the outage of two DC lines

In this situation, it can be instructive to test the stability of the system by tripping an additional line. To do so, the second line is tripped 0.1 s after the first line. In this situation, Figure 4.4 provides the power in a remaining DC line, Figure 4.5a is the voltage at the Hub and Figure 4.5b shows the rotor speed. Even if all signals seems stable the excursion of the rotor speed and the Hub voltage are extreme. In Figure 4.4, the effect of the second link outage can be noticed by the sudden decrease of the power at 1.1 s. However, the overshoot and the control of active power bring onshore are satisfying. This proves that the design of the gain is adapted to the loss of two lines.

The second decrease of V_{Hub} testify the tripping of the second line. In this case the excursion of voltage correspond to 0.25 p.u. which is completely extreme. However the control allows to reach the new reference value quickly. Such a change in the voltage is not damaging for our simulation. However it could be hazardous for some material in a complete model or the real system.

Finally, the rotor speed is also stable even if the maximal value correspond to almost 2.25 Hz. Further analysis on the effect of the frequency should be investigated to determine the harmfulness of such a deviation.

Use of the island as a Hub

Using the island as a Hub means simulating the transfer of power between countries. Initially, each link carries 500 MW from the island to an onshore network. Afterwards, one can imagine a transfer of 500 MW from an onshore network to another. In this case, the power for one link should vary from 500 MW to 0 and the other one from 500 to

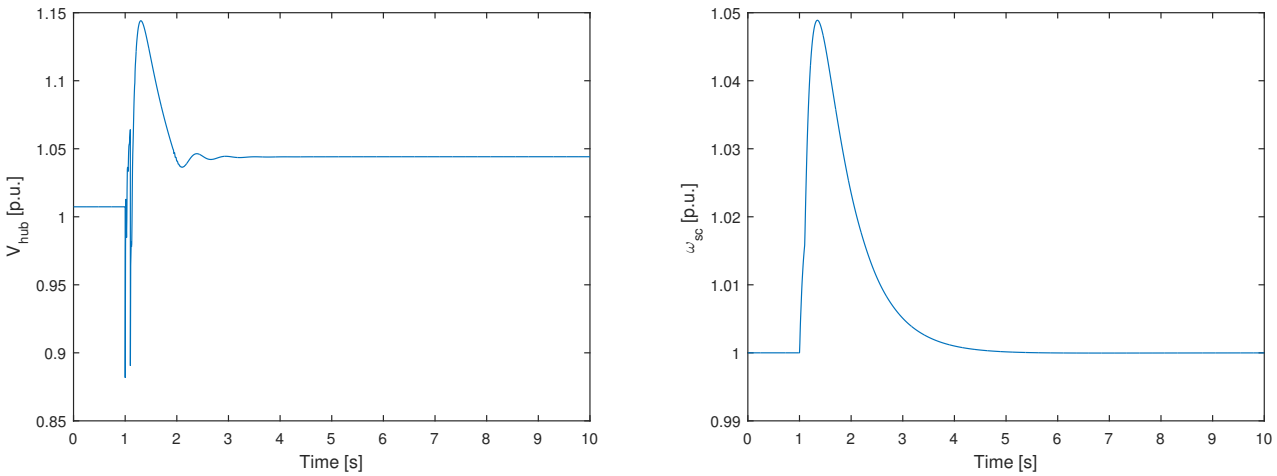

(a) Voltage at the Hub

(b) Rotor speed

Figure 4.5: Outage of two DC lines

1000 MW. However, the power carried by the other links should not change. Figure 4.6a represents the power in each link and Figure 4.6b provides the rotor speed during such an event.

In this case, the Hub Coordinator feels that the power in each link changes. This allows the system to react quickly without the help of the SCs. This explains the global shape of Figure 4.6b. The powers in links 1 and 3 reach quickly and simultaneously the new steady state value. A new simulation can be performed, where the second onshore network changes its rate from 500 MW to -500 MW. In addition to the supplementary 500 MW provided to link 1, the onshore network tries to expel an excess of 500 MW.

Figure 4.7 represents the power in each link. As expected, link 1 reach quickly 1000 MW. However, there is still 500 MW provided by link 2 which have to be evacuated. Due to equal participating factor, the contribution of each link should be the same. However, link 1 is already full due to the nominal power of 1000 MW. Consequently, the 500 MW are spread between the four other links, which leads to 125 MW per link. This explains why the power of link 2 is not -500 MW but well -375 MW. Finally, Figure 4.8 represents the rotor speed. The HC was warned of the transfer of 500 MW between link 1 and link 2 as in the first case. However, there is still additional 500 MW that arrives from link 2. Because the HC was not warned of those 500 MW, the rotor speed starts to change and increase due to the additional power. The HC measures the change in the rotor speed and consequently changes the directives for the power in the DC link. Therefore, the excursion of the rotor speed is due only to 500 MW.

Request of active power on onshore network

The sudden request for active power to support the frequency on an onshore network is close to the previous case. The active power requested on link 1 increases suddenly from 500 MW to 1000 MW. The HC is not warned and begins to change the power in the cable by feeling the rotor speed changes. This rotor speed and the power in all cables are represented in Figure 4.9a and Figure 4.9b respectively.

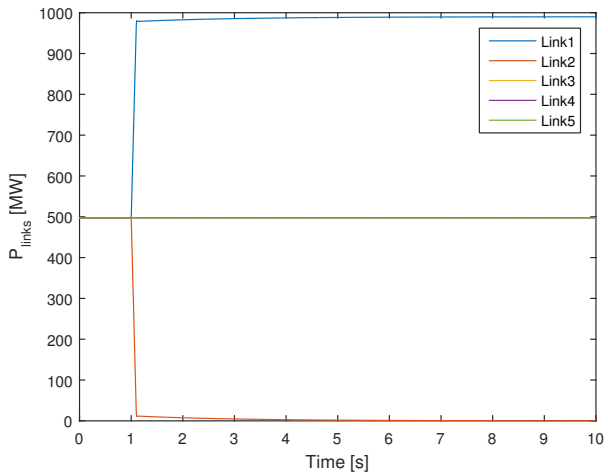

(a) Power in all links

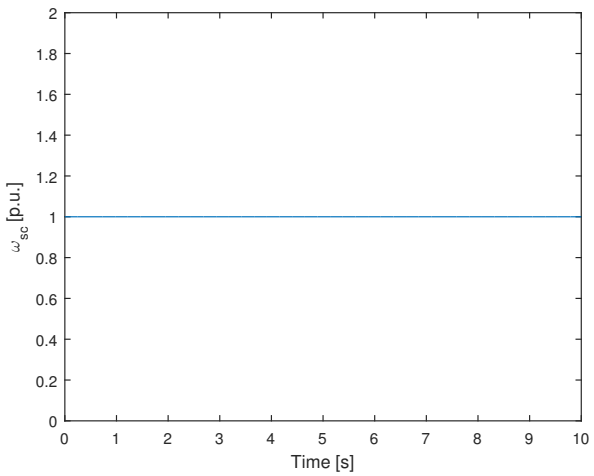

(b) Rotor speed

Figure 4.6: Use of the island as a Hub

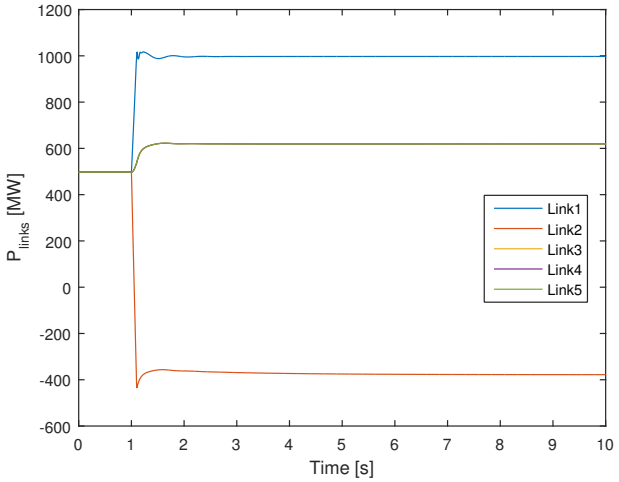

Figure 4.7: Power in all DC lines due to power rate change in Link2 from 500 MW to -500 MW

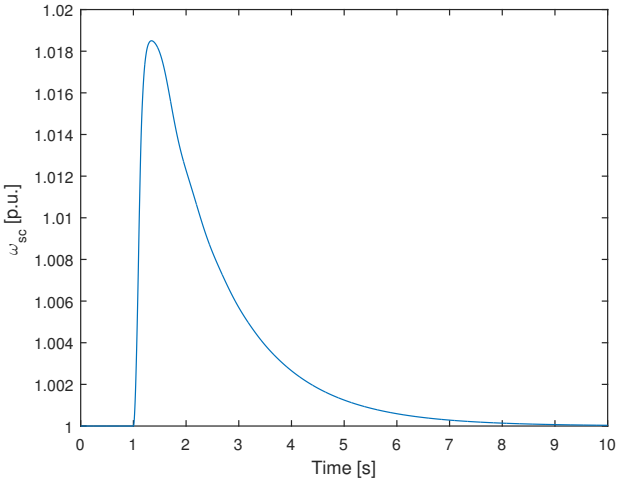

Figure 4.8: Rotor speed in SCs due to power rate change in Link2 from 500 MW to -500 MW

The sudden increase of requested power in link 1 forces the SC to provide it by decreasing its rotor speed. To provide the 500 MW to link 1, every link has to provide a part of its power. Due to equal participating factor, the part is the same for each link, 100 MW, even for link 1. This explains the final value of 900 MW for link 1 and 400 MW for the others. To anticipate the participation of link 1 to the change, a power of 625 MW should be requested, which leads to 500 MW on link 1.

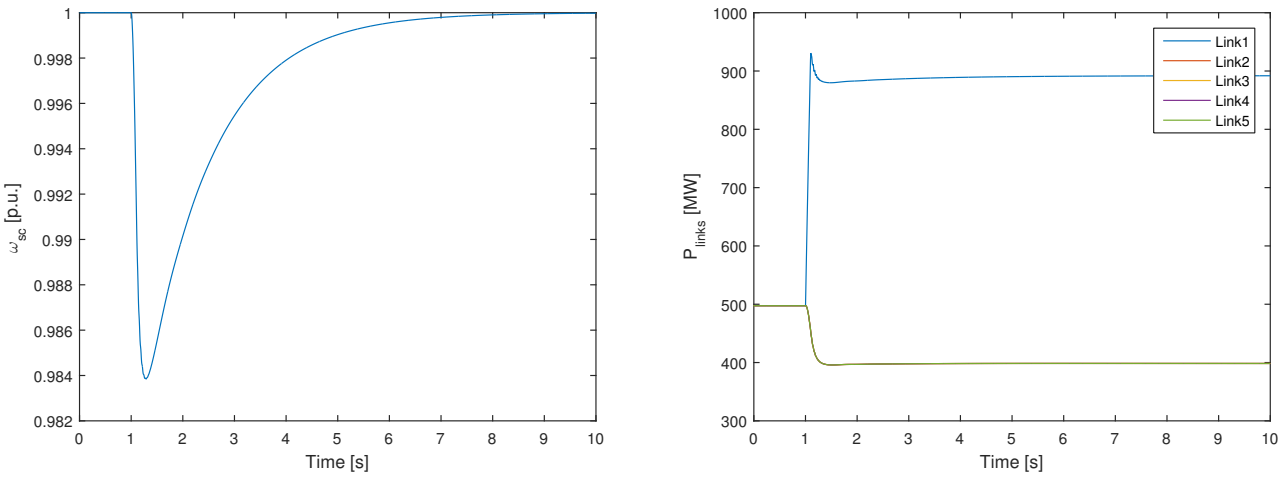

(a) Rotor speed

(b) Active power in all DC lines

Figure 4.9: Request of active power by the onshore network

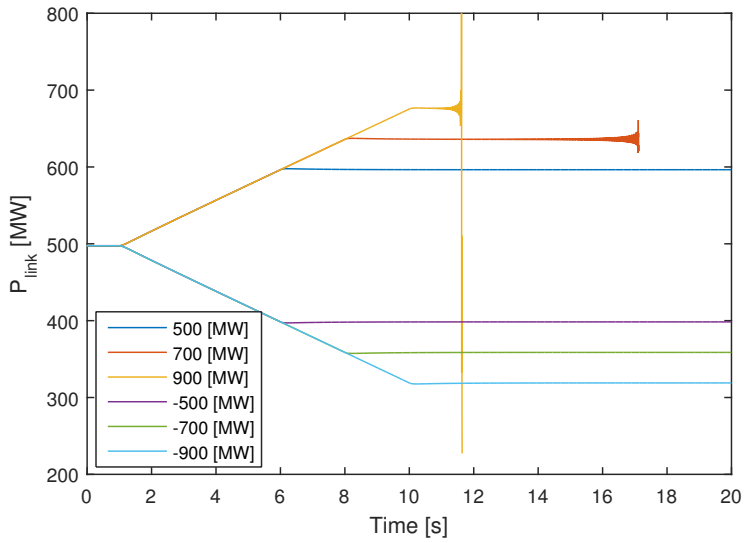

Figure 4.10: Active power in a single DC lines during operating point change

4.2 Important disturbance

All the previous simulations have considered 500 MW as a maximum step. This means that all the considered operating points correspond to a wind power between 2000 and 3000 MW. It could be instructive to study the system at other operating points to ensure that the system is stable whatever the wind power. To do so, several increasing and decreasing powers are applied as disturbances to force the system to function at other operating points. Figure 4.10 shows the change of power in a single DC link due to the changing operating point. In this figure, all the simulations begin at 500 MW. Indeed, the initial operating point has been computed at 2500 MW of wind power, which leads to 500 MW per cable. The power depicted in the legend corresponds to the total change of wind power. A change of 500 MW induces additional 100 MW in each link. This explains the 600 MW in steady state.

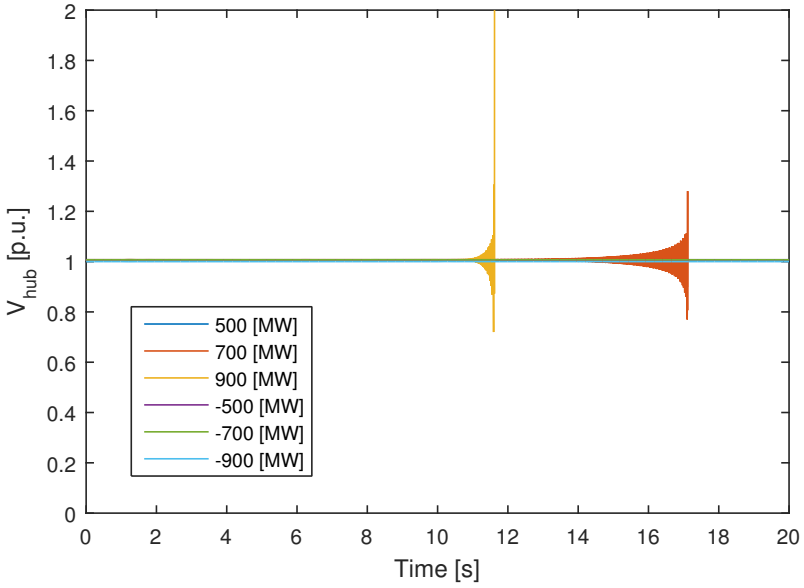

Figure 4.11: Voltage at the Hub during operating point change

The changes in wind power have all a rate of 100 MW/s, meaning a rate of 20 MW/s per cable. The aim is to ensure that instabilities are linked to the new operating point and not to the transition between the previous and the new operating point. As it can be observe in Figure 4.10, a wind power smaller than 2500 MW is never an issue. However, an operating point above 3000 MW seems unstable (600 MW per cable). This means that one or several gains are not adapted to the new operating point.

By investigating the output signals of the system, it seems that the voltage at the Hub is destabilising the system. This one is shown in Figure 4.11. Bigger the new wind power, faster the collapse of the system. The control of the voltage depends essentially on the reactive power (K_{pq} and K_{iq}). In the nonlinear study of the reactive power control (in the previous chapter), a minimal value of K_{pq} has been determined to have a stable system. This minimal value should be linked to the operating point. Therefore, increasing K_{pq} should stabilise the system. Several couples of K_{pq} and P_w have been tested on Ramses, and Figure 4.12 depicts the minimal value of K_{pq} required to stabilise the island at a given value of P_w. As previously, the green dots are the acceptable pairs of K_{pq} and P_w.

Based on this figure, a minimum value of $K_{pq} = 45$ seems necessary to handle all the operating points. Indeed, with a $\Delta P_w = 2500$ MW, $P_w = 5000$ MW and all the links are fully charged. This constrains to change the previous definition of K_{pq} from 13 to 45. Figure 4.13a shows the change of operating point for varying values of P_w with $K_{pq} = 45$ for all VSCs. The legend of Figure 4.13a is the same as the one given in Figure 4.13b. The latter gives the voltage in each situation. The dotted lines correspond to a decreasing wind power. Therefore, the voltage begins to decrease and when the new operating point is reached, the voltage increases suddenly. All the voltages are the same, the only difference is when it reaches the new operating point.

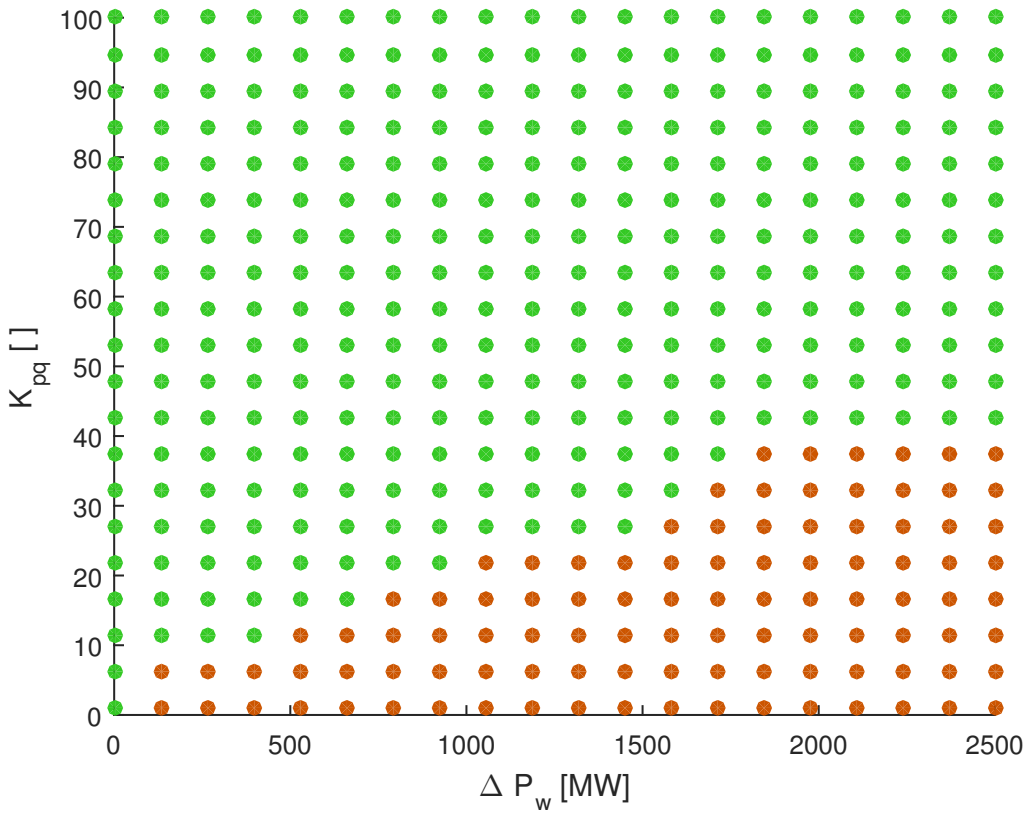

Figure 4.12: Minimum value of K_{pq} necessary to stabilise the system at a given P_w

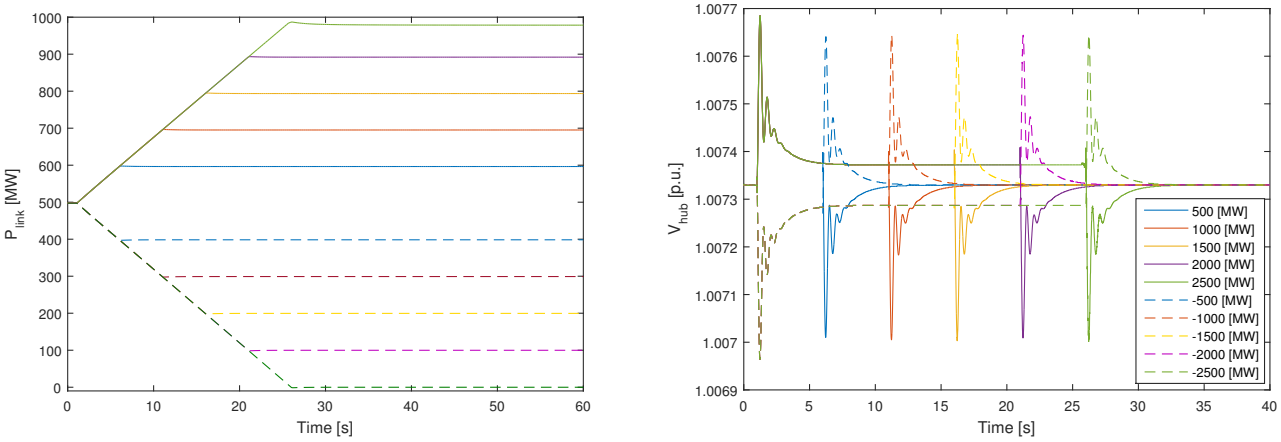

(a) Active power in a single DC line

(b) Voltage at the Hub

Figure 4.13: K_{pq}=45

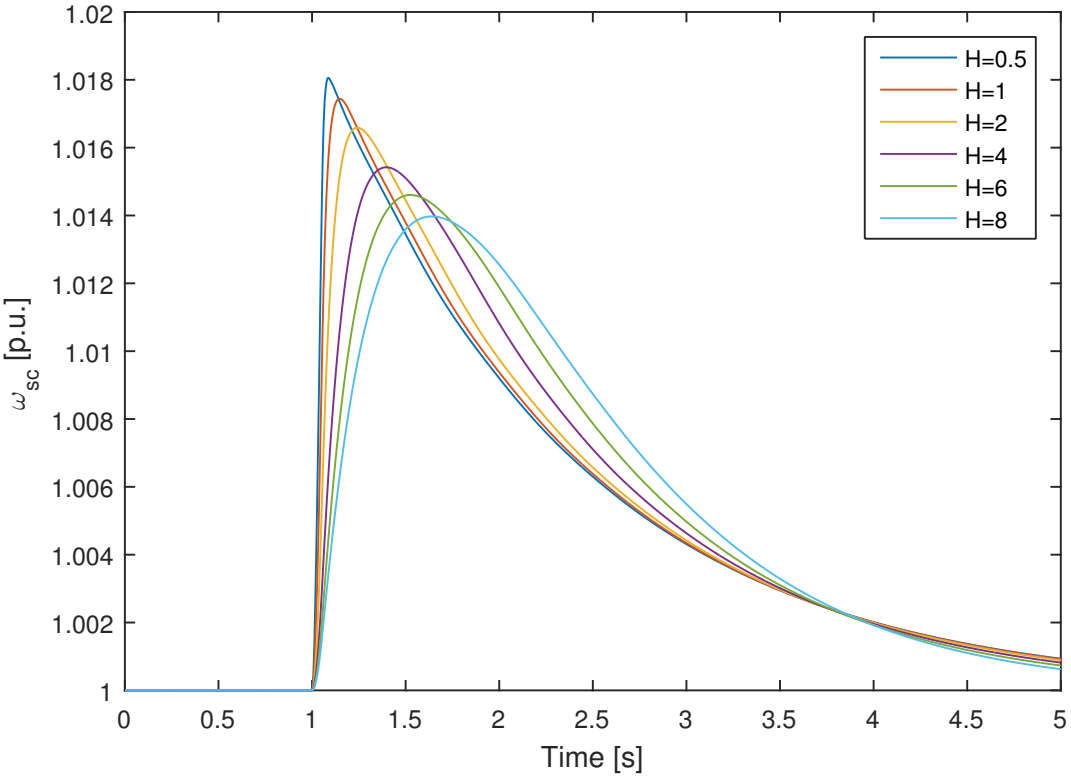

Figure 4.14: Effect of H on the response of the rotor speed of the SCs after D2

4.3 Size of the Synchronous Condenser

Several reasons compel us to study the dimension of the Synchronous Condenser, such as the limited space on the island or the excursion of rotor speed after a disturbance. Two main aspects of the SC are crucial in this project: the parameter H, which reflects the size of the machine and its inertia, as well as the nominal power S_n. These two parameters are discussed separately to be able to distinguish their separated effects on the stability of the system.

Effect of H

In this first analysis, the nominal power of both SCs remains equal to 250 MW. The value of the parameter H is changed automatically and the rotor speed is registered and shown in Figure 4.14. Each situation is simulated with the typical case of a step D2.

The maximal value of $H = 8$ represents the maximal value found in the literature and corresponds to an extreme value. However, it may be instructive to analyse the effect of such a big value. As expected, the excursion of the rotor speed decreases when H increases. Due to its link with the inertia, when it increases, the storage capacity of the machine increases as well. However, the maximal value of ω_{sc} does not change radically even with extreme values such as 0.5 and 8.

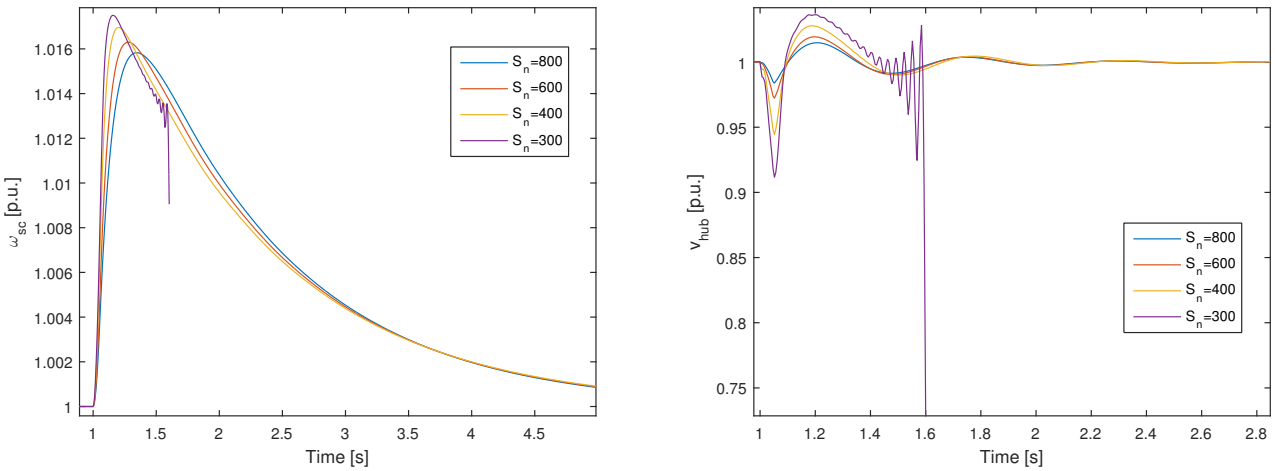

(a) Rotor speed

(b) Hub voltage

Figure 4.15: Study of S_n with D2 disturbance

Two reasons can explain that small values are acceptable and that the response for 0.5 and 8 are not so varying. First explanation is related to the speed of the active power control. Thanks to K_{hc} and K_ω, the speed of the active power control is ensured and the power is quickly conducted towards the VSCs. Therefore, the energy stored in the SC is not that big. This explains that an H of 0.5 is sufficient to store the quantity of energy. Moreover, the second reason is the faster control in case of small H. In the latter, the rotor speed varies faster in the event of a disturbance, so this one is detected faster as well by the HC and then by the gain K_ω. Both events can be seen in Figure 4.14. The increase of the rotor speed is steeper with a small H. The decrease of the rotor speed begins earlier as well. These two observations allow to consider a small value of H and thus a smaller machine, which is an advantage in a project with such limited space.

Effect of S_n

The second parameter under study is the nominal power of the Synchronous Condensers. For now, the total power for both SC together equals 500 MVA. Values of this complete nominal power are tested to observe the impact on the system. Figure 4.15a represents the rotor speed for different values of S_n.

The nominal power does not have a huge impact on the excursion of the rotor speed. However, it seems that a minimal value is required to stabilise the system. Indeed, for a total nominal power of 300 MVA (150 per SC), the response is unstable. Looking at the Hub voltage in Figure 4.15b, it is clearly remarquable that smaller the nominal power, bigger the voltage excursion.

The SCs control the voltage at the Hub through the transformers. Considering a smaller nominal power for both SCs and both transformers, it is more difficult for the SCs to control the voltage. A faster reactive control in the VSC should help stabilising the system. A bigger value of K_{pq} is chosen for all VSCs and the results are shown in Figure 4.16a and Figure 4.16b.

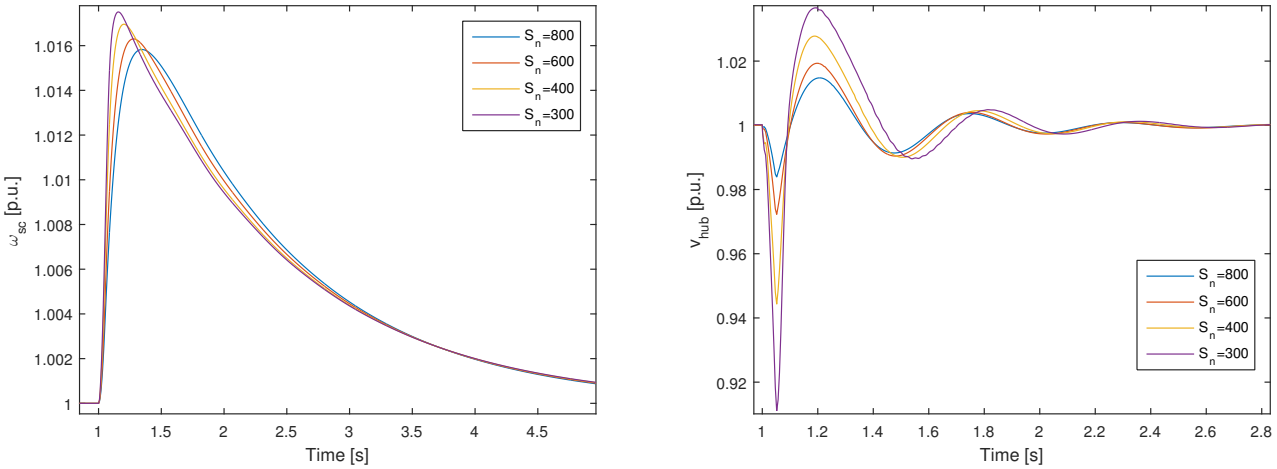

(a) Rotor speed

(b) Hub voltage

Figure 4.16: K_{pq}=100

As expected, the system is stable even with two machines of 150 MVA. With a faster control of the reactive power, the VSCs help the SCs to control the voltage. However, there is a limitation, even with fast reactive control. A total nominal power of 200 MVA has been tested and even with fast control, the system remains unstable. Therefore, a minimal value is required. Even if the system is stable with 300 MVA, the excursion of the voltage at the Hub is significant: almost 0.1 p.u., which is the limit in conventional networks. It is preferred to keep a bigger nominal power. In the end, the choice of 500 MVA seems completely acceptable.

Limitations and future work

Limitations

Along this project, some hypotheses have been made that do not reflect the practical reality. These limitations could be overcome to better fit to the real behaviour of the system.

The first assumption relates to the modelling of the Synchronous Condenser for the small signal stability study. In this study, the SC has been modelled using a classical model consisting in a voltage source in series with a reactance. Considering a more accurate model in the Jacobian could enhance the poles location. However, the nonlinear study shows that the small signal analysis fits well to the nonlinear results, which tends to indicate that this assumption is not crucial so far.

The second limitation is due to the modelling of the wind power. For now, it has been considered as a simple injector of active and reactive power in both simulations. To better fit the actual future system, the wind power could be modelled by a network of cables that would link each wind turbine to the Hub. The inclusion of reactances due to wind turbines induces the addition of shunt reactances to counteract their effects. This increases the requirements in terms of reactive power and Hub voltage control, for which the analysis could be improved.

Future work

Besides the limitations, some further works and advanced analyses could be considered. The first one, as explained Appendix D, could be to study the impact of the frequency on the stability. The frequency of 50 Hz has been arbitrarily chosen to fit the frequency of the onshore network. However, another frequency could enhance the response of the system. A further study could optimise the role of the frequency.

The study of the poles of the linear model is rather complex. It is difficult to determine the poles influenced by a particular gain. An instructive future work could be to study the participating factor of each pole. These ones would indicate which gain has the most influence on a specific pole. This should also allow to work on each pole separately and to target the gains that need to be tuned to meet the dynamic behaviour expected for the system.

In addition, in all the analyses performed during this project, the onshore network has always been represented by a Thevenin equivalent. To have a better overview of the system included in the real onshore network, future simulations could connect the five DC links system to a representation of the Nordic network that already exists for Ramses [26].

Conclusion

The main purpose of this master thesis was to investigate the feasibility of using a Synchronous Condenser as a power balance tool allowing to add inertia to the system. Specifically, this report aims at designing the gains required to control the active and the reactive power of the VSC based on the SC variations.

First, the linear analysis enabled to highlight the stability of the system and the following behaviours of the gains:

- K_{ip} has a small effect on the poles and its minimal acceptable value depends on K_{pp}.
- K_{pp} has a minimal value enterily influenced by the constraints. Its maximum value is linked to K_{ip} and depends also on the constraints.
- Generally speaking, K_{pq} and K_{iq} have the same effect as K_{pp} and K_{ip}, respectively.
- A minimal value of K_ω is required and an increasing value of K_ω required also an increasing value of K_{pp}.
- K_{hc} is mainly linked to K_ω to fit the constraints and its maximum value is linked to the minimal value of K_ω.

Based on these characteristics, specific ranges of values have been tested through nonlinear analysis on Ramses in order to finalise the design of the gains. To do so, several signals of the system have been investigated: the voltage at the Hub, the onshore power, the rotor speed of the SC as well as the settling time of the system. The nonlinear analysis has brought to light important features of each gain:

- K_{pp}, K_{ip} and K_{iq} do not have significant effect on the signals observed.
- K_{pq} needs to reach a minimal value to stabilise the system. This minimal value depends of the operating point, especially P_w, as well as the nominal power of the synchronous condenser.
- K_ω and K_{hc} have a considerable effect on all the analysed signals. The main trade-off was linked K_ω to compromise mainly between the spike of active power onshore and the excursion of the rotor speed.

After all these considerations, a final design of the gains has been chosen.

Finally, the design has been tested on the five link system to investigate additional aspects such as the operating point and $n-1$ criterion. Afterwards, the impact of the SC properties has been evaluated. It has been concluded that the parameter H does not need to be excessively high and that a minimal nominal value is necessary for the SC to ensure the voltage control and the stability of the system. In conclusion, the most important instruction of this project is the feasibility and the stability of the Synchronous Condenser.

Appendices

Appendix A

Main abbreviations

The Table A.1 gives the main abbrevations used in this report.

NSWPH	North Sea Wind Power Hub
HVDC	High Voltage Direct Current
HVAC	High Voltage Alternative Current
NIRO	National Incremental Roll-Out
ICRO	Internationnaly Coordinated Roll-Out
LCC	Line-Commutated-Converter
VSC	Voltage-Source-Converter
TSO	Transmission System Operator
P2G	Power to Gas
SC	Synchronous Condenser
PLL	Phase Locked Loop
HC	Hub Coordinator

Table A.1: Abbreviation table

Appendix B

Phase reactor dynamics and current controllers design

B.1 Phase reactor dynamics

This appendix aims at developing the equations of the phase reactor of the VSC. The phase reactor of the VSC is represented in Figure 2.3. One aims to begin from this representation to develop the equations of the dynamic and compute the block-diagram given in Figure 2.4.

The second Kirchhoff law of the phase reactor gives the following equation which can be rewrite thanks to the phasor representation:

$$v_m - v = R\,i + L\,\frac{di}{dt} \leftrightarrow \sqrt{2}\,\left(re[\overline{V}_m\,e^{j\omega_{ref}t}] - re[\overline{V}\,e^{j\omega_{ref}t}]\right) = \sqrt{2}\,\left(re[R\overline{I}\,e^{j\omega_{ref}t}] + re[L\;\frac{d}{dt}(\overline{I}\,e^{j\omega_{ref}t})]\right)$$

The derivative can be replaced by:

$$\frac{d}{dt}(\overline{I}\,e^{j\omega_{ref}t}) = \frac{d\overline{I}}{dt}\,e^{j\omega_{ref}t} + j\,\omega_{ref}\,\overline{I}\,e^{j\omega_{ref}t}$$

By using this expression in the previous equation, removing all $\sqrt{2}$,all $re()$ and the term $e^{j\omega_{ref}t}$ the following equation is found:

$$\overline{V}_m - \overline{V} = R\overline{I} + L\frac{d\overline{I}}{dt} + j\,\omega_{ref}\,\overline{I}$$

This equation can be divided into two equations, one for each axis (x and y):

$$v_{mx} - v_x = R\,i_x + L\,\frac{di_x}{dt} - \omega_{ref}\,L\,i_y \qquad\qquad v_{my} - v_y = R\,i_y + L\,\frac{di_y}{dt} + \omega_{ref}\,L\,i_x$$

By transform this equation in pu and isolating both current, i_x and i_y, one finds in the laplace domain:

$$i_x = \frac{1}{R + \frac{L}{\omega_N}s}(v_{mx} - v_x + \omega_{ref}^{pu}L\,i_y) \qquad\qquad i_y = \frac{1}{R + \frac{L}{\omega_N}s}(v_{my} - v_y - \omega_{ref}^{pu}L\,i_x)$$

It is possible to rewrite these equation in the (d,q) plan. This is done by replacing x,y by d and q respectively in the previous equation. In this case the angular speed that multiplied Li_y and Li_x is no more ω_{ref}. Indeed, this angular speed is the one of the (x,y) frame. It is replaced by ω_{pll}, the angular speed of (d,q) frame:

$$i_d = \frac{1}{R + \frac{L}{\omega_N}s}(v_{md} - v_d + \omega_{pll}^{pu}Li_q) \qquad \text{(B.1)} \qquad\qquad i_q = \frac{1}{R + \frac{L}{\omega_N}s}(v_{mq} - v_q - \omega_{pll}^{pu}Li_d) \qquad \text{(B.2)}$$

The inverse Laplace transform can be used to express these equations in the time-domain. This gives:

$$\frac{di_d}{dt} = \frac{\omega_N}{L}(-Ri_d + v_{md} - v_d + \omega_{pll}^{pu} L i_q) \qquad \text{(B.3)} \qquad \frac{di_q}{dt} = \frac{\omega_N}{L}(-Ri_q + v_{mq} - v_q - \omega_{pll}^{pu} L i_d) \qquad \text{(B.4)}$$

B.2 Design of current controllers

To design the gains of the current control loop, it is important to define the expected behaviour for the dynamics of the phase reactor. The first parameter considered is the damping ratio ζ which describe the depreciation of the oscillation of the system. A damping ratio of 0.7 is chosen, which is a good trade-off between time response and maximum overshoot of the response[12].

The second aspect of the dynamics is the settling time (t_s). This one described the time necessary to enter in the band limited. The band limited is an accepted error percentage around the reference value. The settling time is choose to avoid interference between several control loop. Indeed, if the response time of two control loops are too close, some interaction between both loop appears. A factor 10 between two response time is necessary to avoid these interactions [12, 27, 28].

All the parameters discussed hereabove are linked by the relation of the settling time. This one, for a second order, underdamped system responding to a step response, can be approximated by:

$$t_s = \frac{-ln(toler)}{\zeta \omega_{osc}} \qquad \text{(B.5)}$$

Where t_s correpond to the settling time, $toler$ to the band limited and ω_{osc} to the natural frequency of the undamped system. This last equation allows to determine the natural frequency of a step response.

Now that all these parameters are determined, it is possible to compute the value of the different gains. Indeed, thanks to previous parameters it is possible to define the characteristic polynomial define by ζ and ω_{osc} [27, 28]:

$$P(s) = 1 + \frac{2\zeta}{\omega_{osc}} s + \frac{s^2}{\omega_{osc}^2}$$

By comparing this polynomial to the denominator of current control loop transfer function, it is possible to design a controller that have the dynamical behaviour expected.

By comparing both polynomial, the gain can be express as a function of the parameters of the second order characteristic polynomial.In these expressions, R and L are given in per unit. These expression are given by:

$$\begin{cases} K_p = \dfrac{2\zeta L \omega_{osc}}{\omega_n} - R \ \ [p.u.] \\ K_i = \dfrac{\omega_{osc}^2 L}{\omega_n} \ \ \left[\dfrac{rad}{s}\right]; \end{cases}$$

By replacing these gains in the transfer function of the current, the bode diagram and the step response of the system can be plotted to visualise if the expected dynamics is respected. This is represented in Figure B.1 and B.2 respectively

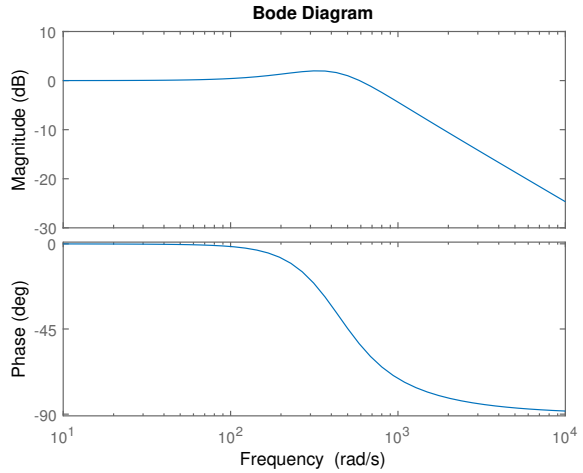

Figure B.1: Bode diagram of the transfer function of the current controller

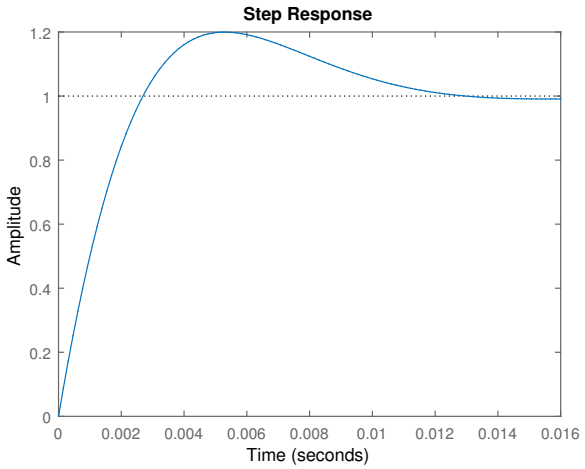

Figure B.2: Step response of the current controller

for time response of 0.01 s, a damping ratio of 0.7 and a tolerance of 5%. As expected the step response enter in a band limited of 5% at 0.01 s and the overshoot in the bode diagram is not too important[28], there is no risk to destabilise the system.

Appendix C

Linear study

C.1 Linearisation

To study the small signal stability, it is necessary to linearize the system of equation given third chapter (equation 3.1 to equation 3.33). To do so, it is necessary to linearise around a value of the states. The indication "^{o}" refers to the initial value of a state around which the system is linearised.

$$0 = \Delta v_x \cos\theta^o + \Delta v_y \sin\theta^o - \Delta v_d - v_x^o \sin\theta^o \Delta\theta + v_y^o \cos\theta^o \Delta\theta \tag{C.1}$$

$$0 = \Delta v_y \cos\theta^o - \Delta v_x \sin\theta^o - \Delta v_q - v_y^o \sin\theta^o \Delta\theta - v_x^o \cos\theta^o \Delta\theta \tag{C.2}$$

$$0 = \Delta i_x \cos\theta^o + \Delta i_y \sin\theta^o - \Delta i_d - i_x^o \sin\theta^o \Delta\theta + i_y^o \cos\theta^o \Delta\theta \tag{C.3}$$

$$0 = \Delta i_y \cos\theta^o - \Delta i_x \sin\theta^o - \Delta i_q - i_y^o \sin\theta^o \Delta\theta - i_x^o \cos\theta^o \Delta\theta \tag{C.4}$$

$$0 = i_x^o \Delta v_x + v_x^o \Delta i_x + i_y^o \Delta v_y + v_y^o \Delta i_y - \Delta P_i \tag{C.5}$$

$$0 = i_x^o \Delta v_y + v_y^o \Delta i_x - i_y^o \Delta v_x - v_x^o \Delta i_y - \Delta Q_i \tag{C.6}$$

$$\frac{d\theta}{dt} = \omega_N \Delta\omega_{pll} \tag{C.7}$$

$$0 = K_{p\omega} \Delta v_q + \Delta M_{pll} - \Delta\omega_{pll} \tag{C.8}$$

$$\frac{dM_{pll}}{dt} = K_{i\omega} \Delta v_q \tag{C.9}$$

$$\frac{di_d}{dt} = -\frac{\omega_N}{L} R \Delta i_d + \omega_N i_q^o \Delta\omega_{pll} + \omega_N \omega_{pll}^o \Delta i_q + \frac{\omega_N}{L} \Delta v_{md} - \frac{\omega_N}{L} \Delta v_d \tag{C.10}$$

$$\frac{di_q}{dt} = -\frac{\omega_N}{L} R \Delta i_q - \omega_N i_d^o \Delta\omega_{pll} - \omega_N \omega_{pll}^o \Delta i_d + \frac{\omega_N}{L} \Delta v_{mq} - \frac{\omega_N}{L} \Delta v_q \tag{C.11}$$

$$0 = \Delta v_d - L i_q^o \Delta\omega_{pll} - \omega_{pll}^o L \Delta i_q + K_p(\Delta i_d^{ref} - \Delta i_d) + \Delta M_d - \Delta v_{md} \tag{C.12}$$

$$\frac{dM_d}{dt} = K_i(\Delta i_d^{ref} - \Delta i_d) \tag{C.13}$$

$$0 = \Delta v_q + L i_d^o \Delta\omega_{pll} + \omega_{pll}^o L \Delta i_d + K_p(\Delta i_q^{ref} - \Delta i_q) + \Delta M_q - \Delta v_{mq} \tag{C.14}$$

$$\frac{dM_q}{dt} = K_i(\Delta i_q^{ref} - \Delta i_q) \tag{C.15}$$

$$0 = \Delta M_p + K_{pp}(P^{hc} - P_i) - K_{pp} K_\omega \Delta\omega_{sc} - \Delta i_d^{ref} \tag{C.16}$$

$$\frac{dM_p}{dt} = K_{ip}(P^{hc} - P_i) - K_{ip}K_\omega \Delta\omega_{sc} \tag{C.17}$$

$$0 = -K_{pq}\Delta Q_i + \Delta M_{qc} - \Delta i_q^{ref} \tag{C.18}$$

$$\frac{dM_{qc}}{dt} = K_{iq}\Delta Q_i \tag{C.19}$$

$$\frac{dv_{dc}}{dt} = \frac{\Delta i_{dc} - \Delta i'_{dc}}{2H_{dc}} \tag{C.20}$$

$$0 = \Delta i'_{dc}R_{dc} - \Delta v_{dc} \tag{C.21}$$

$$0 = \Delta v_{dc} i^o_{dc} P_d + v^o_{dc}\Delta i_{dc} P_d + v^o_{md} S_B \Delta i_d + i^o_d S_B \Delta v_{md} + v^o_{mq} S_B \Delta i_q + i^o_q S_B \Delta v_{mq} \tag{C.22}$$

$$0 = E'_{sc} \sin\delta^o_{sc}\Delta\delta_{sc} + \Delta v_{xsc} \tag{C.23}$$

$$0 = E'_{sc} \cos\delta^o_{sc}\Delta\delta_{sc} - \Delta v_{ysc} \tag{C.24}$$

$$\frac{d\delta_{sc}}{dt} = \Delta\omega_{sc}\omega_N \tag{C.25}$$

$$\frac{d\omega_{sc}}{dt} = \frac{-\Delta P_{sc}}{2H} \tag{C.26}$$

$$0 = i^o_{xsc}\Delta v_{xsc} + v^o_{xsc}\Delta i_{xsc} + i^o_{ysc}\Delta v_{ysc} + v^o_{ysc}\Delta i_{ysc} - \Delta P_{sc} \tag{C.27}$$

$$0 = i^o_{xsc}\Delta v_{ysc} + v^o_{ysc}\Delta i_{xsc} - i^o_{ysc}\Delta v_{xsc} - v^o_{xsc}\Delta i_{ysc} - \Delta Q_{sc} \tag{C.28}$$

$$0 = \Delta v_x - X_e\Delta i_{ysc} - \Delta v_{xsc} \tag{C.29}$$

$$0 = \Delta v_y + X_e\Delta i_{xsc} - \Delta v_{ysc} \tag{C.30}$$

$$0 = \Delta P_{sc} + \Delta P_i \tag{C.31}$$

$$0 = \Delta Q_i + \Delta Q_{sc} \tag{C.32}$$

$$\frac{dP^{hc}}{dt} = -K_{hc}\Delta\omega_{sc} \tag{C.33}$$

C.2 Operating point

From the value given in the operating point part of chapter 3 it is possible to find the initial value of all the states.Due to steady state assumption, all derivative are null, which means:

$$\omega^o_{sc} = 1\ p.u. \tag{C.34}$$

$$\omega^o_{pll} = 1\ p.u. \tag{C.35}$$

The following formulas are based on transformation of equation gave previously and correspond to the initial value of each state:

$$v^o_{xsc} = V_s \cos\delta^o_{sc} \tag{C.36}$$

$$v^o_{ysc} = V_s \sin\delta^o_{sc} \tag{C.37}$$

$$i^o_{xsc} = \frac{P_{sc}\cos\delta^o_{sc} + Q_{sc}\sin\delta^o_{sc}}{V_s} \tag{C.38}$$

$$i^o_{ysc} = \frac{P_{sc}\sin\delta^o_{sc} - Q_{sc}\cos\delta^o_{sc}}{V_s} \tag{C.39}$$

$$v^o_x = v^o_{xsc} + X_e i^o_{ysc} \tag{C.40}$$

$$v^o_y = v^o_{ysc} - X_e i^o_{xsc} \tag{C.41}$$

$$\theta^o = \frac{v^o_x}{\sqrt{v^o_x + v^o_y}} \tag{C.42}$$

$$P^{ini}_i = -P^o_{sc} - P_w \tag{C.43}$$

Here, the notation P^{ini}_i is used to not be confused with the reference value of the active power in the VSC.

$$Qi^o = -Q^o_{sc} - P_w \tag{C.44}$$

$$v^o_d = v^o_x\cos\theta^o + v^o_y\sin\theta^o \tag{C.45}$$

$$v^o_q = v^o_y\cos\theta^o - v^o_x\sin\theta^o \tag{C.46}$$

$$i^o_x = \frac{P^{ini}_i v^o_x + Q^o_i v^o_y}{V_{sc}}\frac{S_B}{S_n} \tag{C.47}$$

$$i^o_y = \frac{P^{ini}_i v^o_y - Q^o_i v^o_x}{V_{sc}}\frac{S_B}{S_n} \tag{C.48}$$

Where S_n is the base power for the VSC and S_B is the base power of the system.

$$i^o_d = i^o_x\cos\theta^o + i^o_y\sin\theta^o \tag{C.49}$$

$$i^o_q = i^o_y\cos\theta^o - i^o_x\sin\theta^o \tag{C.50}$$

$$v^o_{md} = Ri^o_d + v^o_d - \omega^o_{pll}Li^o_q \tag{C.51}$$

$$v^o_{mq} = v^o_q + \omega^o_{pll}Li^o_d + Ri^o_q \tag{C.52}$$

Due to steady state assumption, the equation of the voltage in the capacitor of the DC link becomes:

$$i^o_{dc} = i'^o_{dc} \tag{C.53}$$

$$i^o_{dc} = \frac{v^o_{dc} - V_{dc}}{R_{dc}} \tag{C.54}$$

By replacing this expression in the Kirchhoff's law in the DC link, v_{dc} can be found and is given by the poles of the second degree equation:

$$(v^o_{dc})^2 - v^o_{dc}V_{dc} + (i^o_d v^o_{md} + i^o_q v^o_{mq})\frac{S_B R_{dc}}{P_d} = 0 \tag{C.55}$$

$$v^o_{dc_{1,2}} = \frac{V_{dc} \pm \sqrt{V^2_{dc} - (i^o_d v^o_{md} + i^o_q v^o_{mq})\frac{S_B R_{dc}}{P_d}}}{2} \tag{C.56}$$

The initial value of all the states are not given here but the one necessary to established the Jacobian are computed.

Appendix D

Parameters of one link system and bases

This appendix aims to explain the values of the parameters token in the one link system. First, it is necessary to remain the bases used in this system. Table D.1 gives the value for the different bases. In the system, there is three different bases.The base of offshore network (referenced with index "B"), the base of the AC part of the VSC (index "n") and a base for the DC part of the VSC and the DC link (index "d"). The base power for each part are based on Papangelis, L. (2018) [26]. It can be noticed that the base voltage of the DC and the AC part are equal. Even if the value is the same than for the AC part, it represent different think. In the AC system it is the RMS phase-to-neutral voltage of a three phase system. In the DC part it is the positive value of the voltage. So the base impedance are computed differently.

$$Z_d = \frac{2V_d^2}{P_d} \qquad\qquad Z_n = \frac{3V_n^2}{S_n}$$

Phase reactor

The resistance R with a value of 0.01 p.u. correspond to a resistance of 0.19 Ω. On the same base, the inductance of 0.2 p.u. correspond to a value of 3.8 H. Both are chosen thanks to [26, 33, 30].

VSC capacitance and DC link resistance

To compute the value of the resistance in the DC link, a mean value of the distance between the different countries around the north sea and the potential future location of the NSWPH is computed. This one correspond to 350 km. With a value of 0.011 Ω/km [26, 12], the total value correspond to 3.85 Ω which express in the base gives a value of 0.094 p.u.. The value of H_{dc} aims to simulate the effects of the condenser. The value is choose based on Rault, P. (2014), Denis, G. (2017) [12, 33]. The capacitance effect induces the same effect than the Synchronous Condenser

S_B	100 MVA	V_B	320 kV	Z_B	1024 Ω
S_n	5500 MVA	V_n	320 kV	Z_n	18.62 Ω
P_d	5000 MW	V_d	320 kV	Z_d	40.96 Ω

Table D.1: Bases used in the one link system

and could be used as a battery in case of disturbance. However, the value of H_{dc} is much more smaller than the one of the Synchronous Condenser due to the small value of the capacitance. The link between the capacitance and H_{dc} [33] is given by:

$$H_{dc} = \frac{1}{2} C_s \frac{U_{s,base}^2}{P_{base}}$$

Which means a value of C_s equals to 200 pF.Moreover, the aim here is not to use this energy storage. Indeed, use it means disturb the voltage in the DC cable which lead to instabilities in the cable and maybe onshore if the disturbance becomes too important. This explain why the control of the active power do not have to be too fast. A too fast control without using the SC uses principally the energy storage of the condenser and disturb the behaviour of the DC cable.

Synchronous Condenser

The first parameters used for the SC is H. This one represent the storage capacity of the machine which depend essentially of the weight of the rotor based on the formula:

$$H = \frac{1}{2} J \frac{\omega_{base}^2}{S_{base}}$$

All thinks are fixed in this formula except the value of J which is the moment of inertia of the rotor which in kgm^3. The value of 2 correspond to a small one for a SC [34, 35]. Some SC can have a value of 7 or 8 which mean more storage capacity and better stability in case of disturbance. The value of 2 has been choosed for two reasons. First, a value of 2 is easy to find and an old synchronous generation unit can be easily adapted into a SC of this capacity [38].A value of 7 or 8 need special adaptation or even new creation or this kind of SC [38]. The second reason is to study the system with a small value. Indeed, this solution is a good solution if a simple value of H can be sufficient, not if a special value extremely high and expensive is needed. The second parameter of the SC is X_e. This one is the combination of the SC reactance and the reactance of the transfomer. For the first one, a value of 0.3 p.u. has been chosen and for the second one 0.15 p.u.[31].The addition of both reported in the nominal power of 500 MVA correpond to 0.09.

Frequency

The last parameter is the nominal frequency of the system. It has been choosed to be the same than the onshore frequency. The aim of this study was not to discuss the effect of the frequency on the stability of the system. However, this could be one of the future study point.

Appendix E

Graphs of linear study without HC

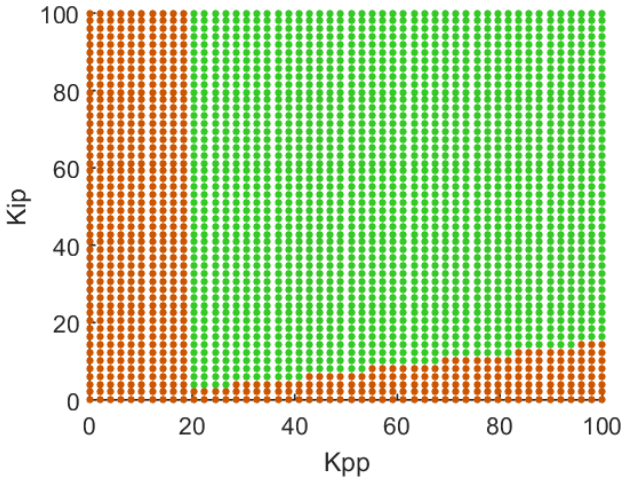

Figure E.1: $K_\omega = 50$

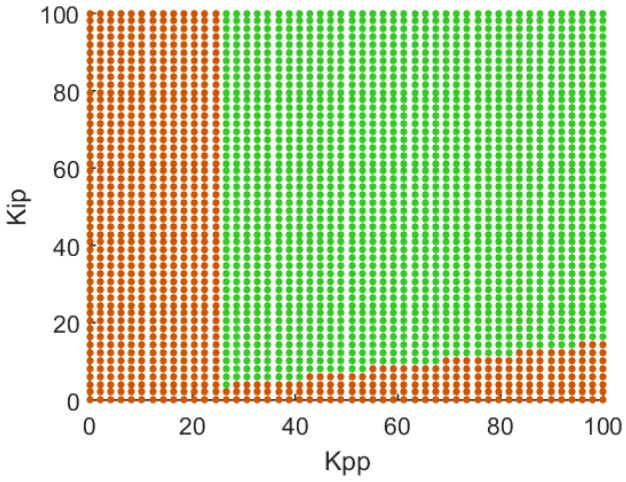

Figure E.2: $K_\omega = 100$

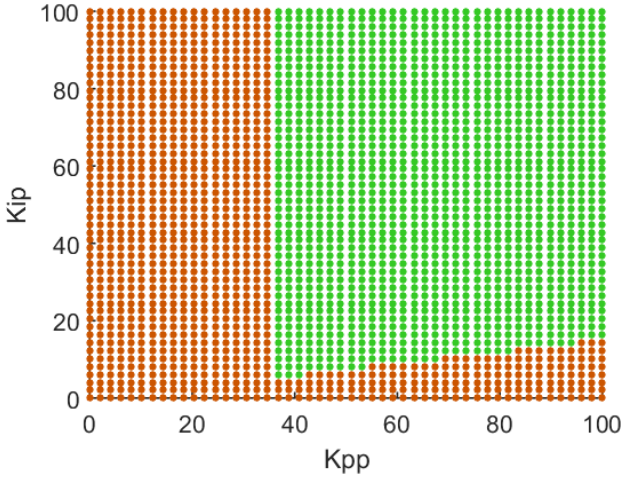

Figure E.3: $K_\omega = 150$

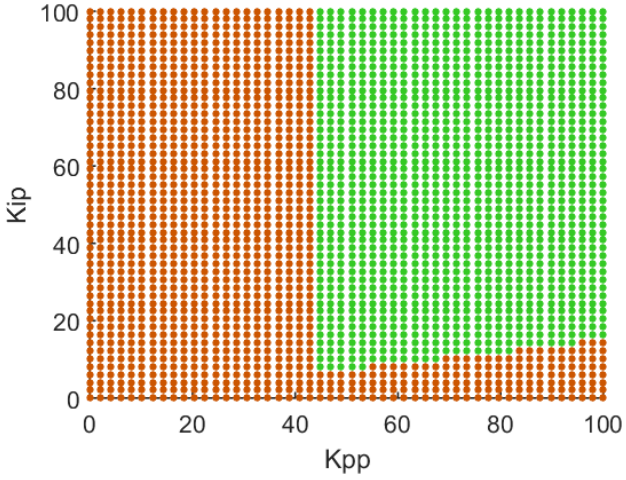

Figure E.4: $K_\omega = 200$

Bibliography

[1] North Sea Wind Power Hub, *Project*. Retrieved from https://northseawindpowerHub.eu/vision/

[2] United Nation, Framework Convention on Climate Change, *Climate: Get the Big Picture*. Retrieved from https://unfccc.int/resource/bigpicture/#content-the-paris-agreemen

[3] S.Mulder.(2017). *Offshore Wind Capacity Dogger Bank*. Retrieved from https://northseawindpowerHub.eu/wp-content/uploads/2017/10/Wind-Capacity-Study.pdf

[4] Ackermann, T. (Ed.). (2005). *Wind power in power systems*. John Wiley & Sons.

[5] NSWPH (2017). *The vision*. Retrieved from https://northseawindpowerHub.eu/wp-content/uploads/2017/11/Concept-Paper-1-The-Vision.pdf

[6] Gullberg, A. T. (2013). *The political feasibility of Norway as the 'green battery'of Europe*. Energy Policy, 57, 615-623.

[7] NSWPH (2017). *PLANNING THE FUTURE TOGETHER,WindEurope Conference 2018 Side event North Sea Wind Power Hub* . Hamburg, September 2018. Retrieved from https://northseawindpowerHub.eu/wp-content/uploads/2018/11/NSWPH-WindEurope-27-September-2018.pdf

[8] NSWPH (2017). *Modular Hub and Spoke*. Retrieved from https://northseawindpowerHub.eu/wp-content/uploads/2017/11/Concept-Paper-2-Modular-Hub-Spoke.pdf

[9] Nguyen, H. T., Yang, G., Nielsen, A. H., & Jensen, P. H. (2018). *Combination of Synchronous Condenser and Synthetic Inertia for Frequency Stability Enhancement in Low Inertia Systems*. IEEE Transactions on Sustainable Energy.

[10] Yan, R., Saha, T. K., & Modi, N. (2015, July). *Frequency response and its enhancement using Synchronous Condensers in presence of high wind penetration*. In 2015 IEEE Power & Energy Society General Meeting (pp. 1-5). IEEE.

[11] Ackermann, T. (Ed.). (2005). *Wind power in power systems*. John Wiley & Sons.

[12] Rault, P. (2014). *Modelling dynamique et commande des réseaux a courant continu multi-terminaux haute tension. Thèse de doctorat en GE-NIE ELECTRIQUE, Doctorat delivre par l'ecole centrale de LILLE.*

[13] Guo, C., Zhang, Y., Gole, A. M., & Zhao, C. (2012). *Analysis of dual-infeed HVDC with LCC–HVDC and VSC–HVDC*. IEEE Transactions on Power Delivery, 27(3), 1529-1537.

[14] Meah, K., & Ula, S. (2007, June). *Comparative evaluation of HVDC and HVAC transmission systems. In 2007 IEEE Power Engineering Society General Meeting (pp. 1-5)*. IEEE.

[15] Little, M., Thomson, M., & Infield, D. (2007). *Electrical integration of renewable energy into stand-alone power supplies incorporating hydrogen storage*. International Journal of Hydrogen Energy, 32(10-11), 1582-1588.

[16] Vandewalle, J., Bruninx, K., & D'haeseleer, W. (2015). *Effects of large-scale power to gas conversion on the power, gas and carbon sectors and their interactions. Energy conversion and management, 94, 28-39.*

[17] Balat, M. (2008). *Potential importance of hydrogen as a future solution to environmental and transportation problems*. International journal of hydrogen energy, 33(15), 4013-4029.

[18] ABB.*Synchronous Condensers for reactive power compensation*. Retrieved from `https://new.abb.com/motors-generators/synchronous-condensers`

[19] Csaba Szabo (2017).*An old tool rediscovered to adress new grid challenges*. Power Engineering International. Retrieved from `https://www.powerengineeringint.com/articles/print/volume-25/issue-11/features/an-old-tool-rediscovered-to-address-new-grid-challenges.html`

[20] Elisa Iannunzio.(2018). *Synchronous Condensers support Australia's clean energy transformation*. Energy Magazine. Retrieved from `https://www.energymagazine.com.au/synchronous-condensers-support-australias-clean-energy-transformation/`

[21] Krause, P., Wasynczuk, O., Sudhoff, S. D., & Pekarek, S. (2013). *Analysis of electric machinery and drive systems (Vol. 75)*. John Wiley & Sons.

[22] Nedd, M., Booth, C., & Bell, K. (2017, August). *Potential solutions to the challenges of low inertia power systems with a case study concerning Synchronous Condensers*. In 2017 52nd International Universities Power Engineering Conference (UPEC) (pp. 1-6). IEEE.

[23] Marken, P. E., Depoian, A. C., Skliutas, J., & Verrier, M. (2011, July). *Modern Synchronous Condenser performance considerations*. In 2011 IEEE Power and Energy Society General Meeting (pp. 1-5). IEEE.

[24] Hsieh, G. C., & Hung, J. C. (1996). *Phase-locked loop techniques. A survey*. IEEE Transactions on industrial electronics, 43(6), 609-615.

[25] Papangelis,L. Van Cutsem,T.(2019). *Generic model of an AC/DC Voltage Source Converter in RAMSES*

[26] Papangelis, L. (2018). *Local and centralized control of multi-terminal DC grids for secure operation of combined AC/DC systems* (Doctoral dissertation, Université de Liège, Liège, Belgique).

[27] Mohan, N., & Undeland, T. M. (2007). *Power electronics: converters, applications, and design*. John wiley & sons.

[28] Aström, K. J., & Murray, R. M. (2010). *Feedback systems: an introduction for scientists and engineers*. Princeton university press.

[29] Papangelis, L., Debry, M. S., Prevost, T., Panciatici, P., & Van Cutsem, T. (2018, June). *Stability of a voltage source converter subject to decrease of short-circuit capacity: A case study*. In 2018 Power Systems Computation Conference (PSCC) (pp. 1-7). IEEE.

[30] Ardelean,M., Minnebo, P. (2015).*HVDC Submarine Power Cables in the World* . JRC Technical Report. European Commission.

[31] Van Cutsem, T. (2017). *Introduction to electric power and energy systems*. Livre de cours.

[32] Co2 Solution Inc.(2001). *Process for generating electricity with a hydrogen fuel cell*. Retrieved from `https://patents.google.com/patent/US6846584B2/en`

[33] Denis, G. (2017). *From grid-following to grid-forming: The new strategy to build 100% power-electronics interfaced transmission system with enhanced transient behaviour*. EC-Lille, Ph. D, 23.

[34] General Electric company(2016). *Systems and methods for controlling an inertia of a Synchronous Condenser*. Retrieved from `https://patentimages.storage.googleapis.com/4f/d8/86/a2433b673efac1/US8384319.pdf`

[35] General Electric company (2015).*Hybrid high-inertia Synchronous Condenser facility*. Retrieved from `https://patentimages.storage.googleapis.com/5e/59/8e/39299ec0cfd7e9/US20150168981A1.pdf`.

[36] Denis, G., Prevost, T., Debry, M. S., Xavier, F., Guillaud, X., & Menze, A. (2018). *The Migrate project: the challenges of operating a transmission grid with only inverter-based generation. A grid-forming control improvement with transient current-limiting control*. IET Renewable Power Generation, 12(5), 523-529.

[37] Zamani, M. A., Yazdani, A., & Sidhu, T. S. (2012). *A control strategy for enhanced operation of inverter-based microgrids under transient disturbances and network faults*. IEEE Transactions on Power Delivery, 27(4), 1737-1747.

[38] Dr. J. M. Fogarty, R. M LeClair (01/2011). *Converting Existing Synchronous Generators into Synchronous Condensers*. Power Engineering

[39] Hildebrand, F. B. (1987). *Introduction to numerical analysis*. Courier Corporation.

[40] Süli, E., & Mayers, D. F. (2003). *An introduction to numerical analysis*. Cambridge university press.

[41] Van Cutsem, T.,*Note théorique du cours ELEC0029*. Retrieved from `http://montefiore.ulg.ac.be/~vct/elec0029/g.pdf`

[42] Sood, V. K. (2006). *HVDC and FACTS controllers: applications of static converters in power systems*. Springer Science & Business Media.

[43] Van Hertem, D., & Ghandhari, M. (2010). *Multi-terminal VSC HVDC for the European supergrid: Obstacles*. Renewable and sustainable energy reviews, 14(9), 3156-3163.

[44] Gomis-Bellmunt, O., Liang, J., Ekanayake, J., King, R., & Jenkins, N. (2011). *Topologies of multiterminal HVDC-VSC transmission for large offshore wind farms*. Electric Power Systems Research, 81(2), 271-281.

[45] Ahmed, N., Haider, A., Van Hertem, D., Zhang, L., & Nee, H. P. (2011, August). *Prospects and challenges of future HVDC SuperGrids with modular multilevel converters*. In Proceedings of the 2011 14th European Conference on Power Electronics and Applications (pp. 1-10). IEEE.

[46] Rodríguez-Amenedo, J. L., Arnaltes-Gómez, S., Aragüés-Peñalba, M., & Gomis-Bellmunt, O. (2019). *Control of the parallel operation of VSC-HVDC links connected to an offshore wind farm*. IEEE Transactions on Power Delivery, 34(1), 32-41.

[47] Palizban, O., & Kauhaniemi, K. (2015). *Hierarchical control structure in microgrids with distributed generation: Island and grid-connected mode*. Renewable and Sustainable Energy Reviews, 44, 797-813.

[48] Denis, G., Prevost, T., Debry, M. S., Xavier, F., Guillaud, X., & Menze, A. (2017). *The Migrate project: the challenges of operating a transmission grid with only inverter-based generation. A grid-forming control improvement with transient current-limiting control*. IET Renewable Power Generation, 12(5), 523-529.

[49] M. Liserre, *Grid following vs. Grid forming Converters : definitions*, Personal communication, May 16, 2019.